THE HIGH-TEMPERATURE OXIDATION OF IRON IN CARBON DIOXIDE

——oOo——

by

F.R.A. JORGENSEN, B.E. Hons. (Adel.)

A Thesis submitted for the Degree of Doctor of Philosophy
in the Department of Chemical Engineering
the University of Adelaide.

January, 1964.

INDEX.

INDEX OF FIGURES.

INDEX OF TABLES.

APPENDICES.

SUMMARY.

The oxidation of iron by carbon dioxide at 200 mm Hg total pressure has been studied over the temperature range from 400-800°C. To follow the kinetics of the early stages of the reaction between iron and carbon dioxide it was necessary to build a vacuum microbalance. This instrument, which utilizes a very sensitive compact optical lever assembly to detect the null point, is capable of obtaining much higher sensitivity than the 1 µg required for this project. A new method of making a non-inductive furnace winding has also been developed.

It was found that for the times of oxidation studied in this project the oxide layer consisted of either wustite or magnetite depending upon whether the temperature of oxidation was above or below the wustite eutectoid temperature at 570°C.

Particular attention has been paid to the early stages of the reaction which proceeded by a mechanism involving the nucleation and growth of an oxide phase on the metal surface. The nuclei appear to form as a result of the metal surface becoming saturated with oxygen and a model has been developed to account for their subsequent growth. This model was successfully fitted to the gravimetric data obtained above 570°C for the initial stages of the reaction.

Above and below 570°C the kinetics of the latter stages of the reaction (as represented by the gravimetric results) obeyed linear and parabolic oxidation kinetics respectively. It was established that the rates of magnetite scale formation were controlled by the diffusion of material - possibly oxygen ions- through the magnetite layer, while the linear rates of the wustite scaling reaction (on both α and γ iron) were controlled by the dissociation of carbon dioxide at the wustite surface.

ACKNOWLEDGEMENTS.

The work described in this thesis was carried out under the supervision of Dr. W.T. Denholm whose encouragement and advice are gratefully acknowledged.

I would also like to thank the following persons and organizations for practical and financial help during the course of the project.

1. Dr. E.C.R. Spooner for reading the text.

2. Mr. W. Boundy for help with the design and construction of the optical lever.

3. Mr. P. Stinburys and the staff of the Bonython Laboratories workshop for assistance with the construction of apparatus.

4. The C.S.I.R.O. for providing a living allowance in the form of a senior post-graduate studentship.

5. The Australian Atomic Energy Commission for a equipment grant.

6. The South Australian Institute of Technology for providing laboratory space and workshop facilities.

This thesis contains no material which has been accepted for the award of any other degree or diploma in any university, and to the best of my belief and knowledge contains no material previously published or written by another person except where due reference is made in the text.

1. INTRODUCTION.

The work described in this thesis forms the first part of a long- term investigation into the high-temperature oxidation of iron alloys in carbon dioxide. Besides being of scientific interest this information also has practical significance in the design of high-temperature gas-cooled nuclear reactors using carbon dioxide as the heat transfer medium.

To understand fully the oxidation behaviour of alloys it is first necessary to know the mechanism of oxidation of the major alloying constituent and then to study how successive increments of alloying elements modify this behaviour. It was thus decided that the work undertaken in this project should be directed towards evaluating the mechanism of oxidation of pure iron in carbon dioxide.

A search of the literature subsequently revealed that much of the previous work in this field had been conducted at temperatures in excess of 900°C and that there was no information about the reaction at temperatures below 600°C. The literature search also revealed that the early stages of the reaction required further study, and that there was some controversy as to the true mechanism of the scaling reaction between iron and carbon dioxide when wustite was the sole oxidation product. In an endeav-

our to resolve this contoversy and to supply some of the missing information it was decided to study the oxidation of iron in carbon dioxide over the temperature range from 400 to 800°C, and to pay particular attention to the early stages of the reaction.

After reviewing the available experimental techniques it was further decided that the investigation would be conducted with the aid of four complementary experimental techniques, namely:-

a) Weight-gain versus time measurements to follow the kinetics of the reaction.

b) Microscopic examination of oxidized surfaces and of polished sections through the oxide layer to provide information regarding the structure and mode of growth of the oxide product.

c) X-ray diffraction analysis of the oxide layer to identify the oxide phases present.

d) Electrometric analysis of oxide scales likely to contain haematite. This is an electrochemical technique and can be used to obtain a quantitative estimation of the amount of ferric oxide in multi- layer scales.

In addition to studying the high-temperature oxidation of iron in carbon dioxide it was also planned to investigate the way in which the electrical capacity

and resistance of thin oxide films varied when these films were subjected to electrochemical oxidation or reduction in an aqueous electrolyte. It was hoped that when a better understanding of these measurements had been obtained that they could be used, in conjunction with other electrochemical parameters, to characterize the residual oxide films left behind on a metal surface by some of the methods of specimen preparation.

Thus the main objectives of this project may be stated as follows:

1) To study the oxidation of iron in carbon dioxide over the temperature range from 400 to 800°C with the view to determining the mechanism of oxidation, and to providing basic rate data which would serve as a basis of comparison to evaluate the performance of iron alloys.
2) To investigate the way in which the electrical capacity and resistance of thin oxide films vary when these films are subjected to electrochemical oxidation and reduction.

In the preparation of this thesis the following order of presentation has been adopted : The thermodynamics of the Fe-C-O system are briefly discussed in section 2 along with a review of the current theories of oxidation together with a survey of the previous work that has been

done to elucidate the mechanism of the reaction between iron and carbon dioxide.

The design and construction of the equipment which consists of a vacuum microbalance, electrochemical apparatus, and gas purification system are described in section 4.

The results are discussed in section 5, recommendations for future work made, and the conclusions drawn in section 6. The thermodynamic calculations and the gravimetric data (in tabular form) are contained in appendices A and B respectively.

2. LITERATURE SURVEY.

2.1 Thermodynamics of the Fe-C-O System.

The mechanism of the oxidation of iron is important both from a purely scientific point of view and as a basis for the understanding of the oxidation behaviour of alloy steels. The number of investigations which have been carried out on this topic is therefore very large. However, the bulk of this work has been performed upon readily available commercially pure forms of iron which have a considerable level of impurities. The effect of these impurities must be allowed for when using the results obtained on these materials as a basis of comparison for the evaluation of alloy steels. Thermodynamic considerations provide one way of estimating the possible effects of these impurities.

An impurity of particular importance which is present to some extent in all forms of iron is carbon. This is the only alloying element which forms gaseous oxidation products and hence its effect is important from the point of view of blistering and flaking of the oxide scale. Thus the effect of the presence of carbon in the iron has been allowed for in the thermodynamic analysis of the iron-carbon-oxygen system.

2.1.1 The Equilibrium Diagram for the Fe-O-C System.

Following Cameron[1] the various phases in equilibrium with carbon dioxide - carbon monoxide gas mixtures have been conveniently represented on an equilibrium diagram (Fig.1). The diagram has been constructed from basic data for a total pressure of 200 mm Hg. Points on the various phase boundaries have been calculated by the simultaneous solution of the equations obtained by considering the thermodynamic and pressure limitations imposed upon the system. The relevant equations and the equilibrium constants derived from them are shown in appendix A.

During the derivation of the diagram it has been assumed that there is no solubility or interaction between iron oxides or iron carbides, also deviations from stoichiometry have not been taken into account. On the graph CO runs from zero at the left to 100% at the right, and the reverse for CO_2, so that the sum of the partial pressures is always 200 mm Hg. Temperature increases from the bottom to the top of the diagram. Over the range of temperatures considered the ferric oxide phase field corresponds so closely with the 100% CO_2 line that it has merely been represented as a thickening of this line. The magnetite region, depending upon temperature, is bounded by either wustite or iron carbide. The region of metallic iron lies

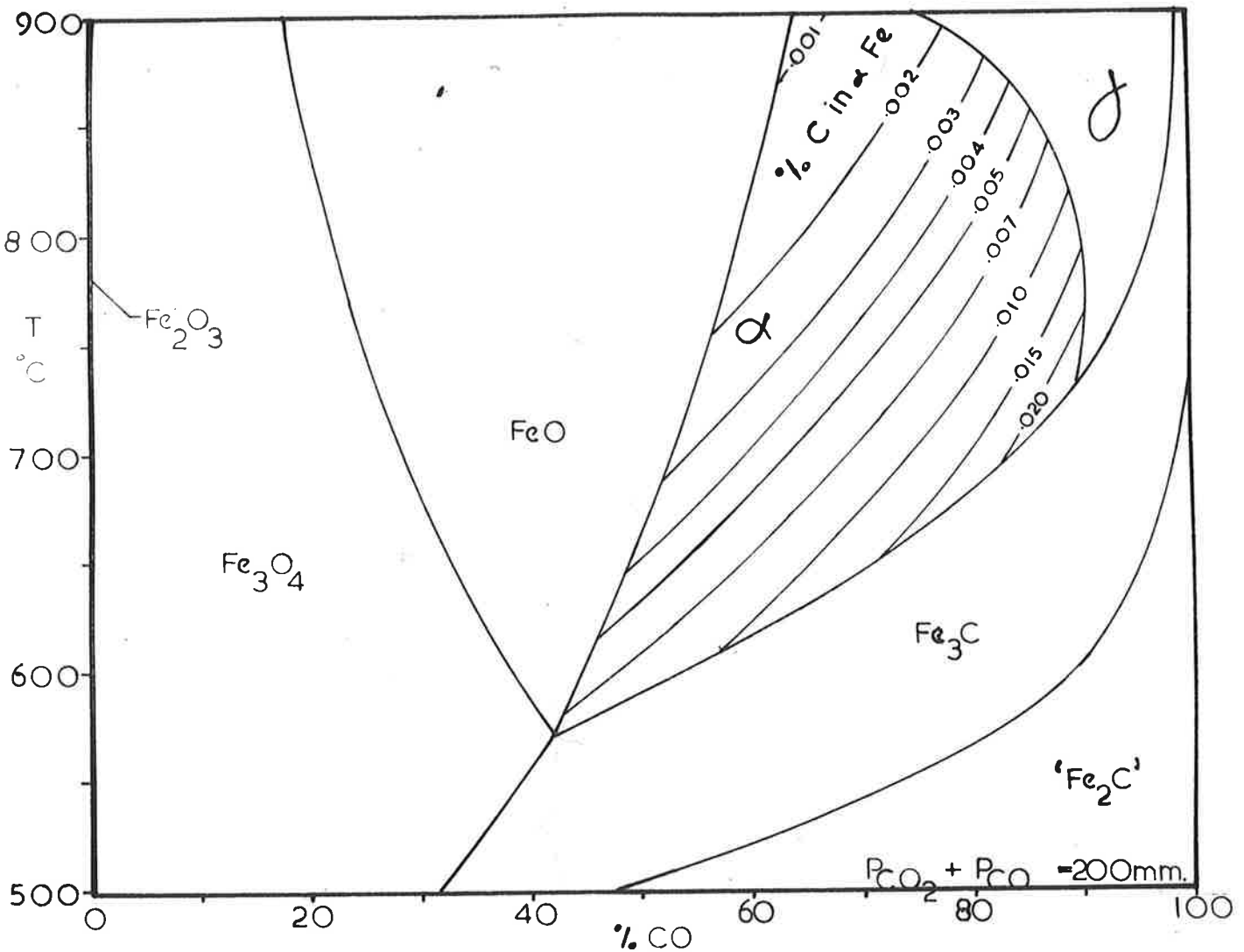

Fig.1 Equilibrium diagram for the Fe-C-O system.

between wustite and cementite and is divided into ferrite and austenite. Equilibrium carbon levels are shown for the ferrite but these values have not been calculated for the austenite where the equilibrium levels are greater than they are in the ferrite.

2.2 Structure of the Iron Oxides.

Many workers have shown that when iron is oxidised above 570°C, in a strongly oxidizing atmosphere, the oxides form in successive layers on the metal surface with the lowest valence oxide next to the metal and the highest in contact with the gas phase.

Wustite (FeO) : The lowest of the oxides is only stable above 570°C, below this temperature it decomposes into Fe and Fe_3O_4. Wustite has a NaCl type cubic lattice formed by the close packing of the relatively large oxide ions with the smaller iron ions arranged in the interstices. The ionic radius for $O^{=}$ is about 1.3 Å, while Fe^{++} and Fe^{+++} have a radius of about 0.7 Å. Reference to the iron-oxygen binary phase diagram[2] shows that the range of existence of this phase is very wide and that it does not include the stoichiometric composition FeO. Jette and Foote[3] have compared the lattice parameters and densities for a series of compositions and have established that these deviations are

brought about by the existence of vacancies on iron lattice sites. Several workers have accurately delineated the boundaries of the phase field, of these the best work is that of Engell[4] and Davies[5] who have shown that vacancies exist on 5 to 13% of the iron sites. In order for the material to be electrically neutral there must be electron holes, - represented as ⊕ - which correspond to the formation of trivalent ions, equal to twice the number of vacancies, - represented as $Fe^{++}_{\square}$.

Magnetite (Fe_3O_4) : This oxide has a spinel type structure and also exists with an excess of oxygen. The excess is smaller than in wustite and the defect concentration is therefore correspondingly less. It follows from the marker and diffusion measurements of Davies and his colleagues[6] that although both cations and anions diffuse in magnetite the bulk of the material transport within this phase is via oxygen ion vacancies.

Haematite (Fe_2O_3) : The haematite (α Fe_2O_3) phase field shows a slight oxygen deficiency and transport of material in this phase is largely by the movement of anions. This material has a rhombohedral structure.

Definite orientation relationships have been

observed at the interfaces between successive oxide layers. A detailed study of the relationship between wustite and iron was carried out by Mehl, Mc Candless and Rhines[7]. It was found that the (100) plane in FeO lies parallel to the (100) plane in iron and that the [110] direction in the (100) plane in FeO lies parallel to the [100] direction in the (100) plane in iron. Taking into account the lattice parameters of the two phases it was suggested that the formation of wustite from iron consists in the expansion of the body centred cubic cell of iron to form a body centred tetragonal cell of axial ratio 1.414. Definite orientation relationships have also been determined for the wustite/magnetite and the magnetite/haematite interfaces. No work appears to have been done to determine the relationship between γ iron and wustite. However, Goldschmidt[8] has examined the relative volumes and structures of the metal and the cubic oxides and obtained numerical comparisons which illustrate the smallness of the adjustments which must be made to fit the lattices together at an interface.

2.3 A Survey of the Mechanisms of Oxidation.

Some of the first systematic work done with the view to furthuring our understanding of the mechanism of the oxidation of metals was performed by Pilling and

Bedworth[9]. These workers considered that the mechanism of the reaction was determined by the relation between the specific volumes of the oxide and the metal. At room temperature the densities of iron in the metal and the oxides are as follows:-

$$\underline{7.85 \text{ g Fe}}_{\text{cc Fe}} \; ; \; \underline{4.43 \text{ g Fe}}_{\text{cc FeO}} \; ; \; \underline{3.74 \text{ g Fe}}_{\text{cc } Fe_3O_4} \; ; \; \underline{3.67 \text{ g Fe}}_{\text{cc } Fe_2O_3} .$$

It is evident that the bulk of all the oxides is greater than the volume of the metal from which they formed and hence the criterion for a compact coherent scale is obeyed. This theory held the field for many years but (at least for work on iron) is now only of general interest.

Following the work of Pilling and Bedworth developments in the theory of oxidation have followed in two different directions. Wagner[10] considered the movement of ions through the oxide layer under the influence of the concentration gradient and the electric field across the layer, and from these considerations obtained a general equation for the rate of growth which was parabolic in form. Cabrera and Mott[11] considered very thin oxide films in which in which the basic assumptions employed in the derivation of the parabolic equation are no longer valid, that is, there is no longer an even distribution of electrical charge throughout the film and the electrical charge at the phase border cannot be neglected. From

these considerations Cabrera and Mott developed the cubic and inverse logarithmic equations for the rate of growth of oxide films. Other rate laws that are sometimes observed obey the linear and logarithmic expressions. The linear relation is usually characterized by a non-protective oxide, although in special circumstances the linear law has been observed to occur with compact scales, in which case it is generally considered that the rate of the reaction is controlled by a phase boundary reaction. The logarithmic equation as derived by Mott[12], from considerations of electron tunnelling at an energy barrier at an interface, is usually characteristic of low temperatures and thin films up to 18 Å thick. This law is also met with in thicker films where the tunnel effect cannot operate, under these circumstances the derivation is usually based upon the formation of cracks and voids in the film[13]. Additional information regarding the above rate laws and the combinations of them that are sometimes observed can be obtained from Kubaschewski and Hopkins[14] book or from Evans[15] handbook on corrosion.

2.4 The Nucleation and Growth of Oxide Films.

The preceding theories suppose that the oxide which forms on the metal is uniform in thickness and that the growth takes place by the movement of ions perpendic-

ular to the surface of the metal. Bardolle and Benard[16] working with iron in low partial pressures of oxygen revealed the process of nucleation and growth during the formation of the oxide film. These observations were later extended to other metals[17-21] and alloys[22-24], and recently to the oxidation of uranium in carbon dioxide[25]. The effect is not limited to the formation of oxide films since Garcia and Fuller[26] have observed it to occur during the growth of sulphide films on copper. These observations are not predicted nor can they be explained by any of the preceding theories.

Benard[27] has described the following stages in the process of nucleation and growth:

> 'At the start of the reaction the metal is covered by a compact oxide film whose thickness increases until it reaches a critical value of the order of several tens of angstroms, which presumeably corresponds to the limit of the influence of the substrate. After this the true oxide phase tends to appear at certain centres of crystallization. The average number of these centres corresponds to a competitive equilibrium fixed by the surface diffusion rates of metal and oxygen at the surface of this base film. Following impingement of the growing nuclei the oxide continues to develop into a layer of appreciable thickness.'

Observation of the nucleation process is only possible under carefully controlled conditions. The temperature must be sufficiently high to promote active surface diffusion, and the oxygen partial pressure must be sufficiently low so that the growth of an oxide is just thermodynamically possible. At oxygen pressures less than the decomposition pressure of the oxide only a chemisorbed film can form but if the conditions are altered so that the oxide becomes stable nuclei will form. There is some evidence to suggest that not only the oxygen partial pressure, but also the composition of the gas may exert a considerable influence on the shape and size of the oxide particles. The work of Gulbransen and Copan[28] has shown the existence of a variety of shapes of oxide particles produced in gas mixtures containing water vapour. To what extent the presence of hydrogen and water vapour contribute to the observed structure (apart from fixing the oxygen partial pressure) is at present not known.

2.4.1 The Initial Oxide Film.

The initial oxide film has its counterpart in aqueous passivation studies where gel-like films grow prior to the nucleation of a true oxide phase[29]. Little is known about the structure and properties of the initial oxide film formed by thermal oxidation as in most cases

it is too thin to be characterized by electron microscopy and electron diffraction. Recent work by Bouillon et al[30] on the oxidation of copper has shown that there is always a competition between the formation of surface oxide and its dissolution in the metal. A decrease in the partial pressure of oxygen favours the dissolution of the oxide which can even completely disappear while at its temperature of formation. The dissolved oxygen modifies the subsequent oxidation behaviour of the metal, and provides a decrease in the incubation time for nucleation, which permits identification of this as the time necessary to accomplish the superficial saturation of the metal with oxygen. The beginning of nucleation would then be precipitation of the oxide.

The initial oxide film probably forms by one of the thin film mechanisms discussed previously in section 2.3. Under these circumstances the oxide would have no structure of its own but would be constrained to fit the underlying metal lattice. For metals such as iron, in which the solubility of oxygen is very low, it would not require very much oxygen to accomplish the superficial saturation of the metal, and it is possible in some cases that only a chemisorbed film is formed and probable in others that complete coverage of the surface may not even result.

2.4.2 The Nature of Nucleation Sites.

Several authors[31,32] have attributed the nucleation of oxides on the surface of metals to the preferential oxidation of metal at the site of dislocations. However, work by Young[33] (using copper of medium and high purity into which he introduced a regular array of dislocations by bending) has shown that the oxide nuclei are only associated with dislocations on the copper of medium purity. It appears that the impurities collect at the sites of the dislocations and it becomes a case of the preferential oxidation of impurities. For the high purity copper the nuclei appeared at random on the surface and were independent of the dislocations in the metal.

Rees[34] has proposed that the nuclei form at aggregations of defects which are produced by the penetration of oxygen atoms or ions into the metal surface. At some stage during their development the aggregation of defects becomes thermodynamically unstable and separates out as a new phase. Because of lattice misfit between the small product crystal and the host phase stresses will be set up which generate dislocations. For those crystals of the product phase in which a screw dislocation has been generated, rapid growth is possible if the screw dislocations intersect the growth interface, and

such crystals would become nuclei. This model can account for the observed fact[35] that the nuclei are often epitaxial with the metal substrate. The orientation of the crystal of the product phase is determined by the host crystal whereas the direction of the screw dislocation is determined by the slip direction in the product crystal. If the host crystal surface is appropriate then the screw dislocation will emerge from the free surface and growth will proceed with the preservation of the inbuilt epitaxial relationship. This model can also be used to explain the results obtained by Hardolle[36] on iron, and Lawless et al[37] on nickel, that the number of nuclei is strongly affected by the orientation of the metal substrate. It can be seen that if the orientation of the product crystals is such that the slip direction, and hence the direction of possible screw dislocations, does not intersect the surface then reaction on such a crystal face will be improbable.

2.4.3 The Rate of Growth of Oxide Nuclei.

Rate measurements made during the initial stages of reaction provide a basis for evaluating reaction mechanisms based upon models of nucleation and growth, providing the distribution of reaction sites is also determined by surface characterization studies of adequate resolution.

Bloomer[38] recognizing the importance of the growth of oxide nuclei in his work on barium films postulated a mechanism involving localized growth from oxide islands associated with favourably located nuclei. For a Wagener type experiment[39] (constant oxygen flow and therefore constant oxidation rate) he obtained a simple growth law of the form

$$S = kt^n.$$

Where S is the sticking probability, and n is a non-dimensional parameter which can be calculated directly from the geometry and mode of growth of the nuclei. For flat circular oxide islands n is 1/2 and for hemispherical oxide islands n is 2/3. This simple model is inapplicable if the growth structures interact or if the nuclei are not all present at the start of the reaction.

Evans[40] has applied probability theory to the two dimensional growth of an oxide to ascertain the manner in which the uncovered fraction y of the surface diminishes with time t, when the oxide extends outwards from the nuclei as circles expanding with a constant radial velocity v. Depending upon whether all the nuclei are present at the instant that the exposure starts, or whether they form subsequently with time on the uncovered portion of the surface Evans has developed the equations

$$y = \exp(-\pi\omega v^2 t^2)$$

$$y = \exp(-\pi \omega v^2 t^3/3).$$

Where ω the nucleation density is defined by stating that the probability of a nucleus being included in an area element δA is $\omega \delta A$. Ω, the nucleation rate is defined by stating that the probability of a nucleus appearing in time element δt on an area element δA is $\Omega \delta A \delta t$. Ronnquist[41] has made a kinetic and a morphological study of the early stages of the reaction between copper and oxygen and has attempted to adapt the above equations to fit his gravimetric results. By assuming that the weight-gain m is proportional to the area covered and by making the approximation that t is very small he has arrived at the following equations

$$m \propto 1 - y \doteq \pi \omega v^2 t^2$$

$$m \propto 1 - y \doteq \pi \Omega v^2 t^3/3.$$

A log-log plotof weight-gain versus time should then have a slope of 2 or 3, depending upon whether the nuclei were all present at the start of the reaction, or whether they formed subsequently with time. Ronnquist has treated his data in this fashion and found that in all cases the slope of the lines was greater than 3. He explains the lack of agreement between the theoretical and experimental results by pointing out that the weight uptake of oxygen was possibly greater than was needed for the growth of the nuclei due to the simultaneous thickening of the basal film.

2.5 The Temperature Dependence of the Rate of Reaction.

The historical basis for the understanding of rate processes is the Arrhenius equation in which it was found that for many processes the specific reaction-rate constant k, could be related to temperature by the relation

$$\log k \propto 1/T,$$

or alternatively

$$k = A \exp (-Q/RT).$$

Two general considerations have been the basis for kinetic studies over the past twenty years. The first is that each individual step in a rate process must be relatively simple and that the reaction path of each step (such as an individual atom jump in diffusion, a molecular decomposition, or the formation of a new chemical bond) involves an activated complex or transition state of maximum energy along the reaction path. Of all possible paths of reaction, the one with the lowest energy barrier will be the most rapid and the major contributor to the overall process. The second general consideration has been that the overall rate, of a complex process involving a series of consecutive steps, is fixed by the rate of the slowest individual step.

The activated complex theory (or transition state theory, or theory of absolute reaction rates) has provided a general form of equation for rate processes and a model which has allowed semi-empirical calculations of

rates for simple processes and has led to more or less successful attempts to calculate theoretical solutions for the simplest gas phase reactions. There are two main principles that are the basis of reaction rate theory(42). First, the activated complex can be treated as any other chemical species even though its life is short. That is an equilibrium constant K^* can be employed for the formation of the activated complex from the reactants. If the standard free energy of formation of the activated complex is ΔG^{o*} then

$$\Delta G^{o*} = -RT \ln K^*.$$

Second, the reaction rate of decomposition of the activated complex is a universal constant equal to $k'T/h$ where k' is Boltzmann's constant, T the absolute temperature, and h is Planck's constant. This corresponds to a rate of $2.1T \times 10^{10}$ seconds^{-1} which is sufficiently high to show that measureable rates are due to the small number of activated complexes formed.

For an individual reaction step to form an activated complex such as

$$A + B = AB^*,$$

and assuming unit activity coefficients, then

$$K^* = C^*_{AB}/C_A \cdot C_B .$$

The reaction rate or number of activated complexes that decompose per unit time is :-

$$\text{Reaction rate} = \frac{k'T}{h} \cdot C^{*}_{AB}$$

$$= \frac{k'T}{h} \cdot K^{*} C_A C_B \ .$$

Where the coefficient of the concentration term is the specific reaction constant. Now

$$K^{*} = \exp -\Delta G^{o*}/RT$$

$$= \exp\left(-\Delta H^{o*}/RT \right) . \exp\left(\Delta S^{o*}/R \right),$$

and the specific reaction rate constant is

$$k = \frac{k'T}{h} . \exp\left(-\frac{\Delta H^{o*}}{RT} \right) . \exp\left(\frac{\Delta S^{o*}}{R} \right) .$$

Furthermore if ΔH^{o*} and ΔS^{o*} are essentially temperature independent it will be noted that the expression is of the form

$$k = aT \exp\left(\Delta H^{o*}/RT \right),$$

where

$$a = k'/h \exp\left(\Delta S^{o*}/R \right).$$

A comparison of this equation and the Arrhenius equation shows that the A term in the Arrhenius equation is no longer constant but is temperature dependent. Most rate measurements are conducted over a limited temperature range, and the accuracy of the experimental results is such, that it is customary to ignore the effect of temperature on the A term in the Arrhenius equation and draw a straight line through the experimental values of ln k vs 1/T and to interpret the rate process in the light of characteristic values of the activation energy.

2.6 The Oxidation of Iron in Carbon Dioxide.

2.6.1 Scale Growth.

When iron is oxidized at elevated temperatures and a relatively smooth compact oxide layer has formed the overall process of oxidation involves both phase boundary reactions and the diffusion of ions and electrons in the oxide layer. Under special conditions the rate may be controlled by the phase boundary reaction and accordingly would be independent of the instantaneous thickness of the oxide layer. Such a case is observed during the oxidation of iron in carbon dioxide before the onset of the diffusion controlled process. Thus Fishbeck et al[43], Schmahl et al[44], and Smeltzer[45], have all observed the occurrence of linear scaling kinetics before the onset of parabolic oxidation. A model that would account for linear, followed by parabolic oxidation has been developed by Evans[46] and Fishbeck et al[43]. If the rate-determining reaction is a boundary effect at the beginning, and becomes diffusion controlled in the latter stages, the reaction may be considered as a flux of material J, which has to overcome a series of resistances. Namely, the diffusion resistance R_d (the diffusion coefficient being taken to be independent of concentration), and the interface resistances R_1 and R_2 at the metal/oxide and oxide/gas boundaries. The driving

force is the difference in concentration, C, between the two interfaces, so that

$$J = \text{Const.} \frac{\Delta C}{R_d + R_1 + R_2} .$$

If the flux of material is approximately constant then

$$J = \frac{d\varepsilon}{dt},$$

$$R_d = a\varepsilon,$$

$$R_1 + R_2 = b, \text{ and}$$

$$\text{Const. } \Delta C = k,$$

where a, b and k are constants and ε is the thickness of the oxide layer. Hence

$$\frac{d\varepsilon}{dt} = k/(a\varepsilon + b),$$

and on integration

$$a\varepsilon^2 + 2b\varepsilon = 2kt,$$

or by combining constants

$$\varepsilon^2 + k_a'\varepsilon = k_b't,$$

the integration constant being zero if $\varepsilon = 0$ at $t = 0$. This corresponds to a generalized parabolic law which involves the possibility that two different processes can be rate-determining during the progress of the oxidation. The interface reaction governed by the term $k_a'\varepsilon$ would be rate-determining in the early stages of oxidation but when the scale becomes thicker this term will become negligible, and the square term will govern the total reaction rate.

The question then arises as to which interface reaction is determining the overall reaction rate. Because the Arrhenius temperature coefficient of their reaction rate constants changed at the $\alpha - \gamma$ change point in iron, Fishbeck et al[43] concluded that the passage of iron into the oxide controlled the reaction. This viewpoint was accepted by Benard and Talbot[47] to explain the occurrence of linear rates in oxygen before the onset of the diffusion controlled reaction. However, Hauffe and Pfeiffer[48] questioned the premise of the rate controlling reaction being at the iron/oxide interface and found experimentally that the linear rate of reaction was proportional to $(p_{CO_2}/p_{CO})^{2/3}$. From this finding these workers have suggested that the overall rate is controlled by the chemisorption of oxygen produced at the oxide/gas interface by the decomposition of carbon dioxide which involves the creation of an electron defect according to

$$CO_2 = CO + O^-(\text{chemisorbed}) + \oplus,$$

followed by the formation of a new lattice site according to

$$O^-(\text{chemisorbed}) = FeO + Fe_D^{++} + \oplus.$$

In addition to using carbon dioxide Pfeiffer and Laubmeyer[49] oxidized iron at low oxygen pressures which were fixed by means of the $Cu_2O - CuO$ equilibrium, and obtained the following relation for the linear rate constant, k_L:-

$$k_L = \text{const.}\ p_{O_2}^{0.7}\ .$$

They considered this to be evidence that the overall rate was being determined by the chemisorption of oxygen. Petit, Yinger and Wagner[50] also questioned the premise that the rate-controlling step was the reaction at the iron/oxide interface and proposed an alternative explanation based upon the dissociative adsorption of carbon dioxide to yield carbon monoxide and adsorbed oxygen, thus

$$CO_2 = CO + O(\text{adsorbed}).$$

The number of equivalents of oxide formed per unit time and unit area, n, is given by

$$n = k'P\,(\,1 + K\,)(\,N_{CO_2} - N^*_{CO_2}\,).$$

Where k' = the rate constant for the reaction,

P = the value of the total pressure,

K = the value of the ratio of the partial pressures of carbon dioxide and carbon monoxide that are in equilibrium with iron and wustite,

N_{CO_2} = the mole fraction of carbon dioxide in the gas mixture, and

$N^*_{CO_2}$ = the mole fraction of carbon dioxide in the gas mixture that is in equilibrium with iron and wustite.

This mechanism differs from the one proposed by

Hauffe and Pfeiffer in that the rate of reaction is determined by the total pressure of CO_2 and CO as well as by the ratio p_{CO_2}/p_{CO}. This conclusion has been confirmed experimentally by Petit, Yinger and Wagner who have shown that the linear oxidation rates at 925 - 1075°C were a linear function of the mole fraction of CO_2 and the sum of the partial pressures of CO_2 and CO.

Arkharov and his associates[51] have made an X-ray study of the scales produced by the oxidation of iron in carbon dioxide at 1000°C for varying lengths of time. Because FeO was the only scale product produced during the early stages of the reaction they have concluded that the initial rate of the reaction was limited by the rate of supply of oxygen to the oxide/gas interface.

Except for a few scattered results obtained below 910°C the bulk of the work that has been discussed so far has been performed upon γ iron. Realizing the absence of data for α iron Smeltzer[45] has determined the kinetics of scale formation on iron in carbon dioxide over the temperature range from 600 - 1100°C. The oxidation rates obeyed linear and parabolic time laws for short and long periods of exposure. An Arrhenius plot of the linear rate constants showed a break at the $\alpha - \gamma$ change point of iron which divided the plot into two portions having slopes corresponding to activation energies of 50.5 and 28.8 kcals/mole for the portions of the plot above and below

910°C respectively. On the basis of these activation energies Smeltzer concluded that the rate of linear scaling was determined by the rate of incorporation of chemisorbed oxygen into the wustite lattice at temperatures lower than 910°C, and by the dissociation of carbon dioxide and incorporation of oxygen into wustite at higher temperatures. An Arrhenius plot of the parabolic rate constants did not exhibit any breaks but was curvilinear over the range of temperature studied. Since the Arrhenius coefficient for the diffusion of vacancies in wustite is linear[52] the curvature of the Arrhenius plot of the parabolic rate constants must be attributed to the variation in wustite composition with temperature.

From the previous discussion it can be seen that the most recent workers[45,50] to have studied the oxidation of iron in carbon dioxide are in general agreement that the linear rates of scaling on γ iron are largely determined by the dissociative adsorption of carbon dioxide onto the wustite surface. Such a mechanism requires a linear dependence of the rate of reaction on $(p_{CO_2} - p^*_{CO_2})$, whereas Hauffe and Pfeiffer have observed a dependence on $(p_{CO_2}/p_{CO})^{2/3}$. Smeltzer[45] has examined Hauffe and Pfeiffer's experimental results and has shown that a good fit is obtained when a straight line plot is made of the linear rate constants versus $(p_{CO_2} - p^*_{CO_2})$ thus the

results of these workers are in agreement with the above mechanism.

Our understanding of the rate-determining process resulting in the linear rates of scaling on α iron in carbon dioxide is not as clear as our understanding of the process on γ iron. Smeltzer[45] has proposed that the linear rates of scaling on α iron are determined by the incorporation of chemisorbed oxygen into the wustite lattice, while on γ iron they are largely determined by the dissociation of carbon dioxide. If such is the case it is difficult to see why the Arrhenius plot of the rate constants exhibits an abrupt change in slope at 910°C as has been reported by Smeltzer and Fishbeck et al. Smeltzer offers a possible explanation for the change occuring at 910°C by stating that the oxidation kinetics at the oxide/gas interface are affected by the different orientation relationships between wustite on α and γ iron. It is considered unlikely that such an explanation would account for the magnitude of the observed change in activation energy from a value of 28.8 kcals/mole to a value of 50.5 kcals/mole. Also Smeltzer bases his conclusions for the incorporation mechanism on the value of the activation energy of 28.8 kcals/mole being equivalent to the value of 30 kcals/mole for vacancy diffusion in wustite. He reasons that the incorporation of oxygen into the wustite lattice during

oxidation is comparable to the formation of a vacancy in the vicinity of an adsorbed oxygen ion and as such the activation energy for this process is comparable to that for the self diffusion of iron in wustite. It should be noted that by similar reasoning it is possible to derive a value of the activation energy of 30 kcals/mole as being characteristic of the reaction occurring at the iron/oxide interface. Thus our understanding of the linear rates of scaling of α iron in carbon dioxide is not clear and additional rate data, obtained under different conditions to those used by Smeltzer, would be helpful in testing any mechanism that may be proposed to account for this reaction.

2.6.2 Film Growth.

Smeltzer[53] has also studied the kinetics of the very first stages of the reaction between iron and carbon dioxide. Using a vacuum microbalance technique he has studied the oxidation of iron in 50% by volume CO_2 - CO mixtures over the temperature range from 590 to 1030°C. In this atmosphere and at temperatures below 835°C, the weight-gain versus time curves were linear throughout the duration of the experimental runs. But at 865 and 895°C, the oxidation rates of the ferritic specimens were only constant until an oxide thickness of 3500 Å was attained. Austenitic specimens oxidized at 920 and 950°C showed no

deviation from linear behaviour even though the oxide thickness was approximately 17000Å. At higher temperatures the deviations from linear growth rate again occurred early in the oxidation process. In all cases the deviations linearity were towards increasing oxidation rates with increasing oxide thickness. That is the weight-gain curves are concave upwards to the time axis. Theoretical expressions having this shape have been been discussed previously in section 2.4.3, and it is likely that Smeltzer has observed the early stages of a process involving the nucleation and growth of an oxide phase on the metal surface.

In assessing the reaction mechanism Smeltzer has shown that the linear rate constants, for film growth at 800°C, are directly proportional to the partial pressure of carbon dioxide greater than the values for the equilibration of wustite with iron. Smeltzer's Arrhenius plot of the linear rate constants for film growth is shown in Fig. 2. The plot indicates a discontinuous change in slope at the $\alpha - \gamma$ transition temperature and a continuously decreasing slope in the range of temperature below 760°C (the Curie point of iron). The activation energies of 60.6 and 33.5 kcals/mole for film growth on paramagnetic α iron and γ iron respectively, were attributed to the dissociation of carbon dioxide and to the incorporation of chemisorbed oxygen into the wustite lattice. The curvature of the plot

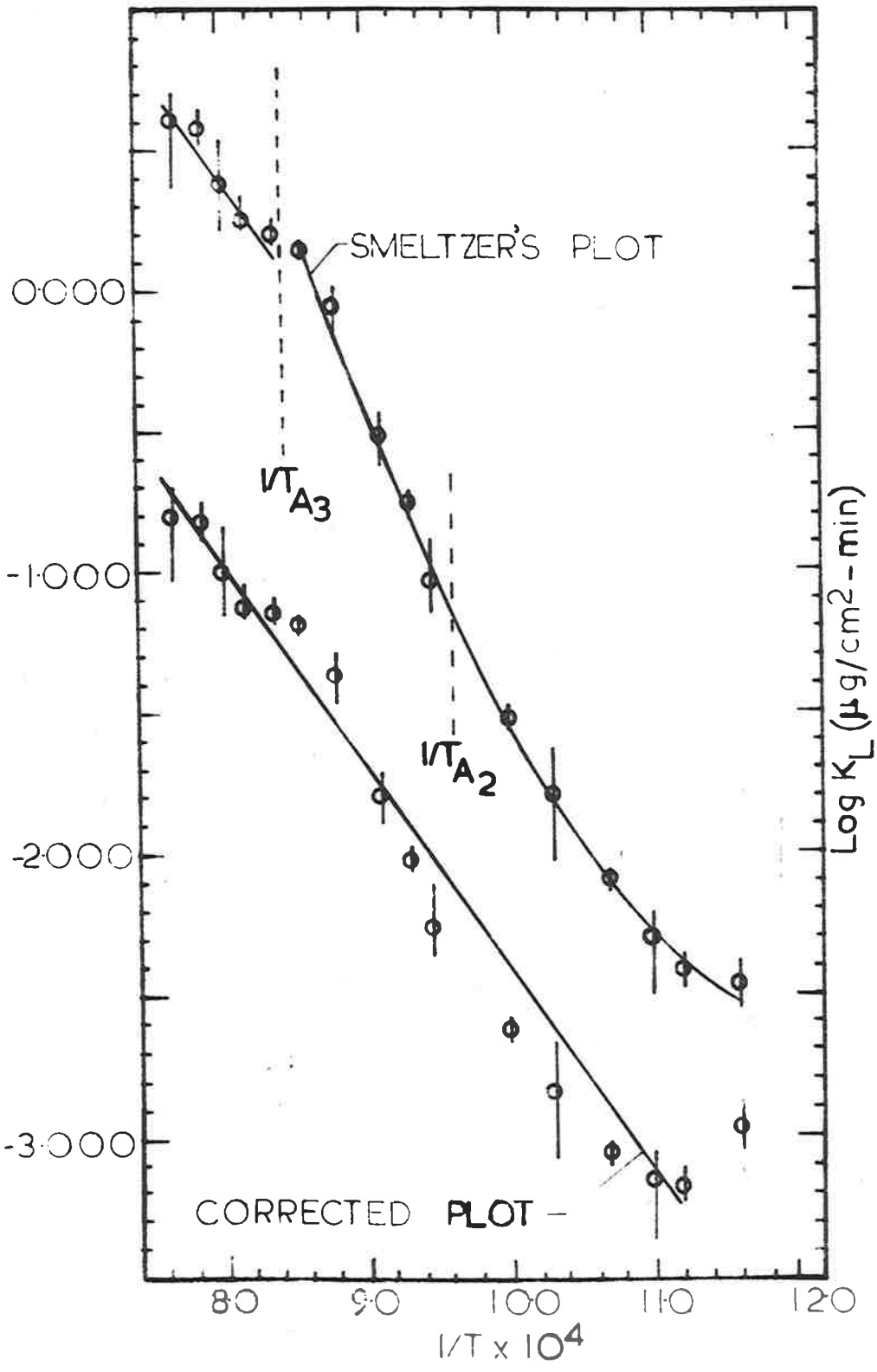

Fig.2 Arrhenius plot of the linear rate constants for film growth.

below 760°C is explained as being due to the variation of the wustite lattice parameter with temperature.

Having determined that the linear rate constants for film growth are directly proportional to ($p_{CO_2} - p^*_{CO_2}$), Smeltzer then neglects the influence of this pressure term on his Arrhenius plot. He states that:-

> 'The expression at 1 atmosphere total pressure for the equilibrium partial pressure of carbon dioxide is,
>
> $$p^*_{CO_2} = (\exp \Delta G^\circ/RT)/(1 + \exp \Delta G^\circ/RT) .$$
>
> Where ΔG° is the standard free energy change for the formation of wustite from iron and carbon dioxide. The temperature variation of this term is relatively small. Consequently, an Arrhenius temperature coefficient of the linear rate constants at constant partial pressures of carbon dioxide may be used to evaluate activation energies for the dissociation of carbon dioxide and the incorporation of chemisorbed oxygen into the wustite lattice. '

This assumption is incorrect; table 1, which has been produced from the equilibrium data of Darken and Gurry[54], shows that in a 50% by volume CO_2 - CO mixture the value of the term ($p_{CO_2} - p^*_{CO_2}$) varies by a factor of 8 over the temperature range under discussion.

If the effect of the variation of ($p_{CO_2} - p^*_{CO_2}$)

Table 1.

The variation of $(p_{CO_2} - p^*_{CO_2})$ with temperature.

T°C	$p^*_{CO_2}$	$(p_{CO_2} - p^*_{CO_2})$
590	52.8%	2.8%
620	55.1%	5.1%
640	56.5%	6.5%
670	56.4%	8.4%
695	60.0%	10.0%
720	61.3%	11.3%
785	64.6%	14.6%
800	65.3%	15.3%
835	66.6%	16.6%
865	67.7%	17.7%
895	68.6%	18.6%
920	69.5%	19.5%
950	70.3%	20.3%
975	71.0%	21.0%
1000	71.7%	21.7%
1030	72.4%	22.4%

with temperature is taken into account then Smeltzer's Arrhenius plot assumes the form shown in Fig. 2. A straight line has been drawn through the corrected points parallel to the upper straight line portion of smeltzer's plot for which he has calculated an activation energy of 33.5 kcals/mole. It can be seen that if the large experimental scatter is taken into account it is now possible, apart from the results at very low temperatures, to fit most of the points by a single straight line, the slope of which would correspond to an activatism energy of approximately 30 kcals/mole. According to Smeltzer's arguement the rate-determining process over the whole temperature range would then be the incorporation of chemisorbed oxygen into the wustite lattice. The results obtained in the temperature range 590 - 620°C cannot be explained by the above mechanism. Although Darken and Gurry's experimental results show that, in this temperature range, a 50% by volume CO_2 - CO mixture is weakly oxidizing , reference to the calculated equilibrium diagram in Fig. 1 shows that under these conditions the gas is carburizing. Hence a possible explanation of the results at the lower temperatures is that the iron was being carburized rather than oxidized.

2.6.3 Conclusions Regarding the Oxidation of Iron in Carbon Dioxide.

A survey of the literature pertaining to the

oxidation of iron in carbon dioxide has revealed that apart from the work of Smeltzer[53], none of the workers in this field have studied the first stages of the reaction between iron and carbon dioxide. They have only been interested in the problem after the reaction has been in progress for some time and a compact uniform oxide layer of appreciable thickness has been interposed between the metal and the gas phase.

Smeltzer's results for the early stages of the reaction between iron and carbon dioxide have been recalculated to show that the Arrhenius plot of the linear rate constants for film growth can, apart from the results at the lowest temperatures, be fitted by a single straight line the slope of which corresponds to an activation energy of the order of 30 kcals/mole. Thus, according to Smeltzer's arguement the rate controlling process over the whole of the temperature range would be the incorporation of chemisorbed oxygen into the wustite lattice. The results at the lowest temperatures have been explained on the basis that at these temperatures the 50% by volume CO_2 - CO mixtures used by Smeltzer were carburizing rather than oxidizing. Also after an initial period some of Smeltzer's weight-gain versus time curves become concave upwards to the time axis. Gravimetric results having this form would be consistent with a process invol-

ving the nucleation and growth of an oxide phase on the metal surface and this facet of the reaction requires further study.

Several groups of workers[43,44,45,48,50] have investigated the scaling of iron in carbon dioxide. However, the bulk of this work has been performed at temperatures above 910°C, that is on γ iron, and as far as can be determined no one has studied the oxidation of iron in carbon dioxide at temperatures below the wustite eutectoid temperature at 570°C. There is general agreement that above 570°C, the rate of scaling of iron is initially controlled by a phase boundary reaction which leads to linear scaling kinetics. As the oxide thickens this relation transforms to the familiar parabolic equation, indicating that the transport of material (mainly iron defects) through the oxide layer has become the rate-controlling process. The most recent workers[45,50] are in general agreement that the linear rates of scaling on γ iron are largely determined by the dissociative adsorption of carbon dioxide at the oxide/gas interface. However, the position regarding the linear rates of scaling of α iron in carbon dioxide is not so clear. Smeltzer[45] considers that the linear scaling rates on α iron are determined by the rate of incorporation of chemisorbed oxygen into the wustite lattice. In the writer's opinion no satisfactory

explanation has been given for the break which has been observed to occur in the Arrhenius plot of the linear rate constants at 910°C, and additional information on the linear rates of scaling of α iron would be helpful in testing any mechanism which may be developed to account for this reaction.

Thus the literature survey has revealed that there is a need for the following work to be done.

1. Study the initial stages of the reaction between iron and carbon dioxide.
2. Study the rates of scaling of iron in carbon dioxide at te mperatures below the wustite eutectoid point.
3. Obtain additional data on the linear rates of scaling of iron in carbon dioxide under different experimental conditions to those used by Smeltzer.

2.7 A Survey of Some Experimental Methods.

2.7.1 Some Methods of Measurement.

2.7.1.1 Gravimetric Method.

Because of its directness and general convenience the gravimetric method is the most commonly used means of obtaining information about oxidation rates. In its simplest form it requires no more than an accurate

balance and a furnace, the metal specimen being attached to one side of the balance and hung in the hot zone of the furnace by an inert suspension wire. When the oxidation is performed in atmospheres other than air, difficulty is experienced in maintaining the composition of the gas constant, as it is impossible to completely seal the furnace and prevent the counterdiffusion of air. At its best this method can only be used to perform rough measurements of the rates of scaling. Accurate weight-gain measurements, particularly if the measurements are in the film range, requires that the oxidation chamber can be completely isolated from the atmosphere. A convenient method is to suspend the sample from a calibrated silica spring, the extension of which gives the increase in weight of the sample during oxidation. The spring is enclosed in a pyrex tube and the extension of the spring is measured by a cathetometer, the eyepiece of which is sighted onto a reference mark on the bottom of the spring. If the refractory tube, in which the oxidation is carried out, is sealed at the bottom and attached to the pyrex tube containing the spring by a conventional vacuum-tight seal, then the oxidation can be conducted in any atmosphere at pressures up to atmospheric. More sensitive than this arrangement is the vacuum microbalance of the type designed and frequently used by Gulbransen[55,69]. The specimen is suspended from the beam of a

very sensitive all quartz microbalance operating in an all glass system. Weight-changes of the specimen are followed by noting the deflection of a pointer on the beam, relative to a fixed pointer, with a travelling microscope. All operations on the specimen, such as degassing and reduction of the initial oxide film, can be carried out in situ. Removal of the initial oxide film is important if measurements of the oxidation rate are to be made in the film range rather than in the scale range. The provision of means of reducing the initial film and the sensitivity of the apparatus makes equipment such as Gulbransen's particularly suitable for measurements of the very early stages of oxidation.

2.7.1.2 Electrometric Method.

The electrometric method of analysis has been developed to determine the thickness of oxide films on metals and hence can be used to determine the rate of oxidation with time in the initial stages of the reaction. The method consists of determining the quantity of electricity needed to reduce the oxidation product either to the metallic state or to a lower state of oxidation. The oxide covered specimen is made the cathode in a suitable electrolyte and the time taken to reduce the oxidation product by a small known current is measured. In the case of a single

oxidation product the cathode potential remains constant whilst there is some reduction to be effected, and when this is complete the potential changes sharply to the potential of hydrogen evolution. The end point of the reduction is taken as the point of inflection of the potential - time curve. When there is more than one oxidation product the potential falls on completion of the reduction of the first to that of the second and so on. It follows that it is not possible to estimate oxides which require for their reduction higher negative potentials than that at which hydrogen is evolved at the current density used.

Cathodic reduction of films of ferric oxide has been used in the past by several groups of workers to obtain a quantitative determination of the magnitude of the films. Davies, Evans and Agar[56] stripped films of α ferric oxide, produced by the oxidation of iron in air at temperatures below 250°C, in 0.1M NH_4Cl solution. They concluded that the reduction took place according to the following equation.

$$Fe_2O_3 + 6H^+ + 2e = 2Fe^{++} + 3H_2O.$$

Cohen et al[57,58] have reported the results of a series of investigations into the cathodic reduction of α Fe_2O_3 which were supported by electron diffraction and microbalance measurements. They concluded that the reduction

took place by the above equation, and that the most suitable electrolyte was a sodium borate - HCl solution buffered at a pH of 7.6. These workers also used NH_4Cl but concluded that it was unsuitable as some dissolution of the film took place. Hancock and Mayne[59] studied the cathodic reduction of the air-formed film on iron and mild steel in 0.2N KCl solution. As Evans and Davies[60] have shown that the air-formed film consists largely of $\gamma\ Fe_2O_3$, Hancock and Mayne assumed the film to consist entirely of this substance, and by a comparison of the quantity of electricity needed to reduce the film and the loss in weight sustained by the specimen during cathodic reduction, concluded that $\gamma\ Fe_2O_3$ was reduced to metallic iron.

2.7.2 Some Methods of Examining the Oxide.

The unambiguous interpretation of kinetic data is facilitated if additional information regarding the progress of the reaction is available from other techniques. The x-ray method can be used to give information relating to identification of oxide phases, crystal size and orientation, and the measurement of lattice parameters. The method is specially suited to the examination of the thicker scales. If these are removed from the metal the ground powder can be used as a specimen for identification; where layers of different oxides are formed it is

frequently possible to separate them and examine each. Glancing angle and back reflection techniques can be used whilst the oxide is still attached to the metal. Stripped films can also be examined by the powder method. For identification purposes it is customary to obtain the complete powder pattern of the material which may then be compared directly with the patterns from known substances without the necessity for determining the crystal structure or indexing the reflections. Otherwise the spacings of the atomic planes are determined from the position of the diffraction lines by Bragg's law and reference made to the A.S.T.M. Index of Crystallographic Data in which materials are listed under the spacings of their strongest diffraction lines.

Microscopic examination of the oxide which has formed on a metal is a useful method of providing information on some of the characteristics of the oxide and the mode of growth. For example microscopic examination of the metal surface during the early stages of the reaction reveals whether the surface of the metal is covered by a uniform film or whether the oxide is spreading from localized growth sites. If the former is the case microscopic examination reveals the extent to which oxidation has taken place on different crystal faces and observation of the interference colours allows a rough estimate to be made of the film thickness of the oxide. In the latter case,

depending upon whether the nuclei are few in number and of sufficient size, it is possible to discern the shape of the nuclei and obtain some idea of their distribution over the surface. The hot-stage microscope enables the metal surface to be examined, whilst it is at temperature and the reaction is proceeding, and should prove a valuable tool in elucidating the reaction mechanism of the early stages of oxidation. Metal specimens carrying oxide scales may be mounted and polished sections through the oxide layer examined under the microscope. The detection multi-layer scale formation in oxides is an obvious example of the use of the metallographic technique. Location, distribution, grain size, shape, and other metallographic characteristics of oxides formed on metals are also features that are observed microscopically. In the past this method has also been used with considerable success to study the movement of inert markers. Although identification of oxides microscopically is possible to a considerable extent it appears that much remains to be done in this field.

2.7.3 The Effect of Specimen Preparation.

Since metallic oxidation is a surface phenomenon the preparation of the surface prior to oxidation experiments is very important. Thus Vernon, Akeroyd and Stroud[61] found that the rate of oxidation of zinc below 225°C was

different for abraded, etched or electrpolished surfaces. Similarly Caplan and Cohen[62] found that different surface preparations had a marked effect on the oxidation of commercial stainless steels. For fundamental work the ideal is to commence the oxidation with a film-free surface. In the past numerous workers, while studying the oxidation of iron, have obtained this condition by reducing the initial oxide film with hydrogen prior to the commencement of the oxidation. It would be expected that some solution of hydrogen in the metal would accompany the reduction of the oxide and it is not known to what extent, if any, that this dissolved hydrogen affects the subsequent oxidation behaviour of the metal.

For alloys however there is no simple treatment that will give the requisite surface. A proper surface for oxidation studies should have a low surface roughness factor and be representative of the bulk composition, that is not enriched in impurities or in one of the alloying elements. Recognizing that with alloy systems some initial oxide film is unavoidable it would appear that the proper preparation is that which gives the least interference with the subsequent oxidation process. Abrasion, the method most commonly used results in a cold-worked distorted layer containing embedded oxide and abrasive which is certainly unrepresentative of the bulk properties of the alloy.

Etching of this surface to remove the worked layer leaves a rough surface which may have been enriched in the more noble metal by preferential dissolution or redeposition. possible alternative methods such as cathodic reduction, ion bombardment and thermal treatment in vacuum, hydrogen, or an inert gas are liable, for alloys at least, to the same faults and to preferential oxidation or volatilization of the alloying elements.

Electropolishing eliminates many of the deficiencies of the abraded surface, but the oxide film left, particularly on polycrystalline specimens is non uniform over the specimen, probably because of variations in both current density and the anolyte layer during electropolishing.

2.7.3.1 Conclusions Regarding the Effect of Specimen Preparation.

The residual oxide films left on a metal surface by some of the means of specimen preparation can have a marked effect on the subsequent oxidation behaviour of a metal specimen. For alloys at least it is possible that the marked differences which have been observed can be attributed to the different residual oxide films nucleating different oxide phases on the metal surface some of which are evidently more protective than others. Our almost complete lack of understanding of why these differences occur is largely due

to the lack of data on the composition, structure, and properties of these residual films.

Denholm[63,64] has used a potentiostatic technique to investigate the passive behaviour of iron and iron-chromium alloys in various electrolytes; electrical measurements made during the course of these tests yielded valuable information regarding the composition and the magnitude of the passive films. It is likely that a similar technique could be used with advantage to study the residual oxide films produced by some of the methods of specimen preparation. The equipment, as developed by Denholm, consisted of a potentiostat incorporating an AC bridge, which, during the course of a potentiostatic traverse, enabled measurements of the apparent electrical capacity of the oxide covered electrode to be made simultaneously with conventional measurements of current and potential. For values of the potential at which ionic changes were taking place in the oxide film very large changes were observed in the value of the capacity, while at other potentials the value of the capacity assumed a value corresponding to the double layer capacity at the electrode-solution interface.

With further development the capacity measurements could prove useful in characterizing oxide films in the following ways. Firstly, in the region where the capacity is independent of the potential, and is dependent only on

the value of the double layer capacity these measurements could be used to determine the real area of the electrode-solution interface and hence used to furnish information regarding the surface roughness of metal surfaces. Secondly, in the region of potential where the capacity measurements appear to be related to ionic changes taking place in the oxide, it is possible that the magnitude of the capacity measurements could be used to determine the quantity of oxide present. Before either of these techniques could be applied to the investigation of unknown oxide films, further developmental work is necessary to try and elucidate the true significance of the capacity measurements. With this aim in mind it was decided to build up oxide films containing a known amount of oxide by the anodic oxidation of iron electrodes and to strip these films by cathodic reduction. During the course of the potentiostatic traverses measurements would be made of the capacity and the quantity of electricity consumed at the electrode. By comparing the capacity readings obtained from oxide films containing different amounts of oxide it was hoped that definite conclusions could be drawn as to the true significance of the capacity measurements.

2.8 Proposals for Experimental Work.

It was noted in section 2.6.3 that the initial stages of the reaction between iron and carbon dioxide required further study. To follow the kinetics of the reaction it was decided to make weight-gain versus time measurements with a vacuum microbalance. As these instruments are not stable when operated at atmospheric pressure it would be necessary to work in the range of pressure where stable operation is attained.

It was subsequently found (see section 3.1.8) that the maximum pressure of carbon dioxide under which the balance would give stable operation was 200 mm Hg total pressure. This pressure limitation proved to be an advantage, for by operating at a reduced pressure the reaction rate was slowed down, and it was possible to study the early stages of the reaction in greater detail than would have been possible if a higher pressure had been used. Since the initial stages of the reaction were to be studied at a reduced pressure it was decided to measure the rates of scaling under the same conditions. It would then be possible to present a suite of results both for the initial and the scaling stages of the reaction all obtained at the same pressure.

Following these conclusions and bearing in mind

the findings of section 2.6.3 it was decided to investigate the oxidation of iron in carbon dioxide at a total pressure of 200 mm Hg, over the temperature range 400 - 800°C. To supplement the kinetic measurements it was decided to follow the progress of the reaction by microscopic examination of the metal surface during the initial stages of the reaction, and to make use of metallographic sections through the scale layer whenever the thickness permitted the use of this technique.

The phases revealed by this study would then be identified by x-ray diffraction analysis of the oxide scales. Also, it was expected that below 570°C duplex scales of magnetite and haematite would be encountered and it was intended to use the electrometric method to determine the amount of ferric oxide in the scales. The amount of magnetite could be estimated from the difference between the electrometric and gravimetric results, thus making it possible to study the rates of growth of the individual oxide oxide layers composing the scales.

In addition to studying the oxidation of iron in carbon dioxide it was also decided to investigate the significance of the capacity measurements made during the course of potentiostatic tests performed upon iron electrodes in aqueous electrolytes, in the hope that when a better

understanding of these measurements had been obtained they could be used to characterize the residual oxide films left behind on a metal surface by some of the methods of specimen preparation.

To accomplish the experimental program it was necessary to build the following equipment:-

a) Vacuum microbalance.

b) Electrochemical apparatus in which to perform the electrometric and potentiostatic tests.

c) Gas purification equipment.

The design, construction and operation of this equipment is described in the following sections.

3. EQUIPMENT AND MATERIALS.

3.1 Vacuum Microbalance.

It was decided that the most convenient way of studying the kinetics of the early stages of the reaction between iron and carbon dioxide was by means of a sensitive weight-gain device. Realizing that monomolecular coverage of oxygen on a specimen having an area of 15 cm^2 corresponds to an uptake of 0.5×10^{-6} g, it was further decided that such a device should have a sensitivity of the order of 1×10^{-6} g, and that it should be capable of carrying specimens weighing in the vicinity of 0.5 to 1.0g. A number of balances capable of detecting mass changes of this order have been reported in the literature[65-70]. Generally speaking they fall into three categories :-

1) Spiral types (helices).
2) Torsional suspensions.
3) Adaptations of gas density balances (pivotal types).

Instruments of the first two categories can be made very sensitive, but installation, operation, and maintenance often require a high degree of experimental skill and patience. In particular quartz helices are susceptible to breakage. Torsion balances of conventional

design are likewise sensitive to shocks and require frequent recalibration. Quartz helices are further limited in that their sensitivity depends upon the load. A study of the various possibilities led to the choice of a microbalance devised by Gulbransen[69]; namely a deflection type with a torsion wire suspension. Such a balance probably has the broadest range of applicability of any of the above types of balances.

Very briefly the method of operation is to suspend a thin sheet of metal from a sensitive quartz beam. Weight changes of the specimen can be followed continuously as various operations are performed upon it. When applied to the oxidation of metals these operations include:-

1) Evacuation to pressures of 10^{-5} to 10^{-6} mm Hg.
2) Reduction of the oxide film with pure hydrogen.
3) Oxidation of the specimen under widely differing conditions of temperature and pressure.

The progress of the reaction is followed by noting the deflection of a pointer on the beam relative to a fixed point on the cradle supporting the beam. It is usual to use a cathetometer or a measuring microscope for this purpose.

The normal type of Gulbransen microbalance has two limitations. Firstly the sensitivity of a given beam assembly is limited by the ability of the measuring device to detect small movements of the beam. Secondly the total oxygen uptake of the balance is limited by the angular movement of the beam which is possible before the beam arrests are encountered. As part of this project it was decided to build a microbalance which would overcome these limitations. It was planned to improve the sensitivity of the balance by using a very sensitive compact optical lever assembly, and to overcome the limitation on the total oxygen uptake by operating the balance as a null point instrument.

3.1.1 The Beam.

The beam was made according to the dimensions given by Rhodin[71]. It was known that such a beam had a sensitivity of 0.01 mm = 1×10^{-6} g and, if the system of measurement under development failed to work, it would then be possible to resort to conventional measuring methods and still have the order of sensitivity required for this project. The beam was constructed of 2 mm transparent fused quartz rod, the overall length being approximately 6 inches. Sealed to the middle of the beam was a 0.001 inch tungsten wire. This wire acted as

the point of suspension in a similar fashion to the knife edge in a conventional laboratory balance. The length and diameter of this suspension wire were so chosen that the restoring moment due to the torque of the wire was only one tenth that of the beam. Tungsten wires spanned the yokes at the end of the beam and served as supports for the specimen and counterweight. A small mirror, attached to the centre of the top face of the beam, reflected light back to the optical lever. The mirror which was extremely small, measuring only 2.0 mm by 2.0 mm, was made by silvering a portion of a microscope coverslip. It was attached to the beam by a drop of shellac.

Before being attached to the beam the tungsten wires were annealed, under tension at 350°C, to relieve strains. The wires were then held in tension and cemented to the beam with molten silver chloride. Care was taken at all stages of the construction to make the beam as symmetrical as possible. Final balancing of the beam was achieved by grinding, and positioning smears of silver chloride. A quartz frame, constructed of 1/8 inch diameter satin-finished quartz rods, supports the beam and was designed to act as a spring. This tends to maintain the beam constant with respect to the frame at the point of support. Since the linear coefficient of expansion

of the tungsten wire was small it was expected that any change in length due to temperature changes would be compensated for by the spring action of the frame.

3.1.2 The Optical Lever.

The microbalance operates as a null point instrument with magnetic restoration to compensate for the oxygen uptake of the specimen. Deflection of the beam from the null point is detected with a very sensitive compact optical lever assembly. The general arrangement of the system is shown diagramatically in Fig.3. The optical lever follows a design developed by Jones and Richards[72, 73] and is shown schematically in Fig.4. The source of light S is a 4 watt, 3.2V miners cap lamp. These lamps are krypton filled and while giving sufficient light to operate the photocells they do not generate enough heat to require special cooling arrangements. An image of S is focussed by the condenser lens L_1 onto the mirror M, attached to the beam. The light from M diverges until it reaches L_2 -a condenser lens similar to L_1- which focuses an image of M, and therefore of S, onto the surface of the photocells. Interposed between L_1 and M and L_2 is a subsidiary system consisting of a lens L_3, near the mirror M, and two gratings G_1 and G_2. G_1 is illuminated by converging light from the condenser lens L_1 and is so situated

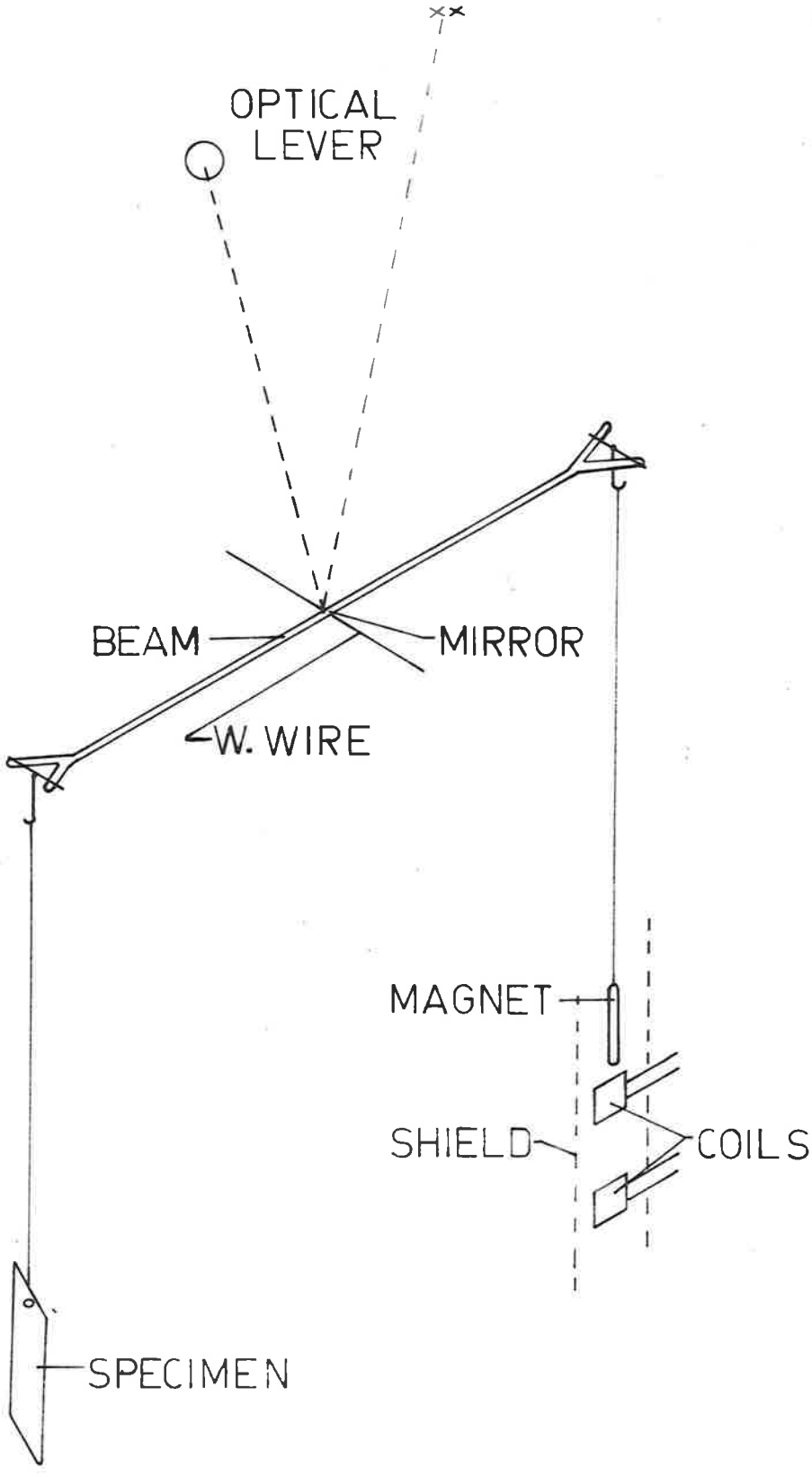

Fig.3 General arrangement of the microbalance.

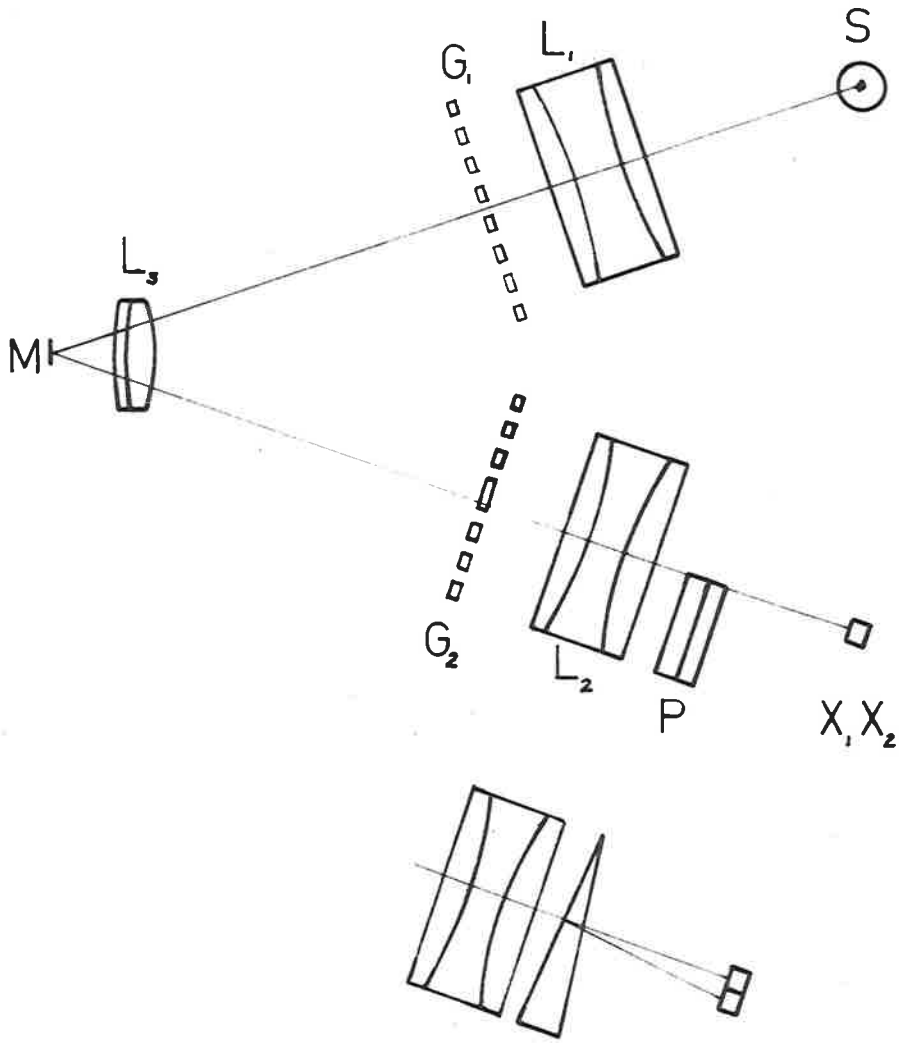

Fig.4 The optical lever.

that the rays diverging from any point on G_1 are made parallel by L_3; after reflection from M these rays return through L_3 to be focussed in the plane of G_2. Thus an illuminated image of G_1 appears in the plane of G_2; this is the standard auto-collimating position, and results in a distortion-free image at unit magnification. If G_1 and G_2 are replicas, G_2 will stop or pass the light from G_1 depending on their relative positions transverse to the light path. G_2 is split into two halves separated by the width of a bar in the gratings, so that when the right half of G_2 passes the light from G_1, the left half of G_2 stops the light from G_1. Viewed from L_2 the effect is that of a divided field, in which the halves go alternately black and white in antiphase as the mirror rotates. A narrow angled prism P, made of perspex, is located behind one half of L_2 with its vertex horizontal to divert the light from this half sufficiently downwards to fall as a focussed image of S on the lower photocell X_1. Light from the other half of G_2 and L_2 is undiverted and forms a focussed image of S on the upper photocell X_2. As M rotates both images retain their positions but their intensities change, due to the varying degrees of overlap between the image of G_1 and the two halves of G_2. The system is operated with about 50% overlap of each half, giving equally intense images

on X_1 and X_2. A slight rotation of M causes one image to brighten and the other to darken; the bridge circuit containing X_1 and X_2 then registers an out of balance current.

The gratings were made by placing strips of black tape on a piece of plate glass which was then photographed. A series of plates containing varying numbers of lines to the inch were then made from the negative. The grating spacing depends upon the application, finer gratings give greater sensitivity at the expense of maximum measureable rotation. The grating spacing found to be best suited to this application was 8 lines to the inch.

The matched photocells X_1 and X_2 (Mullard type no. ORP60) are cadmium selenide photo-conductive devices; they are of the type used for the automatic brightness control on television sets. It is estimated that the sensitivity of the balance could be improved by several powers of ten by using more sensitive photocells, and by equipping the balance with a finer set of gratings. However to realize this increased sensitivity it would be necessary to improve the mechanical and electrical stability of the balance.

To prevent variations in the light intensity due to mains voltage fluctuations, the lamp is fed from

a regulating transformer. When operated continuously at slightly below their rated voltage these lamps will run continuously for a very long time. For instance, the lamp used in this study was still in operation a year after the time it was first switched on. The photocells form two arms of a Wheatstone bridge circuit, the other arms of which are two 25K ohms wire wound resistors. Bridge unbalance is sensed with a 'Scalamp' galvanometer with an internal resistance of 1400 ohms. The bridge supply is regulated by a Zener diode operating from a stabalized power supply. All components of the bridge are housed under constant temperature conditions. The circuit diagram of the bridge circuit and the associated power supply is shown in Fig.5.

3.1.3 The Compensation System.

The specimen is counterbalanced by a small needle-shaped 'Alnico' magnet which is encapsulated in a glass sheath. The magnet hangs inside a copper tube of the vacuum system which is surrounded by two coils. One coil-the taring coil of 2500 ohms resistance- is from an old radio loudspeaker; the other-the balancing coil- has been wound to have a resistance of 33 ohms. Weight changes in the specimen are compensated by altering the current flowing through the balancing coil until

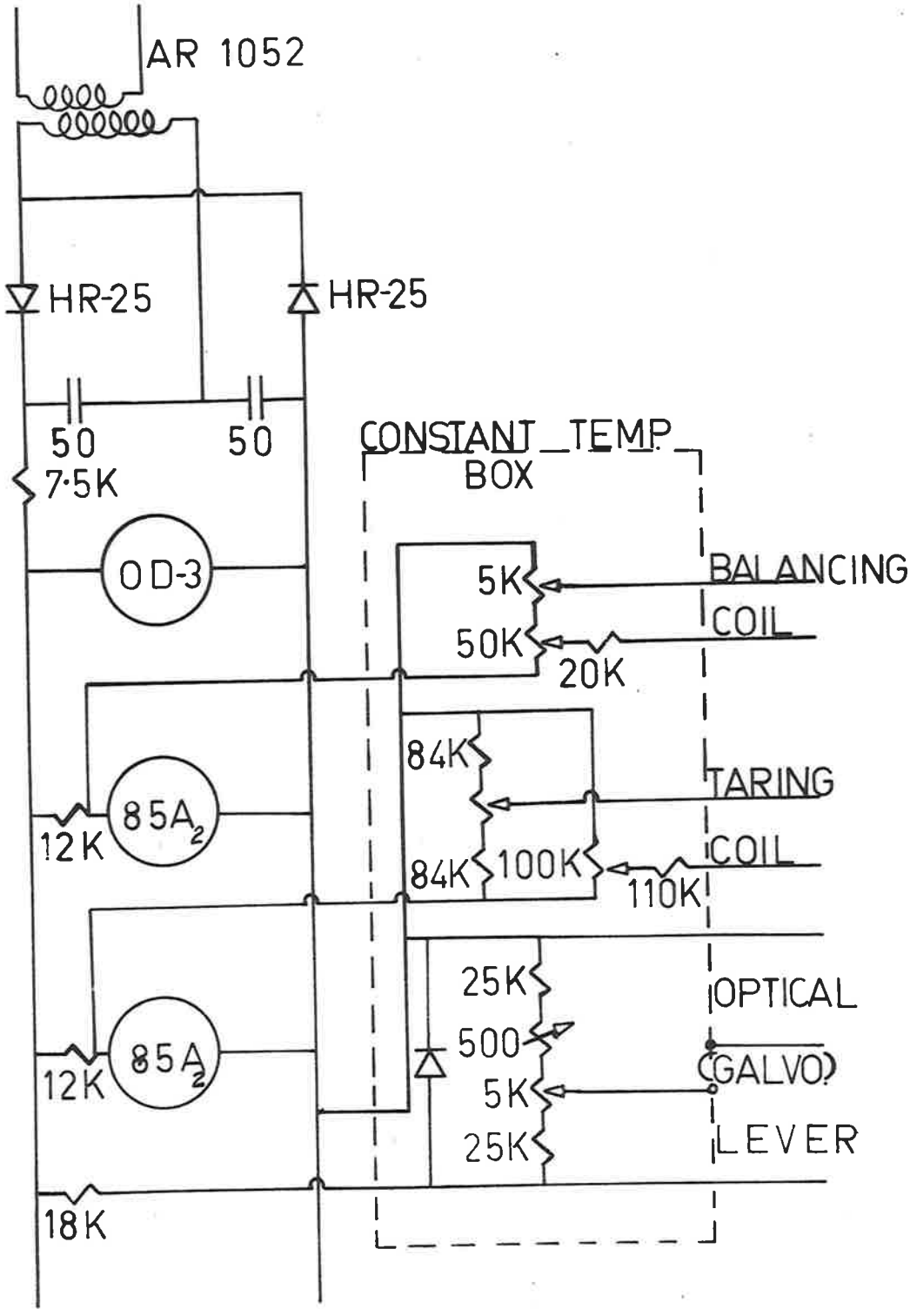

Fig.5 Circuit diagram for the microbalance measuring equipment.

the beam has been restored to its null position. This current is measured with a microammeter. At the commencement of a run the specimens are adjusted to within a few milligrams of the correct weight and the taring coil is used to adjust the position of the beam to the null point. A subsidiary optical lever imaging one end of the beam on the wall of the laboratory is used to detect when the main optical lever has passed through a complete phase change of the gratings.

It is essential that the current passing through the taring coil remains constant for the duration of a run otherwise drifting of the null point occurs. Considerable difficulty was experienced with this problem until it was overcome by using a highly stabalized power supply and by mounting all the temperature-sensitive components of the circuit in a constant temperature box. The circuit diagram for the power supply, balancing and taring coil circuits, and the bridge circuit of the optical lever are shown in Fig.5.

To provide electro magnetic damping, the magnet hangs in the centre of a large copper block, the length of which is several times that of the magnet. This behaves as a single short-circuited turn of very low resistance which is closely coupled to the magnet. Oscillations are quickly damped out by the forces opposing motion which are generated by this mass of copper.

The main structural framework of the microbalance is made of mild steel and initially, stray magnetic fields resulting from this source caused the magnet to deflect sideways and foul the copper block. To prevent this happening, the tube containing the magnet and the taring and balancing coil were surrounded by a Mu-metal shield which effectively screened out these stray magnetic effects.

3.1.4 Constant Temperature Box.

As mentioned in the previous section considerable difficulty was encountered in preventing the null point of the balance from drifting. It was established that the drift was largely due to the effect of ambient temperature changes affecting the value of some of the electrical components. These effects were minimized by air conditioning the room, and by mounting the temperature sensitive components inside a small aluminium box, where they were located in a stream of warm air, the temperature of which was regulated to within $\pm$ 0.1^{o}C by a mercury microswitch. When the temperature falls below the set-point the microswitch closes a sensitive relay which switches on a 15 watt heater lamp. The box is so baffled that the small fan

drawing the recirculating air over the light bulb, blows it over the microswitch and thence onto the electrical components the temperature of which it is desired to keep constant. By such arrangements it was possible to maintain the null point of the balance constant to within $\pm$ 1x10^{-6}g for periods exceeding a day.

3.1.5 The Vacuum Enclosure.

Following the procedure of Powers and Long[74] the balance is contained inside a vacuum-tight brass box, a photograph of which is shown in Fig.6. The silica cradle supporting the balance rests on a large steel plate; the balance case sits over the balance and a detachable vacuum seal is made between it and the steel plate by means of an 8 inch 'O' ring seal. This is a departure from the practice of earlier workers who sealed the balance inside a glass envelope. The present arrangement has the advantage of being very accessible and measures are easily affected to shield the balance from thermal and electrostatic effects, however it does suffer from the disadvantage that the case cannot be flamed to assist out-gassing. The box containing the optical lever rests on top of the balance case and is supported by two pillars. The objective lens of this system projects into the balance case and is housed in a

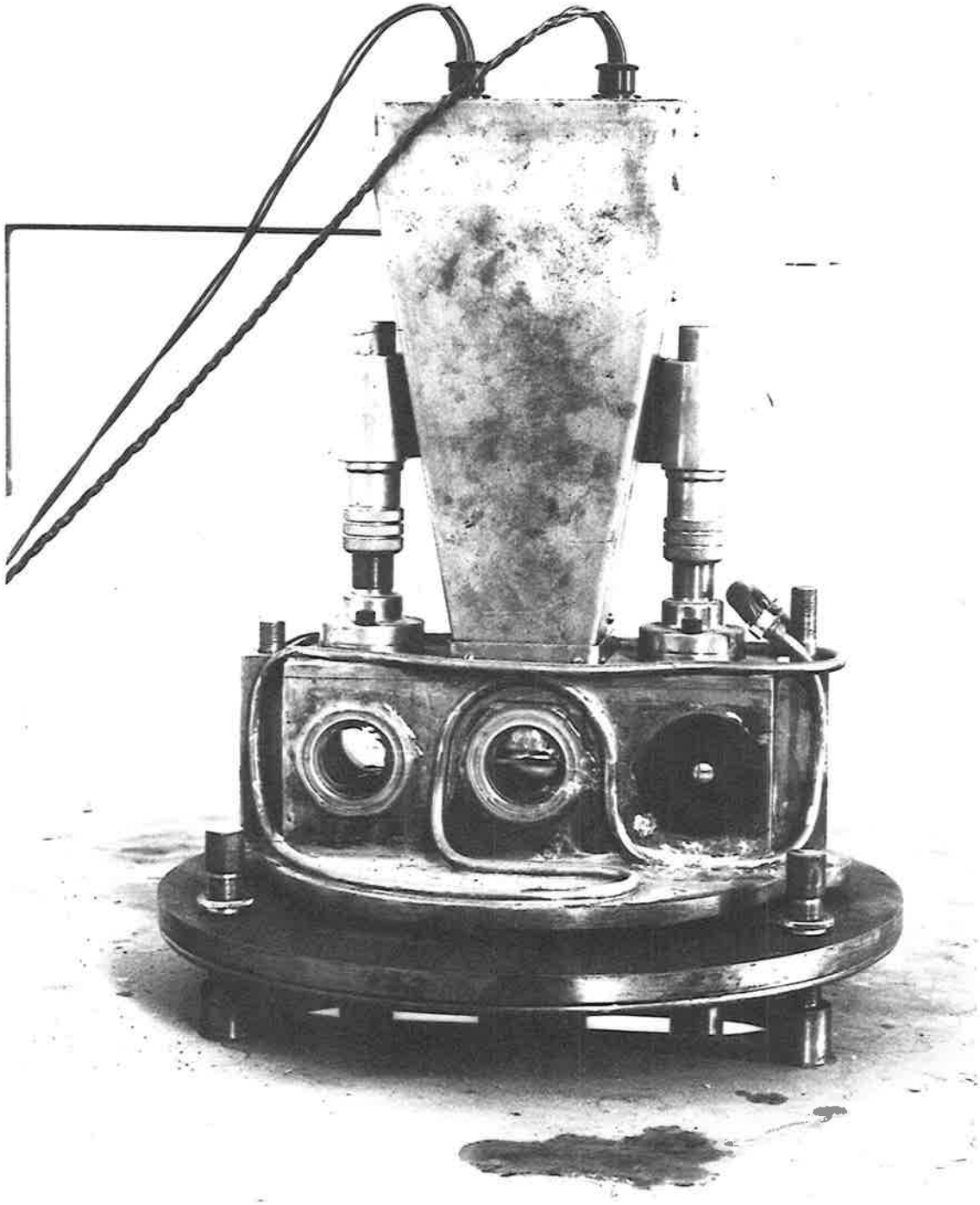

Fig.6 Balance case.

brass well. Light from the optical lever is transmitted to the mirror on the beam and vice versa through a piece of optically flat glass cemented to the bottom of the well with epoxy resin. Additional openings in the sides of the balance case are covered with glass discs, a pair of these portholes have been used to operate the subsidiary optical lever mentioned in section 3.1.3.

Changes in the ambient temperature could have a small effect on the performance of the balance. To minimize this effect copper tubing has been soldered to the balance case and to the plate supporting the balance. Water, maintained to within $\pm$ 1/3°C by a mercury-toluene regulator, is circulated through the tubing by a small pump. To test the efficiency of this procedure in thermostatting the balance a small S.T.C. type F23 thermistor was placed inside the balance case. Over a period of 24 hours it was noted that the resistance of the thermistor did not vary by more than one ohm. As these devices have, at room temperature, a sensitivity of approximately 40 ohms/°C, it was concluded that the variation of temperature inside the balance case was extremely small and that its effect on the balance would be negligible.

The specimens are suspended from one side of the balance on a 0.001 inch platinum wire and hang in a silica tube, the outside of which has been platinized to

shield the specimen from electrostatic effects. This tube is joined to the balance case by a copper tube in the middle of which is a stayed bellows system. By adjusting the stays it is possible to accurately locate the silica tube within the furnace.

The main vacuum line to the balance case enters through a 2 inch 'O' ring seal inthe plate supporting the balance. Vacuum, produced by a two-stage mercury diffusion pump backed by a Rudd Brown rotary oil pump,is measured with a Mc Leod gauge. A Bourdon vacuum gauge is used to measure the pressure of carbon dioxide in the system. To prevent mercury vapour from contaminating the specimen both the diffusion pump and the Mc Leod gauge are separated from the high vacuum side of the system by liquid air traps.

3.1.6 Non-Inductively-Wound Furnace.

Electrically heated resistance furnaces capable of operating in the temperature range 400-800°C have a large heat capacity and take a considerable time to attain temperature. To overcome this difficulty the furnace has been mounted so that it may be brought to temperature away from the specimen then quickly moved into position. The Nichrome resistance windings are carried on a silica former and have been wound in such a fashion that the

magnetic fields resulting from the passage of current through the windings have been eliminated. Thermal insulation of the winding is provided by a 4 inch asbestos drain pipe jacket filled with insulating material. Flanges made from Zeliarc-an asbestos-based insulating board- cover the ends of the jacket and hold the winding in place. The complete assembly locks together between two brass end plates secured by long steel bolts. The brass end plates also carry rollers which run on three vertical guide posts, two of which are made from 1 inch steel bar and one from 2 inch steel tubing. A counter-weight moves inside the steel tube and balances the w weight of the furnace. The combination of the counter-weight and rollers enables the furnace to be quickly positioned around the tube. A photograph of the furnace is shown in Fig.7.

Several non-inductive windings have been made. The first winding was of conventional bifilar construction, but this winding failed after a short service, and a new method of construction has since been developed. In the new procedure two layers of windings are laid on top of each other, the outter layer being wound in the opposite sense to the inner winding. Two windings of this type have since been made. The first of these was made by coating the inner winding with a layer of high quality

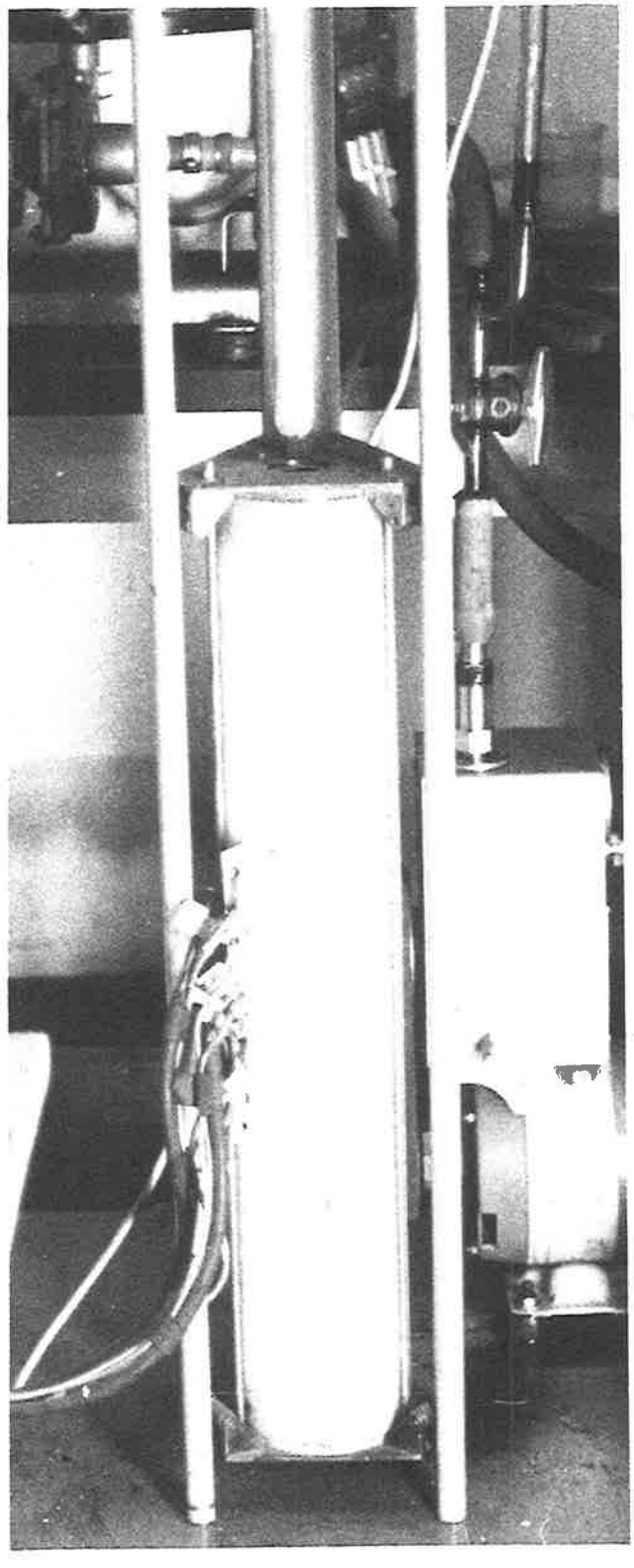

Fig.7 Non-inductively wound furnace.

alundum cement (approximately a quarter of an inch thick) which when fired formed a good base over which the second layer of windings could be laid. However, the failure of some control equipment caused this winding to burn out. A second winding of this type was then made with the two layers of windings separated by several wrappings of 'Refrasil' high temperature insulation tape.

The two windings of the furnace heater unit are connected in parallel. As the outer winding is on a former of larger diameter than that of the inner winding its resistance is greater, and it draws a smaller current. A large variable resistor connected in series with the inner winding is adjusted until the magnetic fields of the windings completely cancell one another. This condition is ascertained by probing with a search coil connected to a cathode ray oscilloscope.

The furnace has a main winding with two end-bands to compensate for heat losses. The main winding is controlled by a Honeywell Brown Pyr-O-Vane temperature indicator controller, using two position control with variacs to set the high and low power inputs. The control measuring element, a chromel alumel thermocouple is positioned at the centre of the furnace adjacent to the tube in which the oxidation is performed. Accurate temperature measurements are obtained with a Pt/Pt-Rh

thermocouple operating in conjunction with a Cambridge workshop potentiometer. This thermocouple is sited in the same sheath as the 'control' thermocouple. The end-bands, which are also non-inductively-wound, are operated in series via a variac. The temperature profile inside the furnace is checked with a thermocouple probe and the power input to the end-bands regulated to correct the temperature distribution. When operated correctly there is a zone twelve inches long at the centre of the furnace over which the temperature does not vary by more than $\pm 5^{o}C$. A typical temperature profile with and without the end-bands is shown in Fig.8.

3.1.7 Antivibration Precautions.

A microbalance is particularly sensitive to shocks and vibrations, accordingly care was taken during the design and construction to incorporate features which would minimize such effects. To damp out vibrations the main frame supporting the balance is of massive construction and has a total weight of approximately 1,000 pounds. This structure is supported off the floor by eight rubber shear mounts (type no. M114/50, supplied by Mackay Silentruba Products). The shear mounts are mounted in pairs, and have been chosen to damp out the vibrations resulting from the motors and vacuum pumps in

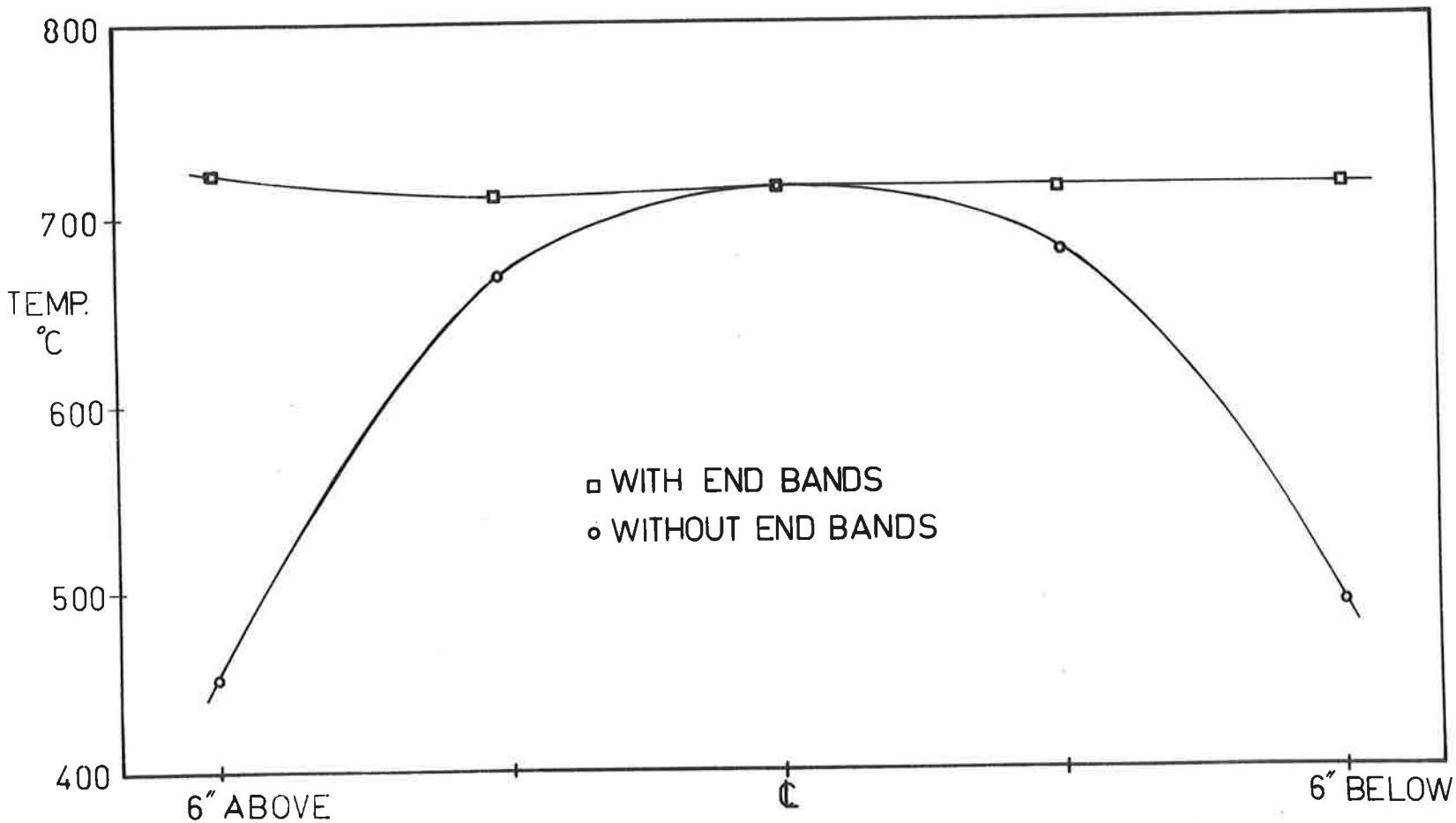

Fig.8 Temperature profile through the furnace.

the laboratory. When the balance is not in use the weight of the frame is supported on jacks.

The vacuum pumps and furnace are mounted on a bridge which spans the base plate of the main frame and is independently supported off the floor. Vibrations from the vacuum pumps are prevented from reaching the balance by the provision of bellows in the pumping line. The system of three bellows is so arranged that when the system is evacuated no mechanical forces are exerted on the pumping line.

3.1.8 Calibration of the Microbalance.

Preliminary adjustments of the number of turns on the balancing coil and its position relative to the magnet were made to obtain the desired sensitivity. The balance was then calibrated by adding known weights and noting the current necessary to restore the beam to the null point. The weights used were three one milligram and two half milligram riders. All possible combinations of the five weights were added to the balance until a total weight-gain of four milligrams had been reached. The resulting calibration curve is shown in Fig.9. As would be expected a linear relationship between the weight-gain and the restoring current was obtained which extrapolated through the origin. The calibration factor

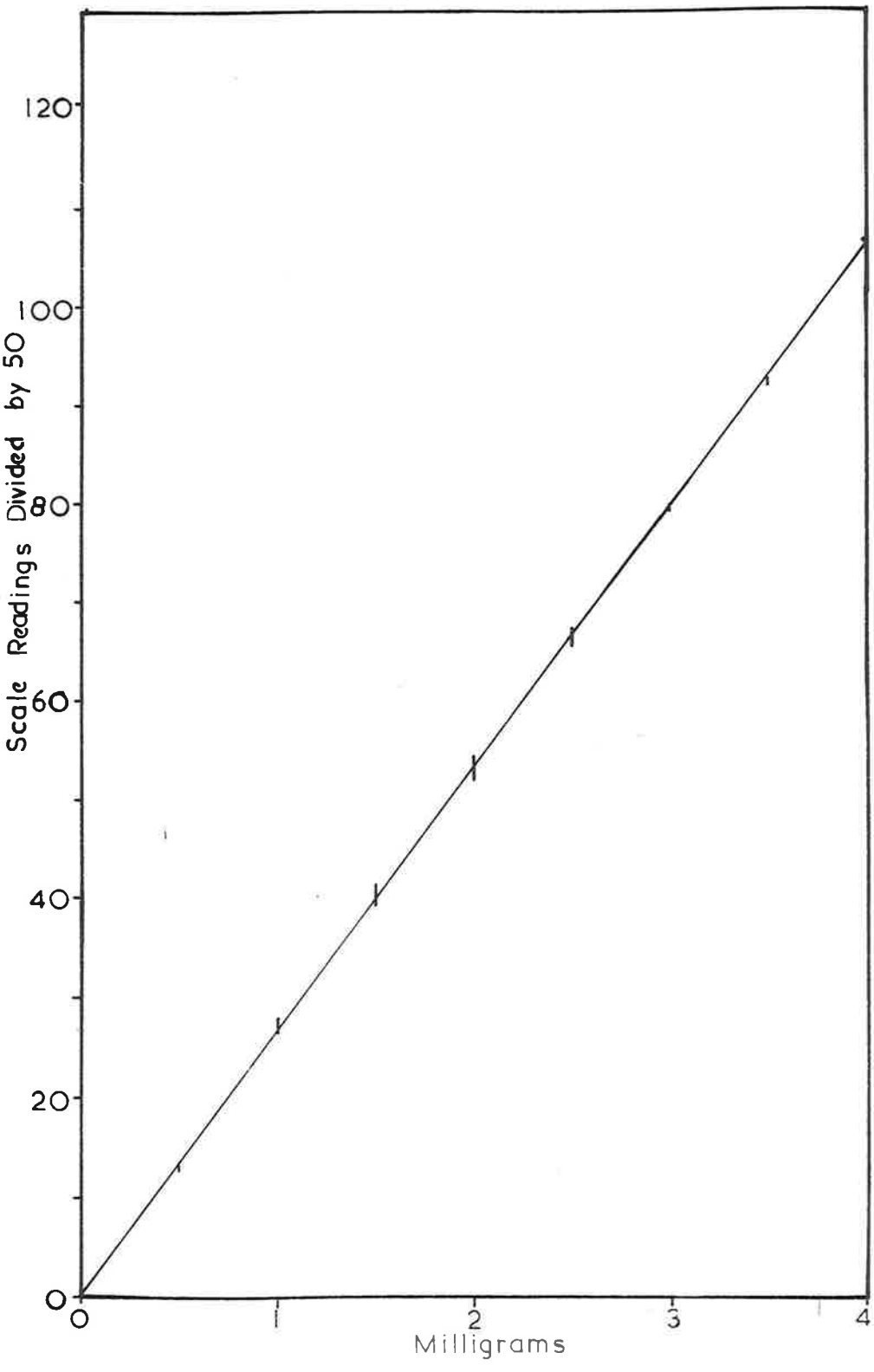

Fig.9 Calibration curve for the microbalance.

was calculated as being 1.33 ± 0.02 scale divisions of the microammeter per microgram. This corresponds to a sensitivity of 0.665 ± 0.01 microamps per microgram.

The balance was then tested for stability. It was found that the maximum pressure of carbon dioxide under which the balance would give stable operation was 200 mm Hg total pressure. Various arrangements of baffles were experimented with inside the balance, and the temperature profile of the furnace was made as uniform as possible; however neither of these measures contributed any appreciable improvement to the stability of the balance when it was operated at more than the above pressure of carbon dioxide. This effect has been noted before by Gulbransen[75] who found that the maximum pressure of oxygen that could be tolerated in a microbalance was one fifth of an atmosphere. He attributed the instability to convection currents and to the thermomolecular flow of gas inside the furnace tube.

3.1.9 Suggestions for Improving the Performance of the Balance.

In its present form the sensitivity of the balance is limited by the accuracy with which the microammeter can measure the current in the balancing coil circuit. The current sensitivity could have been improved

by reducing the number of turns on the balancing coil or by altering its position relative to the magnet. However, as well as increasing the sensitivity such measures also result in a reduction in the total oxygen uptake which can be measured before the meter exceeds full scale and are therefore undesirable. The microammeter was used, in its present application to measure the current, only because it was already present in the laboratory and the sensitivity desired in this project could be obtained by using it. The current could have been measured with greater accuracy, and the sensitivity of the balance improved accordingly, if a potentiometric method of current measurement had been adopted. Such a system would also have enabled a greater range of currents to be measured than is possible with the microammeter.

To fully realize an apparent increase in sensitity the stability of the balance must be such that the drift of the null point, over the period in which measurements are made, is less than the limits imposed by the sensitivity of the measuring system. In the present application, due to the precautions taken to thermostat the balance and to protect it from shocks and vibrations, the beam itself is very stable, and the limitation on the stability is imposed by the necessity to maintain the current in the taring circuit constant for extended periods

of time. The greater range of current measurement possible with a potentiometric method of measurement would enable the taring coil to be eliminated. With only one coil the force on the balance would always be exactly related to the measured current and there would be no possible drift of the null point occuring due to the instability of the taring coil circuit. The stability would then only depend upon the stability of the beam itself.

The fullest possible use has not been made of the great sensitivity of which the optical lever is capable. As mentioned in section 3.1.2 it would be an easy matter to increase the sensitivity of this device by several powers of ten by using finer gratings and better quality photo-electric cells than were used in this study. It would then be possible to use a more robust beam which could accomodate a much greater weight of specimen. By using a 0.004 inch tungsten suspension wire and by fabricating the beam from silica rod having a slightly heavier section than was used in this study it would be possible to construct a balance which could accomodate specimens having a weight in the vicinity of 10 - 20g.

If effect were given to the recommendations made in this section it is felt that a balance could be

built which would have a stability and a sensitivity such that weight changes of the order of 10^{-8}g could be detected in specimens having a weight in the vicinity of 10g. Such a balance would prove invaluable for studying the kinetics of surface reactions.

3.2 Electrochemical Apparatus.

This equipment was designed so that specimens could be vacuum annealed or hydrogen reduced and then introduced to the electrometric cell without intermediate contact with the air. This was accomplished by preparing the specimens in a chamber positioned directly above the electrometric cell and separated from it by a large stopcock. The specimen was mounted on the end of a long rod which entered the top of the preparation chamber through an 'O' ring seal. On completion of preparation the chamber was evacuated, filled with a cover gas and the specimen lowered into the cell through the stopcock. Provision was made to remove oxygen from the electrolyte by alternately bubbling oxygen-free nitrogen through the solution and then boiling it under vacuum. The removal of oxygen ensured that no current was used in the reduction of oxygen at the electrode surface.

3.2.1 Preparation Chamber and Specimen Holder.

The preparation chamber was made from a 30 inch length of one inch diameter silica tubing, the working section of which was surrounded by an electrically heated furnace. Temperatures in the furnace were controlled by a Honeywell Brown Pyr-O-Vane temperature indicator-controller. The specimen was held in the preparation chamber on the end of a 5 foot length of surface-ground stainless steel tubing which entered the preparation chamber through an 'O' ring seal in a brass block. This block was cemented with epoxy resin to a spherical glass joint by means of which it was possible to position the specimen within the oxidation chamber. The tube was also used to conduct electric current to the specimen and it was water-cooled to protect it from the high temperatures encountered in the preparation chamber.

The specimens had a working area of 5 cm^2 and were connected by a long thin tail to a tag which was clamped into the end of the stainless steel tube. Temperature gradients in the furnace were thus eliminated as the tail was sufficiently long to enable the end of the water-cooled tube to be clear of the furnace. Appropriate gas connections were made to the preparation chamber and vacuum was produced in the system by a Jena mercury diffusion pump backed by an Edwards 2SC 20 rotary oil pump.

3.2.2 The Electrometric Cell.

The apparatus for removing oxygen from the electrolyte and for performing the electrochemical measurements is shown in Fig.10. It was a modified version of the equipment used for a similar purpose by Mills and Willis[76]. The electrolyte was contained in a 2-litre reservoir flask and was freed of dissolved oxygen by alternately evacuating and filling the apparatus with oxygen-free nitrogen. After four cycles of this treatment sufficient electrolyte was forced into the cell to cover the working area of the electrode.

The cell was a four necked flask; three of the necks admitted electrodes while the fourth was used to make a connection to the flask containing the electrolyte. The electrodes used were as follows:-

working electrode	:	test specimen
auxiliary electrode	:	Pt wire
reference electrode	:	Ag-AgCl electrode

The reference electrode had a short Luggin capilliary and was specially designed so that the shielding extended practically to the tip of the electrode. Stray pick-up effects thus entirely eliminated.

3.2.3 Electrical Measuring Equipment.

This equipment was a modified version of that

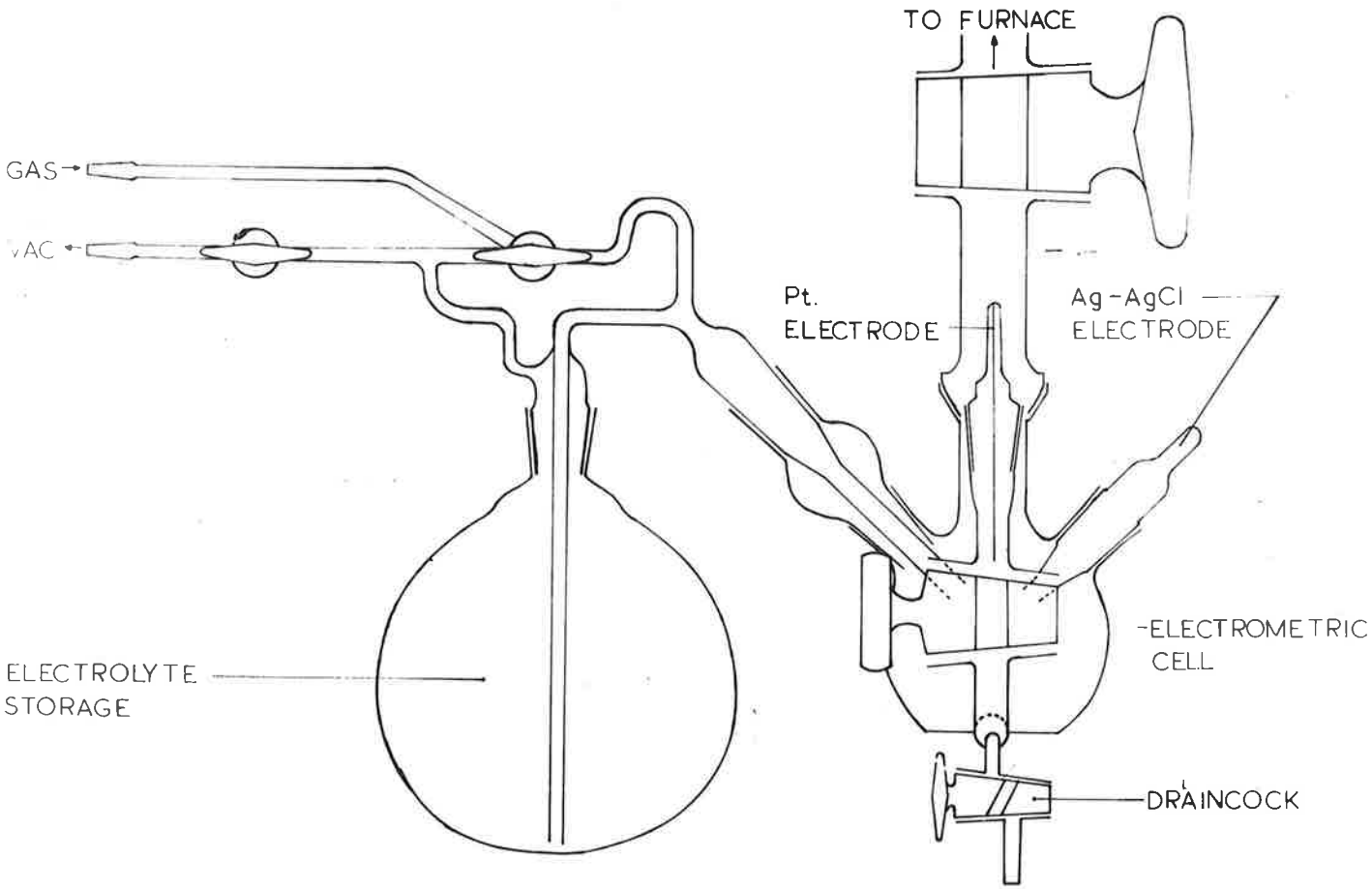

Fig.10 Electrometric cell.

devised by Denholm[77] to study the aequeous corrosion of iron and iron chromium alloys. Briefly it consisted of a potentiostat to set the potential of the specimen at any desired level with the direct current necessary to maintain this potential being recorded on a Honeywell Brown high speed recorder. Superimposed on the direct current was an alternating current with a square-current wave form which polarized the specimen between ±10 M.V. of the set potential point. These small potential excursions were analysed by an impedance bridge which enabled measurements to be made of the capacity and resistance of the oxide covered specimen.

A schematic diagram of the equipment is shown in Fig.11. The square wave current was generated by a Schmitt trigger, the output of which was supplied across two networks; the first consisted of a high resistance in series with the cell containing the test electrode, the second consisted of a high resistance in series with a comparison network, or analogue, composed of a resistance and capacitance in parallel. When the outputs of the X and Y amplifiers were applied to the plates of a cathode ray oscilloscope a straight line at 45° indicated matching of both the resistance and capacity, a loop indicated mismatch of the resistance, while variations from 45° indicated mismatch of the capacity.

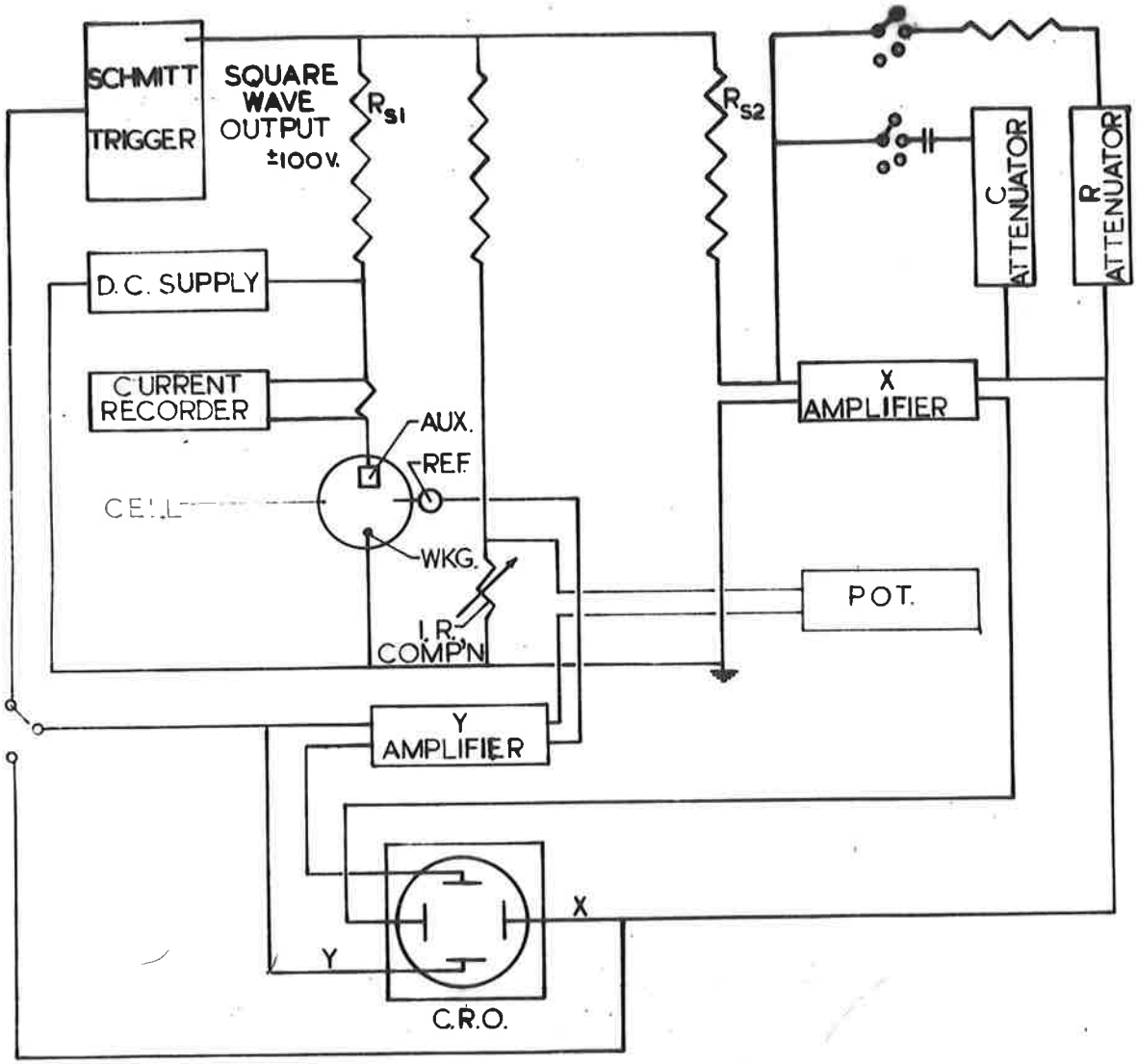

Fig.11 Block diagram of square-current-wave bridge.

By using square wave excitation it was possible to separate the series and parallel components of the resistance. Series resistance resulted in two parallel lines in the c.r.o. trace while parallel resistance produced curvature of the trace. A compensating resistor built into the equipment allowed for the effect of the series resistance to be eliminated. This is an important feature as at high current densities the series I.R drop from the tip of the reference electrode to the specimen could cause appreciable errors in the potential readings.

The Schmitt trigger caused reversal of the square-current wave when the potential reached the level of 10 M.V. on either side of the set point. The whole equipment thus acted as a self-excited oscillator providing two-position control of the potential about the set point. When a direct current was required for an electrode process this was supplied by assymetry of the square wave on the time axis. The assymetry was compensated for by a direct current supplied from a high resistance source which was adjusted to return the c.r.o. trace to the middle of the X axis. Under these conditions the total current supplied to the electrode was steady D.C. with a symmetrical square-wave form current superimposed.

The current measuring system sampled both the steady D.C. from the external source and the D.C. compon-

ent due to any slight residual assymetry. The A.C. component was filtered by a long time constant R-C filter network. The current recorded by the Honeywell Brown potentiometric recorder was thus the true D.C. passing across the electrode/solution interface.

3.3 Materials and Gas Purification Equipment.

3.3.1 Materials.

For a fundamental study of any gas-solid reaction it is essential to use the purest materials available as impurities in both the gas and solid phases can have a marked effect on the oxidation behaviour of the specimen. Two forms of iron of differing impurity content were used in this study. The early experiments were performed with specimens of Armco iron enamelling sheet, spectrographic analysis of which revealed the presence of the following impurities:-

Mn	Cu	Si	Al	Cr	Ni
0.07%	0.04%	0.001%	0.02%	0.01%	trace

Carbon was determined by chemical means and found to analyse 0.02%.

Some time after the commencement of the project a sample of high purity iron became available and this material was used in the latter part of the experimental

program. The high purity iron was supplied by the Battelle Memorial Institute and had been prepared from a special grade of electrolytic iron which had been further purified by vacuum melting and zone refining. Before dispatch this material had been analysed according to the methods described by Heffelfinger et al[78], and the analysis contained in Table 2 was supplied with the material.

Initial supplies of carbon dioxide were obtained from a local supplier but analysis of this gas by officers of the Australian Atomic Energy Commission showed that the moisture content of the gas was of the order of 600 ppm, while the oxygen content was approximately 7,000 ppm. Clearly such gas was unsatisfactory and further supplies of carbon dioxide were obtained from the Colonial Sugar Refining Co. Ltd., of Sydney. This gas, with further purification, was used during the whole of the experimental program. The gas from this latter source is produced by a fermentation process and as such does not contain any carbon monoxide. Draycott and Smith[79] have reported that the main impurity present in this gas is air, with up to 200 ppm of oxygen and 800 ppm of nitrogen being encountered. The moisture content was below 50 ppm while other impurities were present as traces.

The hydrogen and oxygen-free nitrogen were supplied by C.I.G. (Aust.) Ltd., and the major impurities

Table 2.

Analysis of Battelle Iron.

Amounts are given as parts per million.

Aluminium	15	Magnesium	< 5
Antimony	< 5ND(a)	Manganese	< 0.1
Arsenic	< 5ND	Molybdenum	< 5ND
Beryllium	< 0.2	Nickel	20
Boron	< 5	Phosphorus	9
Cadmium	< 5ND	Silicon	10
Calcium	< 10ND	Tin	< 5ND
Chromium	5	Titanium	< 1ND
Cobalt	5	Tungsten	< 5ND
Copper	7	Vanadium	< 1ND
Lead	< 1ND	Zinc	< 10ND
		Zirconium	< 1ND

(a) ND means not detected. Detection limits are given.

Carbon	10	parts per million.
Oxygen	28	"
Nitrogen	2	"
Hydrogen	0.2	"
Sulphur	10	"

present in these gases were oxygen and moisture.

3.3.2 Gas Purification Equipment.

Gas purification trains have been built to remove water vapour and oxygen from the carbon dioxide and hydrogen used in this project.

Moisture is one of the most troublesome impurities as very small quantities can have a profound effect upon the rate and rate of growth of the oxide product. Apart from those desiccants such as barium perchlorate and calcium chloride which rely on chemical reaction to remove water the most common drying agents in use are either silica gel or activated alumina. However a new group of materials known as molecular sieves have recently been developed. These highly selective adsorbents have a greater adsorptive capacity and can yield lower dew points in the gas being dried than is possible with silica gel or activated alumina. The molecular sieves - type no. 4a - used in this project were supplied by the Union Carbide Corporation of Roseville N.S.W. Molecular sieve driers have been provided on the carbon dioxide and hydrogen gas purification systems.

The molecular sieves were in the form of pellets and a 10 inch bed of this material was contained inside a 2 inch diameter copper tube the outside of which was

was surrounded by a pyrotenax heater. Prior to a run the bed was activated by heating it to 300°C. The adsorbed water released during this operation was flushed from the system by a stream of gas which flowed through the bed in a direction countercurrent to that taken by the gas during the adsorption cycle. The bed was then allowed to cool to room temperature before the drying operation commenced. Braycott and Fox[80] have used molecular sieves to dry carbon dioxide and have obtained moisture contents of less than 5 ppm. It is considered that the same order of purification was being attained in this project.

Oxygen was removed from the gases by chemical means. In the hydrogen gas purification system the gas was passed over a hot copper catalyst maintained at 400°C, which caused any oxygen present to combine with hydrogen to form water. This was subsequently removed from the gas stream by a molecular sieve drier. Although the nitrogen was nominally oxygen-free it contained an appreciable quantity of oxygen and this had to be removed by passing the gas over a freshly reduced copper surface maintained at 400°C. Two furnaces containing copper turnings were used to perform this operation and while one was removing oxygen the other was being reduced.

Neither of the operations just mentioned were

feasible for removing oxygen from the carbon dioxide. It was decided to use a method developed by Draycott and Herr[81] for this purpose. In this method the oxygen was removed by passing the gas over reduced pyrolusite which was heated to 150 - 180°C. Regeneration of the pyrolusite was accomplished by passing hydrogen counter-currently at a temperature of 300°C. Unfortunately the bed capacity was reduced to some extent after each regeneration and after two reductions the pyrolusite was replaced by a fresh batch. According to Sidgwick[82] when MnO_2 is reduced at the temperatures used in this study MnO is the end product. During the oxygen removal cycle this material oxidizes to form Mn_3O_4 and Mn_2O_3. Measurements made with a Hersch oxygen meter indicated that the oxygen content of the purified carbon dioxide was less than 10 ppm.

The details of construction of the pyrolusite furnace are shown in Fig. 12. The all copper construction was typical of the gas purification furnaces. Temperatures in the furnaces were measured with cromel-alumel thermocouples which were connected, via a multipoint thermocouple switch, to a Cambridge temperature indicator. Power inputs to the furnaces were regulated by means of a bank of Sunvic energy regulators. Construction of the gas purification system was greatly facilitated by running

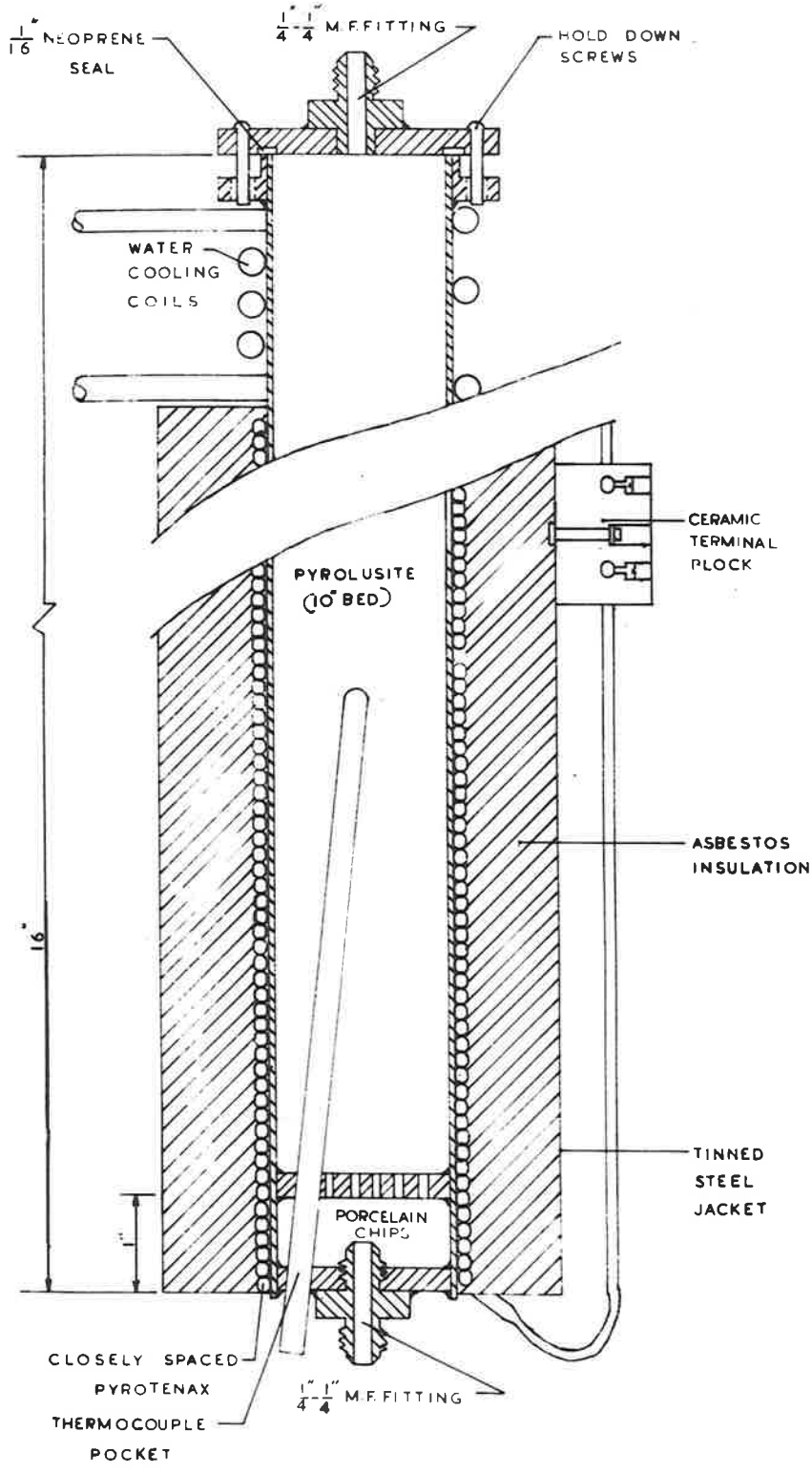

Fig.12 Pyrolusite furnace.

all the gas lines in 1/4 inch annealed copper tubing and by making extensive use of standard refrigeration valves and fittings. The arrangement of the gas purification system is shown schematically in Fig. 13.

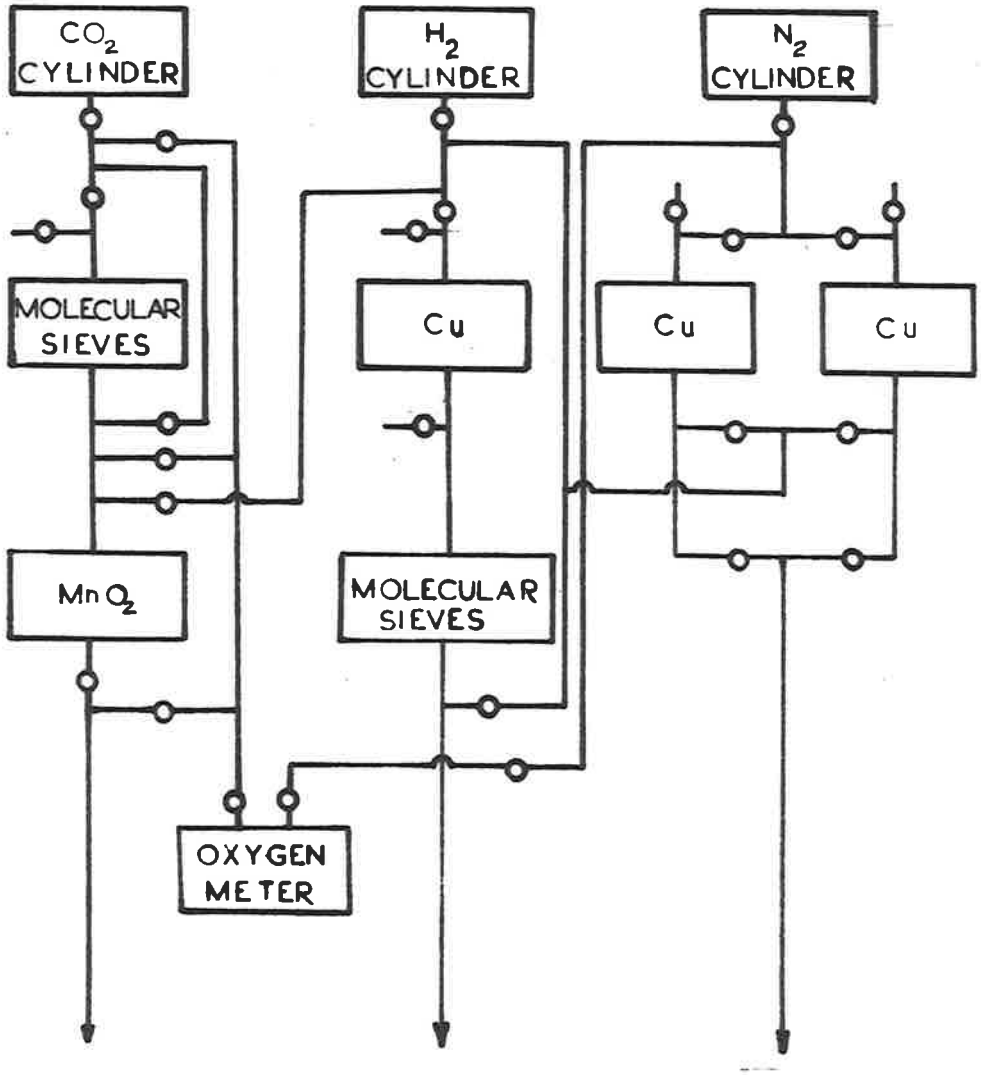

Fig.13 Schematic diagram of the gas purification system.

4. EXPERIMENTAL PROCEDURES AND EXPERIMENTAL RESULTS.

4.1 Electrochemical Tests.

Use has been made of an electrochemical technique to analyse the scales formed below 570°C for ferric oxide. It was expected that at these temperatures (i.e. 400 - 570°C), and for the times of oxidation studied in this project, the scales would consist of two oxide layers - namely an outer layer of haematite with an inner layer of magnetite. Knowing the total oxygen uptake from gravimetric measurements it would then be possible to determine the ferric oxide electrochemically and to estimate the magnetite by difference, thus making it possible to study the rate of growth of the individual oxide layers composing the scale.

The residual oxide films left behind by some of the methods of specimen preparation such as abrasion, etching, and electropolishing, can, under certain conditions have a marked effect on the oxidation behaviour of a metal. Little is known about the structure and properties of these thin films and it is not known how they affect the subsequent oxidation behaviour of the metal. It was felt that measurements of the electrical capacity and resistance of these thin residual films, when coupled with other electrochemical parameters such as potential, and the quantity of electricity needed to

oxidize or reduce the oxide to another oxidation state, could prove useful in determining the thickness and composition of these residual films. However, before these measurements could be used as an analytical tool further developmental work was required to discover the true meaning of the electrical capacity and resistance measurements.

4.1.1 Investigation of the Capacity and Resistance Measurements.

It was decided to investigate the significance of the capacity and resistance measurements by forming oxide films containing known amounts of oxide by the anodic oxidation of iron in aqueous electrolytes. During the course of the anodic polarization, measurements of the electrical capacity and resistance of the oxide covered electrode were to be made along with measurements of the current and the potential. The latter pair of parameters would enable a quantitative and qualitative identification of the oxide product to be made. Correlations were then to be sought between the capacity and resistance measurements and the amount of oxide on the surface of the specimen.

In defining the experimental conditions and in the interpretation of the results use has been made

of a pH-potential equilibrium diagram a short description of which follows.

The pH-potential diagram for the iron-water system, shown in Fig. 14, has been reproduced from Pourbaix's book[83]. It has been constructed from equilibrium data for a temperature of 25°C.

Fig. 14 shows-

1) The areas of thermodynamic stability of :-

   a) Water, stable between the lines (a) and (b) which represent the reactions

      $2H^+ + 2e = H_2$, and

      $4OH^- = O_2 + 2H_2O + 4e$.

   b) Iron stable in the area bounded by lines (19), (10),(20).

   c) Solid oxidation products $Fe(OH)_2$, Fe_3O_4 and Fe_2O_3 in the areas so named.

   d) Soluble oxidation products of which the two most important are the ions Fe^{++}, stable in acid solutions of low oxidising power, and FeO_2H^-, stable in alkaline solutions of low oxidizing power.

2) The relative predominance of the different forms of iron existing in the dissolved state. The lines 1 to 8 divide the diagram into fields of predominance of Fe^{++},

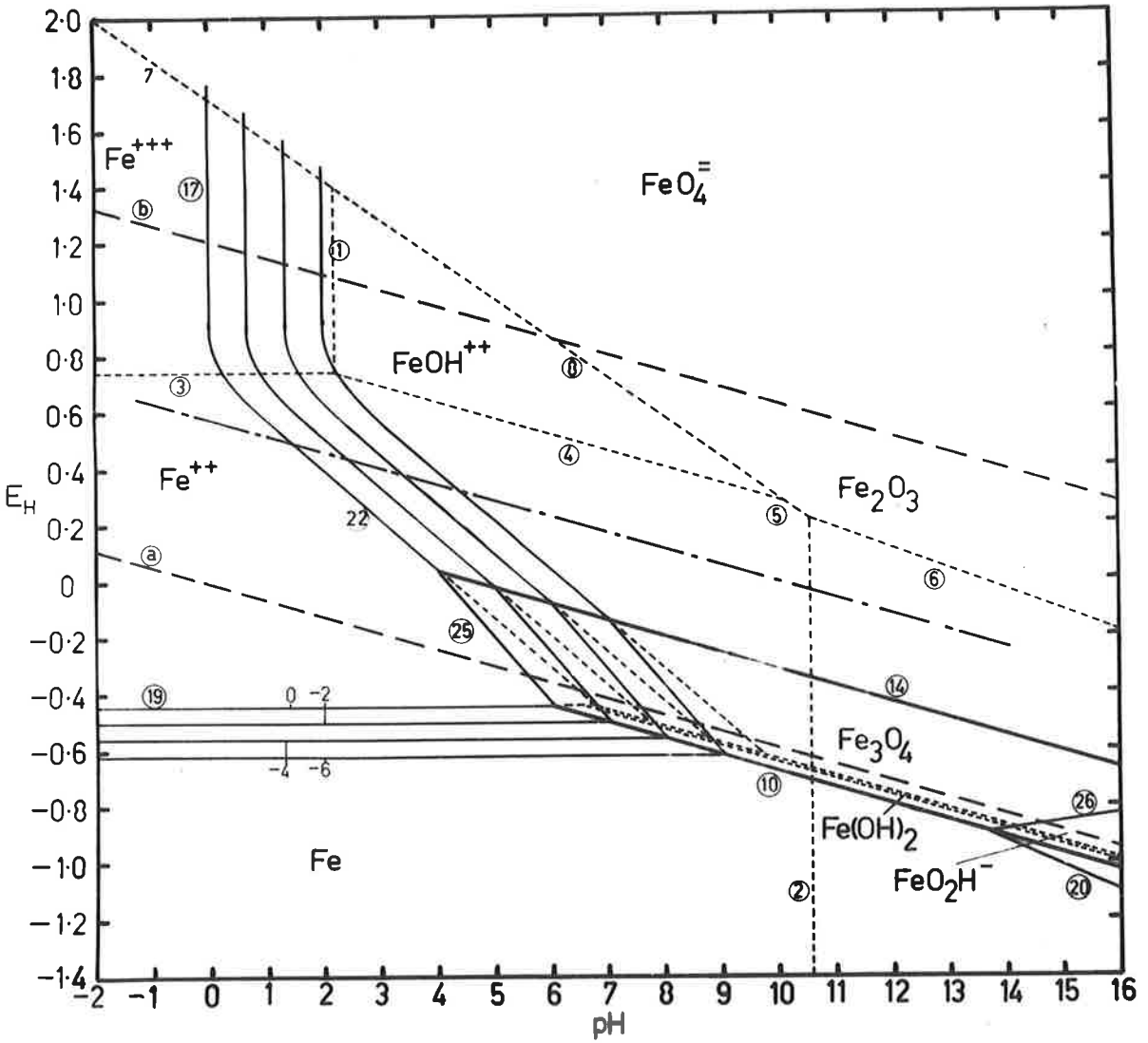

Fig.14 pH-potential diagram for the Fe-H_2O system.

Fe^{+++}, $FeOH^{++}$, FeO_4^{--}, and show the condition of equal activity in solution of each of these ions. The areas of stability of the soluble oxidation products Fe^{++} and FeO_2H^- are bounded by families of lines. Each line refers to a particular concentration of iron in solution.

The following convention has been followed in the construction of the pH-potential diagram.

1) Full lines refer to equilibria between liquids and solids.
2) Bold lines refer to equilibria between two solids.
3) Dotted lines refer to equilibria between dissolved ions.
4) Dashed lines refer to equilibria between water and its products of decomposition.

In some electrochemical studies unbuffered solutions can be tolerated provided that the solutions are well stirred, however in film forming studies the metal/solution interface becomes covered with a gelatinous or porous layer and stirring cannot prevent pH changes at the interface. Under these circumstances it is essential to use buffer solutions to control the pH of the electrolyte. The choice of a suitable electrolyte is complicated by the fact that a buffer agent only covers a limited range of pH and furthermore the use of such a system introduces a foreign anion into the system. Each anion has its effect

on the electrode processes, but the presence of these effects must be tolerated if buffer solutions are to be employed to fix the pH.

Denholm[77] has studied the effect of the addition of various anions on the electrode processes that occur at an iron electrode in an aqueous solution. From this study it would appear that the borate ion is largely an indifferent anion and hence borate buffer solutions have been used in the present application. These solutions have a buffering action which extends over the pH range from 8 to 10. Reference to the pH-potential diagram shows that in this range it is thermodynamically possible to form oxide films by anodic oxidation.

4.1.1.1 Experimental Procedure.

A series of electrolytes were prepared in the pH range 8 - 10 by adjusting the pH of a saturated boric acid solution with 5.0 N caustic soda solution. A measured quantity of 0.1 N potassium chloride solution was then added to give 10^{-5} N chloride ion concentration which was sufficient to operate the Ag-AgCl reference electrode. All the electrolytes were prepared from A.R. quality chemicals and distilled water.

As the starting point of the potentiostatic traverses specimens of Armco iron, previously prepared by abras-

ion on 600 grade silicon carbide paper, were freed of any residual oxide film by annealing in dry hydrogen at 800°C for one hour. The specimens were then lowered into the cell without intermediate contact with the air and sufficient electrolyte was blown into the cell to cover the working area of the specimen. The initial potential of the specimen was found by adjusting the potential of the specimen until the current drawn by the specimen was less than 10^{-7} amps/cm^2 which was the smallest current that could be measured with the equipment.

After the initial potential of the specimen had been found the potential of the electrode was altered in 20 M.V. steps with the current being allowed to settle to a steady value between potential increments. This procedure was repeated until the specimen had been polarized to a potential above the Flade Potential which is shown on Fig. 14 as a line of short and long dashes. At these potentials the pH-potential diagram shows that Fe_2O_3 is the stable solid phase. During the course of the potential traverse measurements of the capacity and resistance of the electrode were made with an A.C. bridge. On the completion of a test a sample of the electrolyte was run off and the reference electrode removed from the cell. The pH of the electrolyte was checked, and the potential of the Ag-AgCl reference electrode measured relative to a saturated calomel

half cell with a Jones model B pH-electrometer. This reading enabled the potential measurements to be expressed on the hydrogen scale of potential.

4.1.1.2 Experimental Results.

The Honeywell Brown recorder gave a record of current versus time. Steady state values of the current, I, were read from this record and the total quantity of electricity, Q, consumed at any time was obtained by graphical integration of the chart record. Plots of E vs log I and E vs Q were then made. The capacity and resistance, expressed as $\mu F/cm^2$ and $mhos/cm^2$ respectively, were also plotted as a function of potential. Two typical results obtained at pH 8 and 10 are shown in Figs. 15 and 16 respectively.

At any given pH the current consumed by the electrode processes increased as the potential was made more noble until a maximum value was attained after which it decreased to, and remained approximately constant at, a very low value. Increasing the pH of the electrolyte decreased the maximum value of the current drawn by the electrode processes and this behaviour was reflected in the E-Q curves which involved smaller total amounts of electricity. It was only at the highest values of the pH, i.e. at pH 9.5 and 10, that a second arrest corresponding

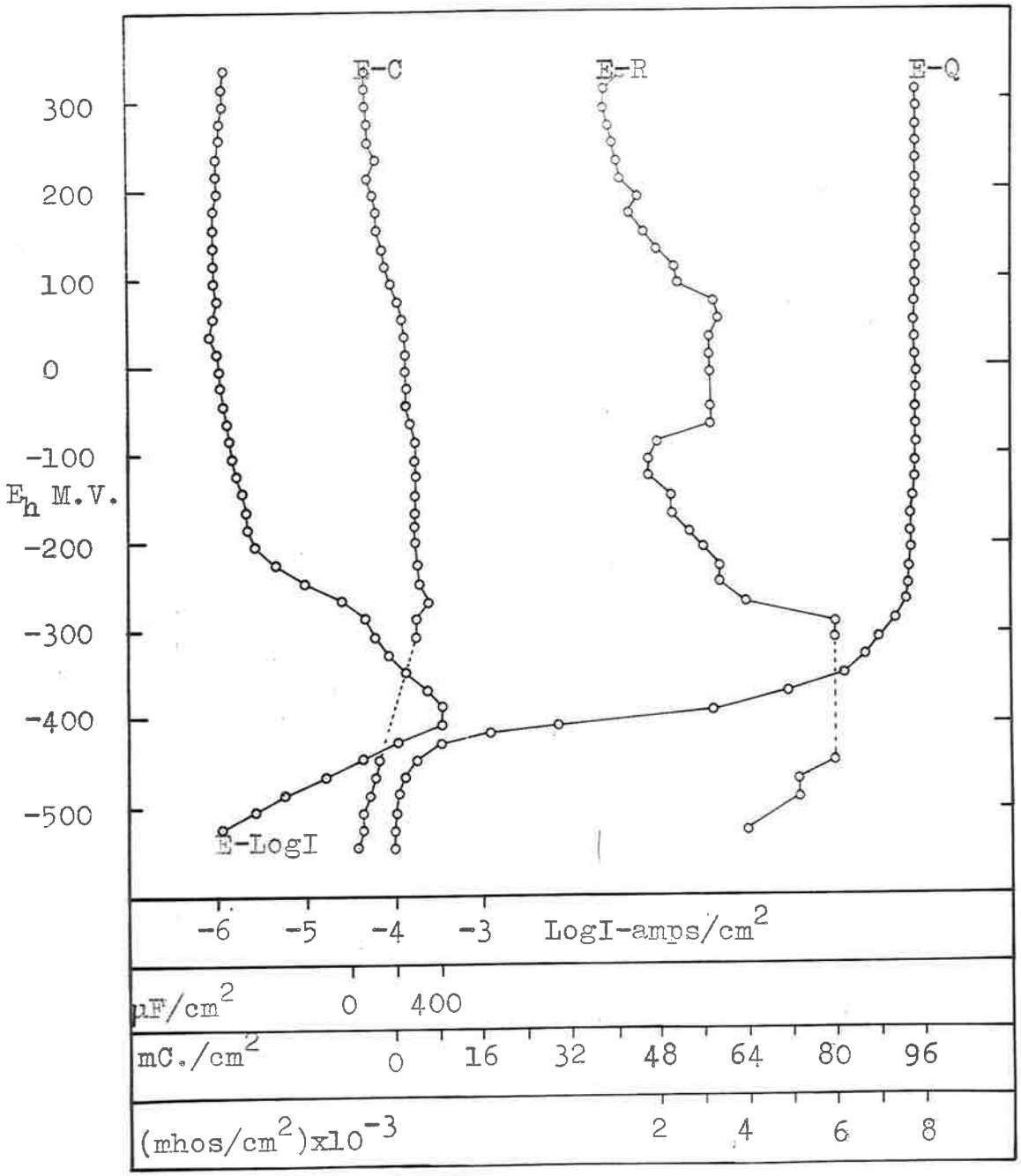

Fig.15 Electrochemical investigation - pH 8.

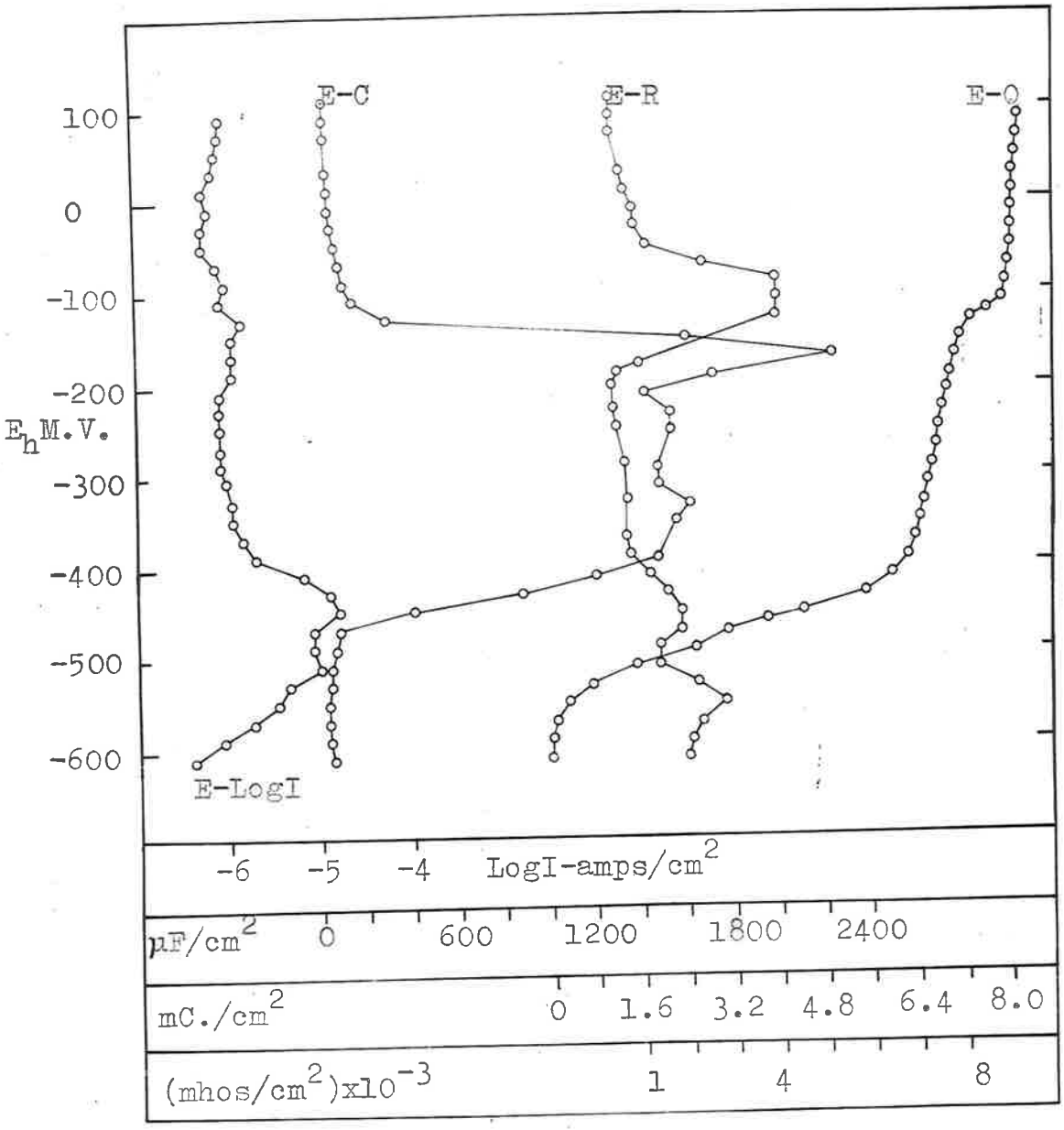

Fig.16 Electrochemical investigation -pH 10.

to the oxidation of Fe^{++} to Fe^{+++} in the film became detectable in the E-Q curves.

The capacity curves are characterized by the following :-

a) Very low values of the capacity at the beginning and end of the potential traverses.

b) A plateau in the E-C curves.

c) The appearance of a peak value of the capacity in the results obtained at pH 9.5 and 10 which corresponds to the appearance of a second arrest in the E-Q curves.

Some typical values of the capacity are contained in table 3.

Table 3.

Characteristic Capacity Values.

pH	8.0	8.5	9.0	9.5	10.0
C(initial) $\mu F/cm^2$	30	66	30	60	56
C(plateau) $\mu F/cm^2$	300	300	250	400	1500
C(peak) $\mu F/cm^2$	-	-	-	2300	2800

The resistance curves show considerable scatter, however it is apparent that the general trend exhibited by these results is for the conductivity to decrease as the potential becomes more noble. Superimposed on this behaviour there is , at pH 9.5 and 10.0, a peak value of the

conductivity which coincides with the appearance of both the peak in the E-C curves and the second arrest in the E-Q curves. This behaviour appears to be related to the transformation of Fe^{++} to Fe^{+++} oxidation states in the film.

4.1.2 Electrometric Analysis of Oxide Films.

The electrometric method of analysis as developed by Cohen et al[57,58] has been used to analyse the scales formed below 570°C for ferric oxide.

4.1.2.1 Experimental Procedure.

Specimens of Armco iron were prepared by abrasion on the various grades of silicon carbide paper, degreased by swabbing with benzene and acetone and dried in absolute alcohol. They were then placed in the apparatus and annealed overnight in a dry hydrogen atmosphere at 800°C. The next morning the temperature of the furnace was adjusted to the reaction temperature and the hydrogen pumped from the system. After a vacuum anneal for one hour at the reaction temperature purified carbon dioxide gas was admitted to the system to a total pressure of 200 mm Hg. The specimens were then oxidized for varying lengths of time at different temperatures under identical conditions to those used in the microbalance.

At the end of the test period the reaction was terminated by evacuating the system and lowering the specimen out of the furnace. Purified nitrogen was then admitted to the system and the specimen was lowered into the cell.

The electrolyte used was a sodium borate-HCl solution buffered at a pH of 7.6. Prior to an experiment the electrolyte was freed of any dissolved oxygen by alternately evacuating and filling the system with oxygen-free nitrogen. Sufficient electrolyte was then blown into the cell to just cover the working area of the specimen, after which the stopcock separating the cell from the preparation chamber was opened and the specimen lowered into the cell. Immediately the reference electrode had been positioned close to the surface of the specimen and the initial potential found, current was supplied to the specimen at a current density of 15 $\mu a/cm^2$. Readings of potential versus time were then commenced.

4.1.2.2 Electrometric Results.

If the specimen had any ferric oxide upon its surface the potential versus time curve, obtained when the specimen was subjected to cathodic polarization at a constant current density, would show two potential arrests. The first arrest would result from the reduction of any ferric oxide present whilst the second arrest would result

from the evolution of hydrogen. The cathodic reduction of magnetite requires a considerable overpotential which polarizes the specimen into the region of hydrogen evolution. Indeed Huch, Beck and Cohen[58] have stated that under the conditions used in this study magnetite is not reduced, however more recent work by Sewell, Stockbridge and Cohen[84] has shown that it is possible to accomplish some reduction of magnetite under these conditions, but that the process occurs at the very low current efficiency of less than 17%. Thus it is not possible to estimate magnetite by electrometric means.

The result of an electrometric analysis performed upon a specimen of hydrogen-annealed Armco iron, oxidized in carbon dioxide at 200 mm Hg total pressure for 1500 minutes at 460°C, is shown in Fig. 17. According to Fig. 19 the weight-gain of oxygen sustained under these conditions should be approximately 120 $\mu g/cm^2$.

Upon the application of the cathodic current the specimen rapidly polarized until a potential of approximately -900 M.V. on the hydrogen scale of potential had been attained. Reference to Fig. 14, the pH-potential diagram, shows that this value of the potential is more negative than the hydrogen evolution potential. Because there was no potential arrest at more noble values of the potential it was concluded that no ferric oxide was present and that

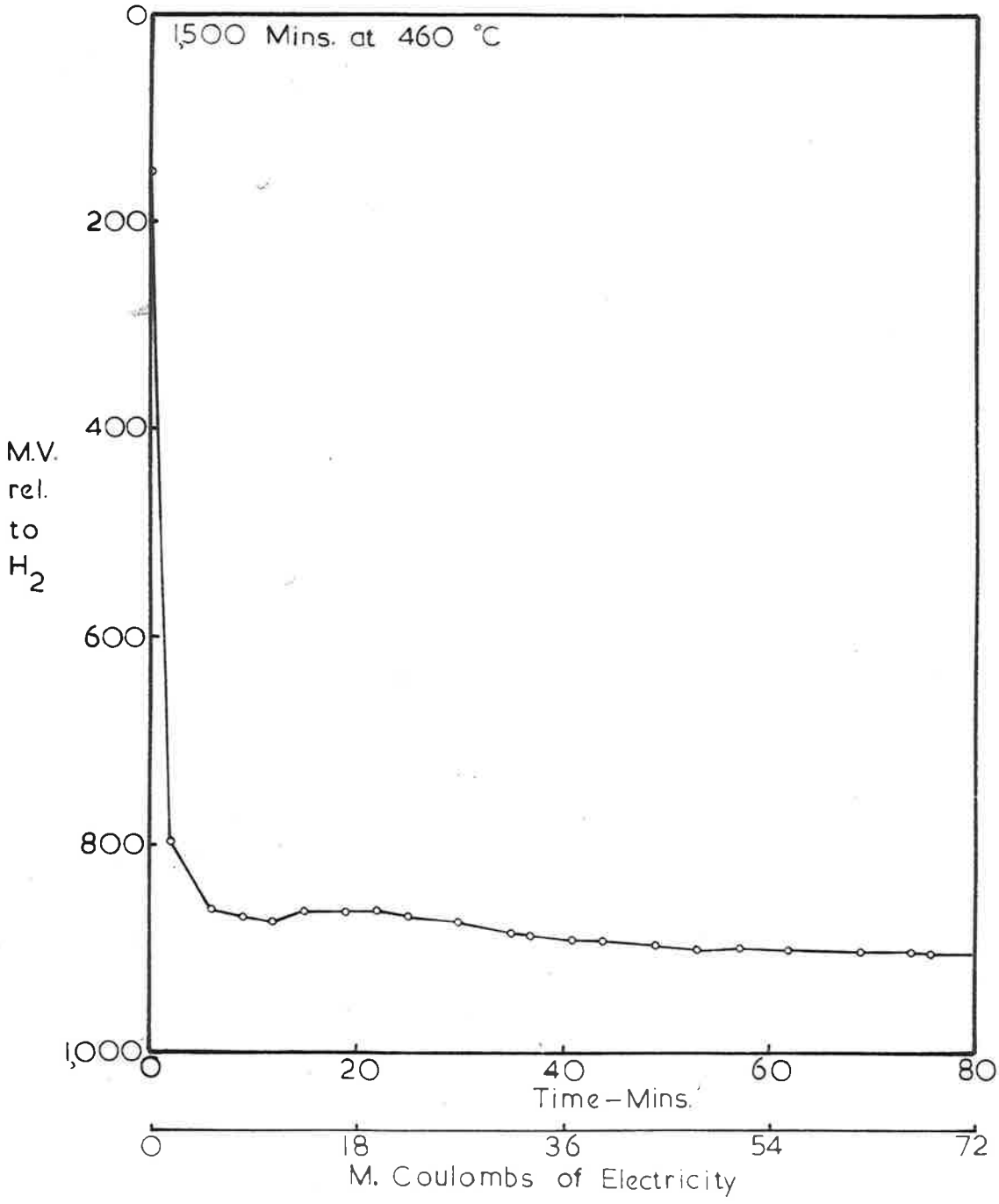

Fig.17 Electrometric analysis.

the oxide film consisted entirely of magnetite. Similar results were obtained for specimens that had been oxidized at different temperatures.

The absence of ferric oxide from the oxide film was surprising and endeavours were made to check the composition of the oxide by other means. As ferric oxide is optically active a series of specimens were examined under a microscope equipped with polarizing facilities. No evidence of any optically active material was found. Subsequent x-ray diffraction analysis also failed to reveal the presence of ferric oxide. It was thus established that, under the conditions used in this study, the oxides formed below 570°C consisted wholly of magnetite.

4.2 Gravimetric Tests.

4.2.1 Experimental Procedure.

Iron previously rolled to strip 0.008 inches thick served as the stock from which rectangular coupons of metal, 3.5 cms x 1 cm were cut to use as specimens. After drilling a hole near one end, the specimens were wet abraded through the various grades of silicon carbide paper, dried in absolute alcohol, and accurately measured with a micrometer. They were then degreased by swabbing with benzene and acetone, and, after a final wash in absolute alcohol, the specimens were quickly dried and loaded

onto the microbalance. The oxidation chamber was then evacuated to 10^{-5} mm Hg total pressure and one of the standard methods of specimen preparation was embarked upon.

Two different methods of specimen preparation were adopted. One series of specimens was hydrogen annealed while another series was vacuum annealed prior to the commencement of oxidation. For the hydrogen annealed specimens the procedure was as follows:- When a vacuum of 10^{-5} mm Hg had been attained the system was closed off from the pumps and hydrogen was admitted to the system. After several flushings of hydrogen the pressure was adjusted to one atmosphere and the furnace was raised around the specimen. The specimen was then annealed overnight at a temperature of 800°C. The next morning the temperature of the furnace was adjusted to the reaction temperature and the system was evacuated for one hour. Purified carbon dioxide was then admitted to the system until a total pressure of 200 mm Hg had been attained. The balance was quickly tared to the null point, zero time was recorded, and readings of weight-gain versus time commenced. For the vacuum annealed series of specimens the procedure was essentially the same as for the hydrogen annealed specimens except that the hydrogen anneal was dispensed with. After the initial evacuation the furnace, already heated to the reaction temperature, was raised around the speci-

men and the vacuum anneal for one hour at this temperature commenced.

4.2.2 Experimental Results.

The weight uptakes of oxygen have been expressed as $\mu g/cm^2$ of apparent geometric area. At any given temperature it is possible to separate the weight-gain versus time record into two parts. The first portion corresponds to the region where the reaction is controlled by a nucleation and growth process; the second part is observed when an appreciable thickness of oxide has built up on the metal and one of the scaling laws are obeyed. Also it has been noted in section 4.4 that above 570°C the scale was composed of wustite, while below this temperature it was composed of magnetite. The change in composition alters the mechanism of oxidation and a different type of weight-gain versus time record was obtained depending upon whether the temperature of formation was above or below the wustite eutectoid point (i.e. 570°C). Thus the gravimetric results have been presented as the early and the latter stages of oxidation with a further subdivision within each group depending upon whether the temperature of formation was above or below 570°C.

4.2.2.1 Results for the Early Stages of Oxidation.

The weight-gain versus time records obtained for the early stages of the reaction between hydrogen annealed Armco iron and carbon dioxide are shown in Fig. 18. At the start of the reaction the rate accelerates with time and the curve is concave upwards until the rate reaches a maximum after which the rate decreases. The overall effect is to give a curve which is approximately sigmoidal in shape. It should be noted that the reactions at 620, 580 and 550°C are initially slower than the reaction at 520°C. Curves having the same shape as those in Fig.18 have also been obtained for a series of vacuum annealed specimens. These latter experiments were mainly performed upon samples of Battelle iron, but above 570°C a complete set of results has also been obtained using decarburised Armco iron. It was found necessary to decarburize the Armco iron prior to the vacuum anneal otherwise it preferentially decarburized when carbon dioxide was admitted to the system. Attempts were made to decarburize this material by vacuum annealing it, in situ, on the balance at 890°C. However, it was found that it took six hours at this temperature before the material had decarburized sufficiently to start gaining weight when gas was admitted to the system. The specimens were ultimately decarburized by packing them in ferric oxide and heating them

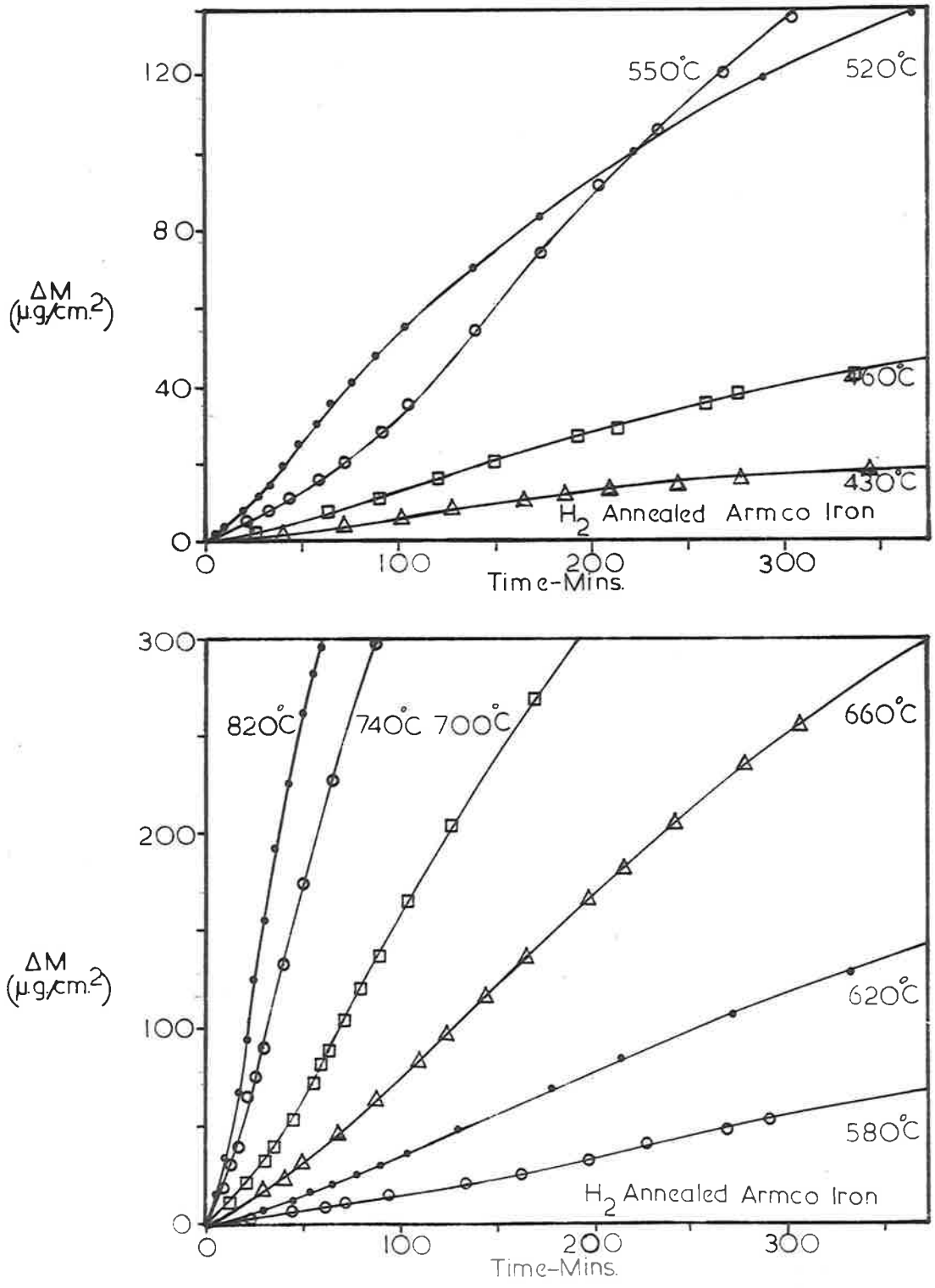

Fig.18 Gravimetric results for the early stages of oxidation.

at 800°C for four hours under a vacuum of 10^{-3} mm Hg. This procedure lowered the carbon content of the Armco iron to a very low level. Any oxide left on the surface was easily removed during the preparation of the specimen.

4.2.2.2 Results for the Later stages of Oxidation.

The gravimetric results for the later stages of oxidation are shown in Figs. 19 and 20. Below 570°C the results show a continuous relationship between weight-gain and time, the slope of which decreases as the thickness of oxide on the metal increases. At any given temperature there is a large difference between the weight-gains sustained by the hydrogen annealed Armco, and the vacuum annealed Battelle iron series of specimens. Above 570°C the results show a rectilinear relationship between weight-gain and time. In this case there is no marked difference in behaviour between the two series of specimens, the slopes of the straight lines being approximately the same in both cases. The slight displacement of the lines relative to one another is due to the different behaviour exhibited by the two series of specimens during the nucleation and growth phase of the reaction. The slopes of the straight line regions of Fig.20 are recorded in table 4.

At temperatures above 660°C the uptake of oxygen

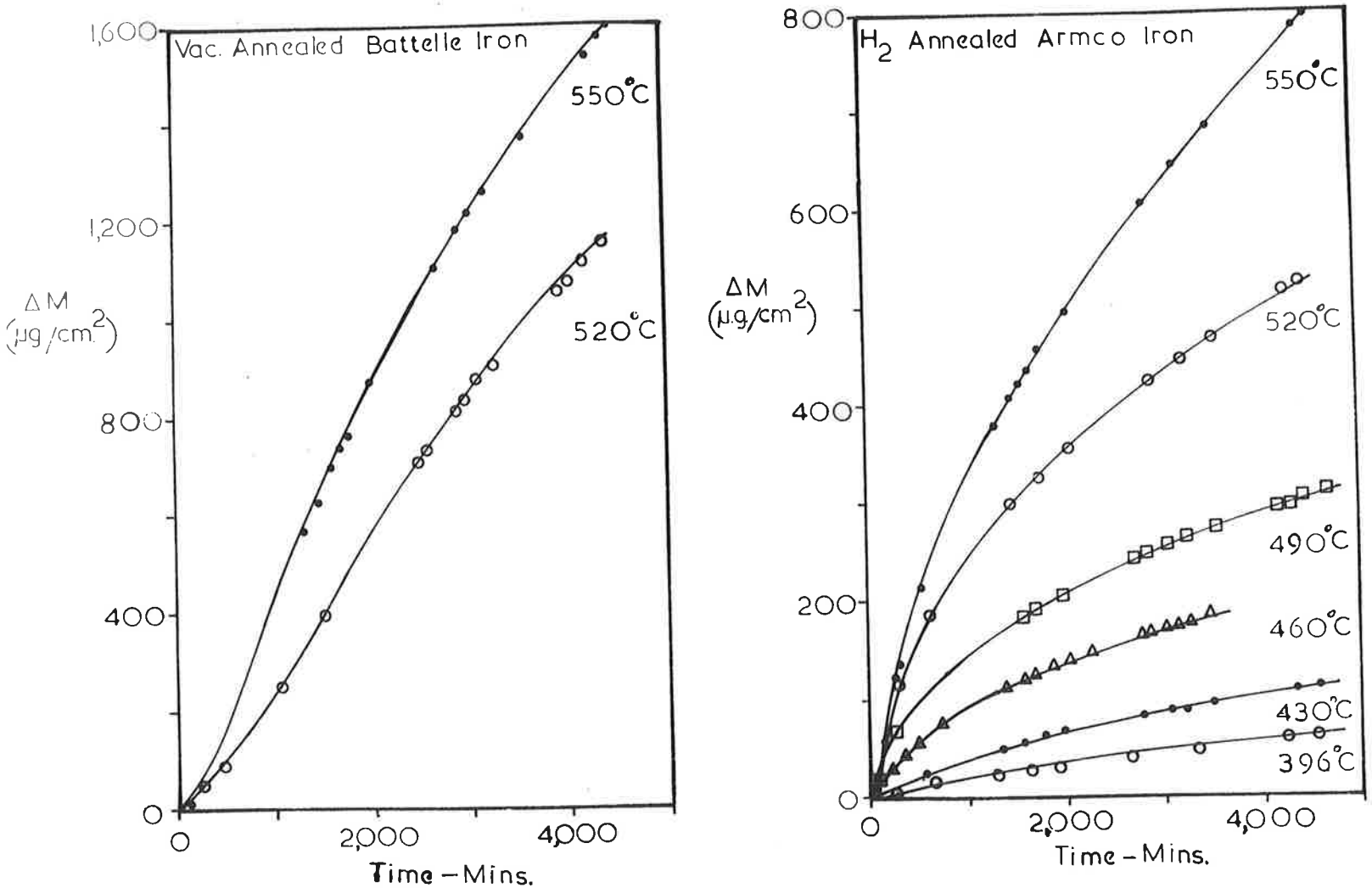

Fig.19 Gravimetric results for the latter stages of oxidation, < 570°C.

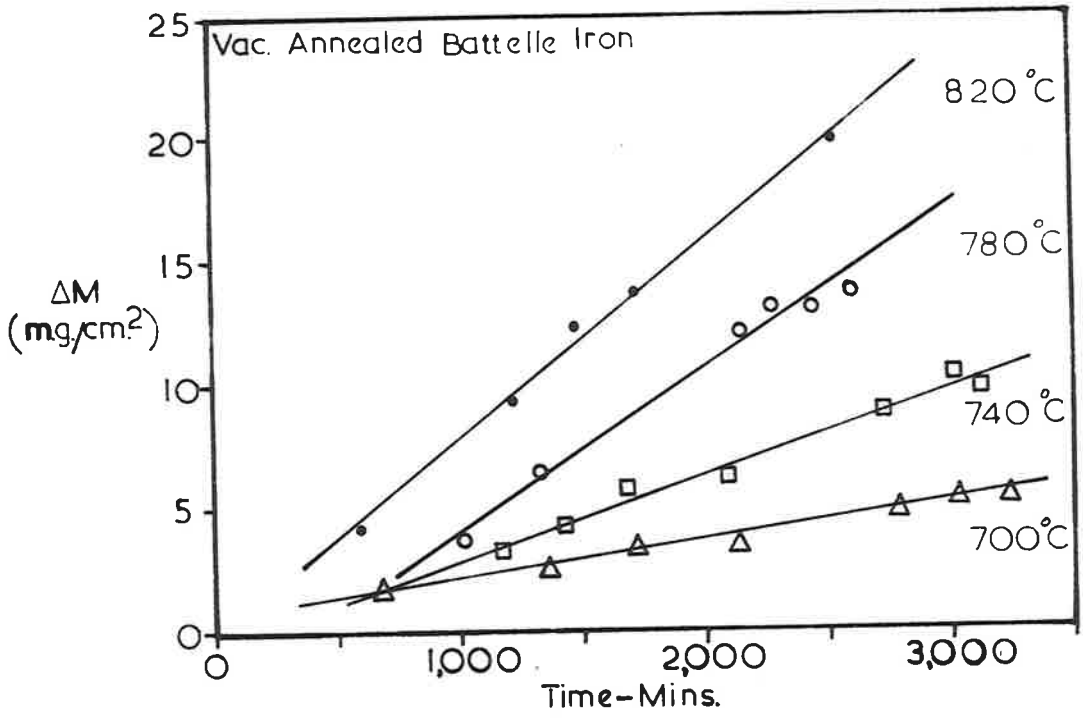

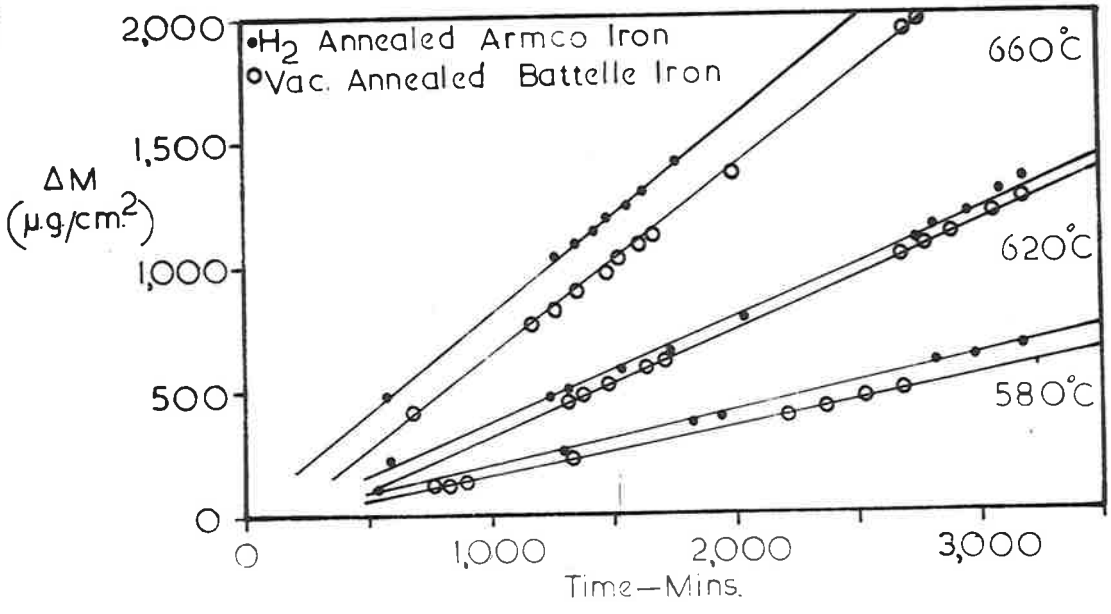

Fig.20 Gravimetric results for the latter stages of oxidation > 570 °C.

Table 4.

Linear rate constants for wustite scale formation.

T°C	K_l (mg/cm^2)/min. (H_2 annealed Armco iron)	K_l (mg/cm^2)/min. (Vac. annealed Battelle iron)
580	0.207	0.202
620	0.403	0.429
660	0.803	0.777
700		1.51
740		3.51
780		5.45
820		7.84

during the later stages of oxidation was more than could be conveniently measured on the balance and a new weighing procedure had to be adopted. A series of specimens were prepared, accurately weighed, placed inside a furnace, and given identical treatment to those oxidized on the microbalance. After being oxidized for varying lengths of time specimens were removed from the hot zone of the furnace. At the end of a run the specimens were again weighed and from the difference between the initial and the final weighings the weight-gain of oxygen was calculated.

The oxidation of iron by carbon dioxide involves the production of one mole of carbon monoxide for every mole of carbon dioxide consumed. As the experiments were performed in stagnant atmospheres it was unavoidable, particularly at the higher temperatures, that some build up of carbon monoxide would occur during the progress of the reaction. Increasing amounts of carbon monoxide in the gas phase would have the effect of reducing the oxygen potential of the gas and hence the rate of reaction. However, Smeltzer[45,53] has shown that in carbon dioxide - carbon monoxide gas mixtures the linear rates of wustite scale and film formation are directly proportional to $(N_{CO_2} - N^{*}_{CO_2})$, that is at any given temperature the rate of reaction is proportional to $(p_{CO_2}/p_{CO_2} + p_{CO})$. It can be seen that a small increase in the term p_{CO} would

have a negligible effect on the rate of reaction.

As the balance case and the associated pumping lines had a volume of approximately 5 litres it has been calculated that at 25°C and 200 mm Hg total pressure the amount of carbon dioxide contained within the system would be 0.0538 g moles. For a specimen having an area of 7.5 cm^2 an oxygen uptake of 1 mg/cm^2 would correspond to the production of 0.000234 g moles of carbon monoxide. This would represent a carbon monoxide content in the gas phase of approximately 0.86%. Consequently the procedure was adopted of completely changing the gas within the balance whenever the oxygen uptake of the specimen approached 0.5 mg/cm^2. This procedure limited the maximum carbon monoxide content of the gas, attained during an experiment, to 0.43%.

4.3 Metallography.

Microscopic examination of the oxide was undertaken to provide additional information regarding the mode of growth and the structure of the oxide with which to supplement the kinetic data obtained from the microbalance. During the initial stages of the reaction the surface of the metal was viewed directly under the microscope, but as the reaction progressed and the oxide became thick enough to be mounted, polished sections through

the oxide layer were then examined.

Examination of the metal surface during the early stages of the reaction revealed that the specimens were completely covered by a thin oxide film. From the interference colours it was concluded that this film was extremely thin and that it varied in thickness from grain to grain of the underlying metal. Scattered over the surface of this basal film were oxide nuclei which appeared as dark coloured dots when viewed through the microscope. As the reaction progressed the nuclei grew in size until they completely covered the surface. During this phase of the reaction some impingement of the nuclei took place. This phase of the reaction was also accompanied by a marked increase in the surface roughness of the oxide layer as some of the nuclei ingested their neighbours and grew at a very rapid rate. Metallographic sections through the specimen revealed that peculiar growth forms occurred during this stage of the reaction.

Difficulty was experienced in obtaining a suitable mounting and polishing procedure for the metallographic sections. Most of the common mounting materials proved to be too soft and considerable relief occurred during polishing. This left the specimen unsupported and caused the oxide to break up, thus allowing large pieces to be torn from the mount. This difficulty was largely overcome by mounting

the specimens in Formvar (a plastic with a polishing rate approaching that of steel). The specimens were mounted in this material according to the procedure described by Hardy and Hopkins[85], and then wet abraded through the various grades of silicon carbide paper. The polishing operation was performed on a Syntron vibratory polishing machine using three grades of alumina which were supported on hard nylon cloths.

Photomicrographs of some of the polished sections are shown in Figs. 21 and 22. The metal and the oxide appear in the photomicrographs as white and grey coloured phases respectively. As a further precaution against relief occurring during the polishing operation the specimens were either mounted in pairs, back to back, or between two pieces of iron. These methods of mounting are illustrated in Figs. 22a and 22c. As mentioned previously there is a transition stage between the time that the nuclei nearly cover the surface of the metal until the time that a uniform oxide topography is assumed. During this stage a considerable increase in the surface roughness of the oxide occurs. Figs. 21a and 21b illustrate the irregular nature of the surface during this stage of the reaction, and also some of the peculiar growth forms which were observed to occur.

As the reaction proceeded further the irregular-

a. 780°C
540 $\mu g/cm^2$
X 350

b. 780°C
540 $\mu g/cm^2$
X 350

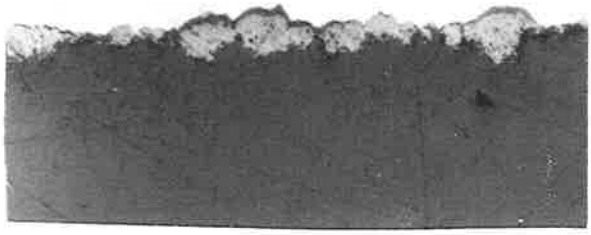

c. 780°C
2600 $\mu g/cm^2$
etched 10 secs.
in warm dil. HCl
X 350

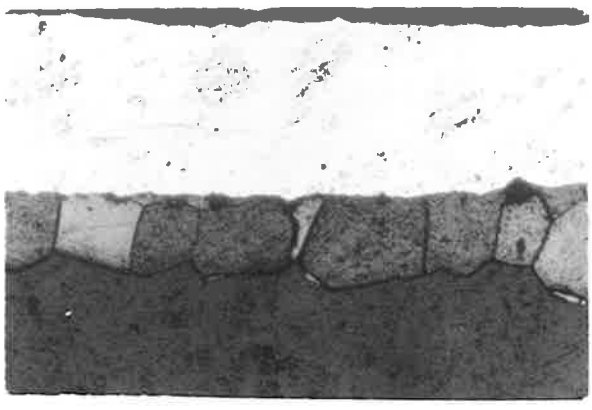

Fig.21 photomicrographs of metallographic sections.

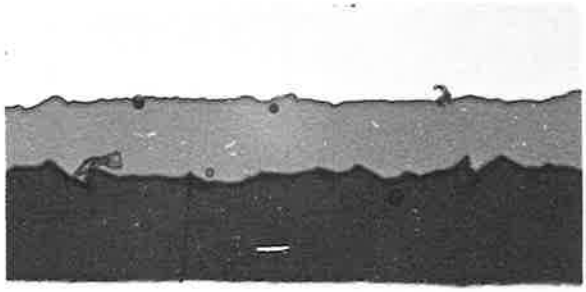

a. 780°C
2600 µg/cm²
X 350

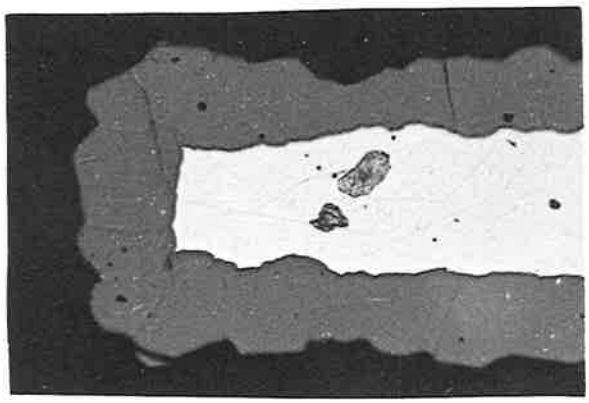

b. 740°C
3120 µg/cm²
X 350

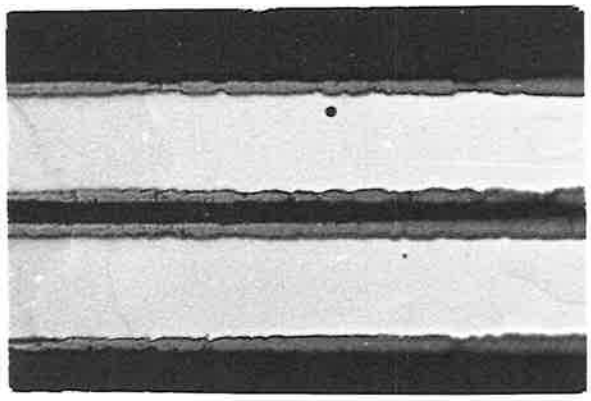

c. 550°C
1620 µg/cm²
X 350

Fig.22 Photomicrographs of metallographic sections.

ities were reduced until a relatively uniform topography was obtained as is shown in Figs. 22a, 22b and 22c. These photomicrographs show the presence of only one scale layer. No duplex scales were encountered on any of the metallographic sections examined. Also the oxide that has formed is protective and is free from cracks and voids and no blistering has occurred. Fig 22b illustrates the way in which the wustite scale layer has conformed to the end of the specimen, and that no end effects have occurred due to uneven oxidation in this region of the specimen. Only a few specimens were etched but it was established that the grain size of the oxide increased with increasing temperature. Fig. 21c shows the large grain size present in a wustite scale formed at 780°C.

4.4 X-Ray Diffraction Analysis.

The various oxide phases produced during the oxidation study were identified by means of an x-ray diffractometer. Copper Kα radiation was produced in a Philips PW1009 x-ray generator. The diffractometer (made by Crystal Structures Ltd., Cambridge, England) employed a source to image distance of 10 inches with 2 degree Soller slits in the incident and reflected beams. The nickel filter was placed on the detector side of the exit Soller slits.

The counting train employed a Philips proportional counter with pulse-height discrimination driving a Honeywell Brown recorder. This system eliminated the background count due to fluorescence from the iron specimen. The diffractometer was set up using a standard silicon powder sample and was accurate to within 0.05 degrees of 2θ. A scanning rate of 20 degrees of 2θ per hour was employed.

A series of specimens were prepared for x-ray diffraction analysis by oxidising samples of iron for varying times at different temperatures. Phase transformations on cooling were prevented from occurring by rapidly 'quenching' the specimens from the reaction temperature. This was accomplished by quickly removing the furnace from around the specimen and allowing it to cool to room temperature. The specimens were then transferred to the specimen holder of the goniometer and were scanned through values of 2θ from 20 to 120 degrees. The 2θ values of the diffraction peaks were read from the recorder chart, converted to d values, and compared with the standard x-ray diffraction patterns for the iron oxides given in the A.S.T.M. standards. On the basis of this comparison it was subsequently established that the oxide phases present were either wustite or magnetite, depending upon whether the temperature of formation was above or below the wustite eutectoid point (570°C). Some typical results are shown in the

following tables.

No attempt was made to obtain full powder patterns as the d values of the standard diffraction patterns for haematite, magnetite and wustite are sufficiently different to enable identification to be made solely on the basis of the positions of the diffraction peaks. The relative intensities of the diffraction peaks differed markedly from those given in the standard patterns, being dependent on such factors as the thickness, grain orientation, and grain size of the oxide layer. For this reason the relative intensities have not been included in the following tables.

In addition not all the diffraction peaks given in the standard patterns were detected. However, reference to tables 5,6 and 7 shows that sufficient peaks were obtained to establish definitely that, depending upon whether the temperature of formation was above or below 570°C, the oxide present consisted wholly of either wustite or magnetite. In addition to the oxide peaks the diffraction patterns, particularly for specimens with thin oxide films, also showed the presence of the α iron substrate.

Table 5.

X-ray diffraction analysis of a magnetite scale.

(Temp. of formation 550°C; Weight-gain 1620 $\mu g/cm^2$;

Battelle iron.)

This Study		A.S.T.M. d values	
2θ	d	Fe_3O_4	α Fe
-	-	4.86	
30.1	2.97	2.97	
35.5	2.53	2.53	
-	-	2.425	
45.1	2.010	2.097	
-			2.0268
53.4	1.715	1.714	
57.0	1.615	1.615	
62.6	1.484	1.484	
65.1	1.4328		1.4332
72.0	1.312	1.326	
-	-	1.279	
75.0	1.266	1.266	
-	-	1.209	
-	-		1.1702
-	-	1.120	
89.4	1.096	1.091	
-	-	1.048	
-	-		1.0134
-	-	0.988	
-	-	0.968	
-	-	0.938	
-	-		0.9064

Table 6.

X-ray diffraction analysis of a wustite scale.

(Temp. of formation 780°C; Weight-gain 930 mg/cm^2; Armco iron.)

This Study		A.S.T.M. d values	
2θ	d	FeO	αFe
36.1	2.488	2.486	
42.0	2.151	2.153	
44.7	2.027		2.0268
60.8	1.523	1.523	
65.1	1.433		1.4332
72.7	1.300	1.299	
82.4	1.170		1.1702
-	-	1.243	
91.4	1.077	1.077	
-	-		1.134
102.5	0.988	0.988	
106.2	0.964	0.963	
-	-		0.9064

Table 7.

X-ray diffraction analysis of a wustite scale.

(Temp. of formation 780°C; Weight-gain 13700 $\mu g/cm^2$; Battelle iron.)

This Study		A.S.T.M. d values	
2θ	d	FeO	αFe
36.0	2.495	2.486	
41.8	2.160	2.153	
-	-		2.0268
60.7	1.526	1.523	
-	-		1.4332
72.8	1.299	1.299	
-	-		1.1702
76.7	1.242	1.243	
-	-	1.077	
-	-		1.0134
102.5	0.988	0.988	
106.3	0.963	0.963	
-	-		0.9064

5. DISCUSSION OF RESULTS.

5.1 The Electrical Capacity and Resistance Measurements.

The E-C curves indicate that the capacity measurements can be divided into three sections (see table 3).

a) Capacities of about 30 - 70 $\mu F/cm^2$ corresponding to the electrical double layer capacity which were exhibited at the start of the anodic polarization when there was no oxide film on the surface.

b) Capacities which range from 300 up to 1500 $\mu F/cm^2$ (depending on the pH of the electrolyte) which appear to be related to reversible electrochemical reactions occurring at the electrode surface.

c) Peak values of the capacity which occur at potentials slightly in excess of those corresponding to the Fe_3O_4/Fe_2O_3 equilibrium potential, after which the capacity rapidly decreases to values which are equal to or smaller than double layer capacity.

The value of the capacity of the electrical double layer on mercury is about 16 $\mu F/cm^2$[86,87], the apparent area being taken as equal to the true area; with other electrodes the value of the capacity per unit area will depend on the method of surface preparation as this would vary the true area of the electrode surface. Thus capacity measurements made in the range of potential where the

electrode exhibits double layer capacity may be used to gain some idea of the surface roughness of the electrode surface. On the assumption of the above value of the double layer capacity the surfaces of the hydrogen reduced electrodes used in this study would have surface roughness factors which range from 2 to 4.

As the peak values of the capacity and conductance occur at potentials in the vicinity of the Fe_3O_4/Fe_2O_3 equilibrium potential a possible explanation of these results is that a rapid reversible equilibrium was occurring between the ferrous and ferric cation sites in the film. It would be expected that the magnitude of these measurements would depend upon the composition of the film and as such they could be used to furnish information regarding the defect composition of thin films. At more noble values of the potential the remaining ferrous sites in the were rapidly oxidized and the capacity and conductance measurements decreased in value until the film assumed the proportions of an inert dielectric film placed between the electrode and the electrolyte. Under these circumstances the capacity measured less than double layer capacity and depended upon the thickness and the dielectric properties of the oxide film.

The absence of a clearly defined second arrest in the potential versus quantity curves (E-Q curves)

rendered it impossible to use these results to estimate the amount of oxide formed upon the electrodes. Thus it was not possible to fulfill the main aim of this part of the experimental program which was to compare the capacity and resistance measurements made upon oxide films containing known amounts of oxide. Evidently the bulk of the current consumed in the establishment of the first arrest in the E-Q curves was being expended on the formation of iron ions in solution and it was only at the highest values of the pH that a measureable amount of oxide was formed upon the surface of the specimen. To achieve higher values of the pH than were used in this study it would have been necessary to employ carbonate buffer solutions. However as the pH-potential diagram for the $Fe-H_2O-CO_2$ system[88] shows that under some conditions it is thermodynamically possible to get carbonate formation, further test work in this range of pH was not embarked upon. Instead it was decided that a more fruitful approach would have been to form oxide films of known quantity and composition by thermal oxidation and recommendations to this effect are contained in section 5.6.

5.2 Decarburizing.

All the specimens were prepared by wet abrasion on silicon carbide papers and as a result of this method

of preparation they were covered with a thin hydrated oxide film. The vacuum annealed series of specimens initially lost weight during the vacuum anneal due to the dehydration of this residual film, but after a short period of time the Battelle and decarburized Armco iron commenced to oxidize and slowly gain weight. However, the ordinary specimens of Armco iron continued to lose weight, and lost weight at an accelerated rate when carbon dioxide was admitted to the system. Those specimens of Armco iron which were hydrogen annealed lost weight during the hydrogen anneal due to the dehydration and reduction of the initial oxide film. These specimens gained weight when vacuum annealed and immediately commenced to oxidize when carbon dioxide was admitted to the system. As the Armco iron used in these experiments contained approximately 0.02% carbon the different behaviour exhibited by the ordinary specimens of this material during the vacuum annealing and subsequent oxidation stages is attributed to a preferential decarburizing reaction.

If the ordinary specimens of Armco iron were left in the carbon dioxide atmosphere for long enough they started to oxidize and gained weight at a much greater rate than was experienced with any of the other specimens. Examination of the specimens shortly after they had started to gain weight revealed some interesting features. Firstly the oxidation product was not evenly distributed over the sur-

face of the metal; the greatest thickness of oxide being formed at the bottom of the specimen. Secondly in some cases it was possible to stop the reaction and observe that oxidation had taken place on the bottom of the specimen while the top was still unoxidized. Fig. 23 shows a photograph of a specimen which had been oxidized to this stage and reveals the band-like structure of the oxide which results. Evidently the carbon monoxide produced during the decarburizing of the bottom portion of the specimen was rising about the specimen and hindering the decarburizing of the top portion. Decarburizing of the bottom of the specimen would proceed rapidly and reach sufficiently low limits for oxidation to take place while the top was still decarburizing. The band-like structure of the oxide would be a result of the diffusion pattern set up around the specimen. It is also likely that once the oxidation starts the very rapid rate of oxygen uptake is associated with cracking of the oxide layer due to a continuation of the decarburizing reaction.

5.2.1 Decarburizing Limit.

Reference to Fig. 1 shows that iron is the stable phase over a wide range of gas compositions. Dissolved in the ferrite is a certain amount of carbon which is in equilibrium with the gas phase. The equilibrium carbon levels are shown by the diagonally sloping lines which traverse the

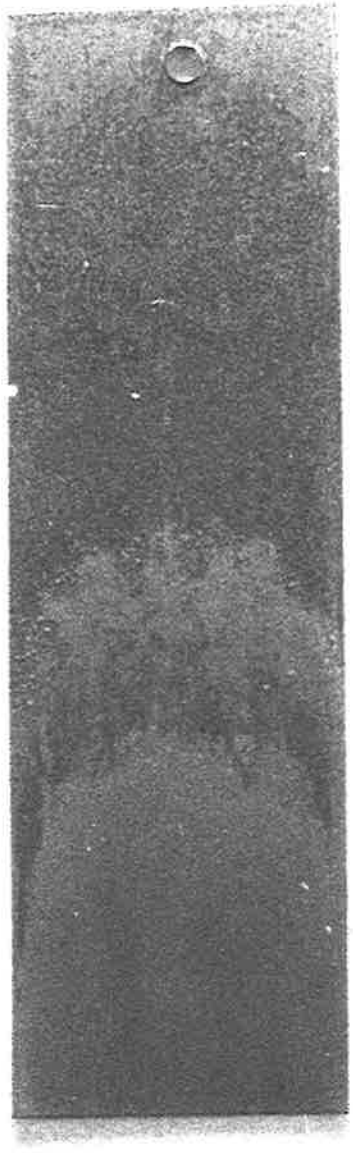

Fig.23 Photograph of a decarburized specimen.

the iron phase field and are terminated at the phase boundaries. If the composition of the gas is made more oxidizing than that in equilibrium with iron - that is by increasing the carbon dioxide content of the gas - it becomes thermodynamically possible for the iron to oxidize and become covered with an oxide layer which would hinder the decarburizing reaction. It is unlikely however that any oxide would form until the carbon content of the surface had been reduced to that corresponding to the Fe/FeO limit. That is the material would preferentially decarburize because any oxide produced would be reduced by the carbon monoxide generated by the decarburizing reaction. Carbon contents corresponding to the Fe/FeO limit have been read from Fig. 1 and are shown plotted as a function of temperature in Fig. 24.

At any given temperature a specimen having a carbon content in excess of that shown in Fig. 24 should undergo a preferential decarburizing reaction until the carbon content of the surface had been reduced to that corresponding to the Fe/FeO limit. Thus the Armco iron used in these experiments would be expected to decarburize preferentially since its carbon content was approximately 0.02%. Similarly iron having a carbon content of 0.004% would also be expected to decarburize at temperatures above 650°C. Smeltzer[53] has used iron containing this percentage of carbon in his investigation of the oxidation of iron in a 50% CO-CO_2 mixture at

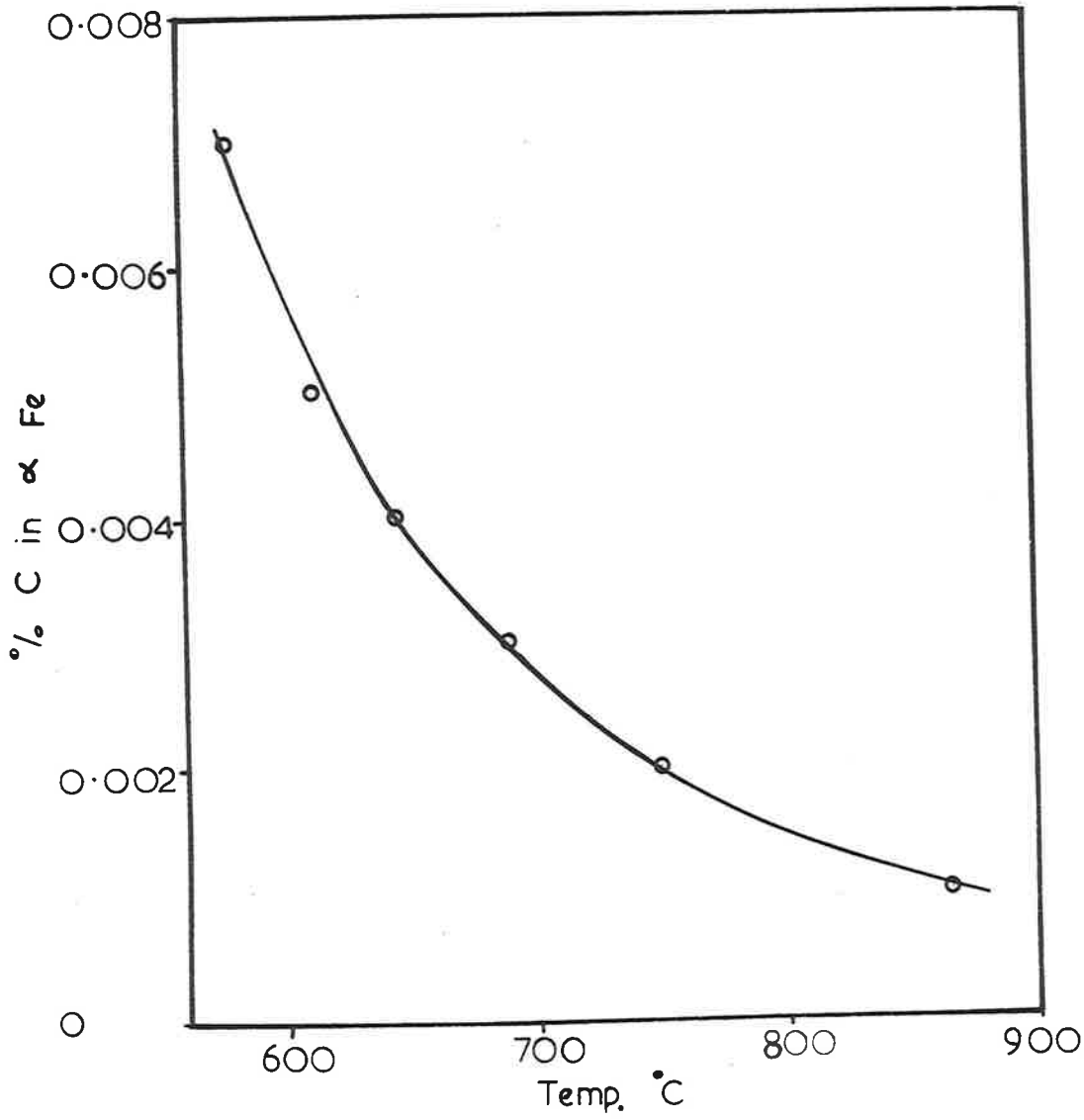

Fig.24 Decarburizing to the Fe/FeO limit.

200 mm Hg total pressure. Although he makes no specific mention of having encountered decarburizing it is very likely that he has, and that his elaborate heating procedure can be explained on this basis. Prior to oxidation Smeltzer annealed his specimens under a vacuum of 10^{-5} to 10^{-6} mm Hg, during the heating period of approximately 3 hrs. to 890°C, and annealed them for a further 3 hrs. at this temperature before adjusting the temperature of the furnace to the reaction temperature. Such a procedure could have been used to reduce the carbon content of his specimens to a very low level.

One of the effects of the hydrogen anneal on the Armco iron was to virtually eliminate all the carbon from the specimens. Calculations have been made in Appendix A which show that, by annealing specimens of Armco iron in an atmosphere of dry hydrogen at 800°C, it is thermodynamically possible to obtain carbon contents of 0.00018%. Such material would not decarburize. The Battelle iron used in this project had a carbon content of 0.001% and no evidence of decarburizing was obtained with this material. However, Fig. 24 shows that if this material had been oxidized in the temperature range 880 - 910°C this behaviour may have been encountered. (The restriction of 910°C is placed upon the upper limit of temperature, since at this temperature the $\alpha - \gamma$ transformation occurs in iron, and the

equilibrium carbon levels in austenite are much greater than they are in ferrite.)

5.2.2 Blistering and Flaking of the Oxide.

When an iron-carbon alloy is placed in an oxidizing atmosphere the specimen undergoes a preferential decarburizing reaction until the carbon content of the surface layers of the metal has been reduced to such an extent that it possible for oxide formation to occur. Accompanying this phase of the reaction is the establishment of a diffusion gradient of carbon from the surface into the interior of the specimen. The amount of carbon eliminated would depend upon:-

a) the thickness of the specimen
b) the initial carbon content of the specimen
c) the rate of diffusion of carbon within the specimen.
d) the rate of removal of carbon at the metal/gas interface.

Such factors can probably explain the observations of Upthegrove and Murphy[89] that mild steel oxidized in carbon dioxide did not blister whereas that subjected to a more rapid oxidation in air did blister. The steel oxidized in carbon dioxide would have a lower overall carbon

content before oxide formation occurred than that oxidized in air. Evidently the residual carbon content of the steel that was oxidized in air was sufficient to cause blistering whilst that of the steel oxidized in carbon dioxide was not.

Once an oxide layer has formed the removal of carbon from the specimen by direct reaction with the gas phase is no longer possible and the carbon content of the surface of the metal would tend to increase due to the continued diffusion of carbon from the interior of the specimen. When the carbon content of the surface exceeds that corresponding to the Fe/FeO limit it becomes possible for the carbon to react with the oxide and produce pressures of carbon monoxide which would certainly rupture the oxide. However, Engell[90] has analysed the scales formed on a series of iron-carbon alloys and has shown the presence of a small but definite amount of carbon in the oxide layers. It is evident that some carbon can escape by way of solution in the oxide. Also Warner[91] has recently shown that wustite is slightly porous and it would thus be possible for the gaseous oxidation products to escape by diffusion through these pores. Blistering would then only occur at the metal/oxide interface if the amount of carbon being transported through the pores as gaseous oxidation products required too high a pressure differential across

the oxide.

5.3 The Nucleation and Growth of an Oxide Phase on a Metal Surface.

Some theoretical expressions concerned with the rate of nucleation and growth of an oxide phase on a metal surface have been considered in section 2.4.3. The weight-gain versus time curves resulting from these expressions have the common feature that initially the curves are concave upwards to the time axis. Experimental gravimetric curves having this shape have been produced during the oxidation of copper by Wagner and Grunewald[92] and by Tylecote[93]. Similarly the curve for a magnetite layer growing laterally beneath a ferric oxide layer was also demonstrated, by Davies Evans and Agar[56], to be concave upwards. In each case the form of the curve was attributed to the oxide growing from localized sites and spreading to cover the surface of the metal.

As mentioned in section 4.2.2.1 curves having this shape have been obtained during the present study for the early stages of the reaction between iron and carbon dioxide. This indication that the early stages of the reaction were proceeding by a mechanism involving the nucleation and growth of an oxide phase was confirmed by microscopic examination of the surface of a series of speci-

mens oxidized into the concave upwards portion of the weight-gain versus time curves. It was observed that the oxide did not cover the metal surface uniformly but collected at localized sites, the density of which varied from grain to grain of the underlying metal.

5.3.1 The Nucleation of an Oxide Phase.

If it were possible to obtain a clean metal surface and to expose it to an oxidizing atmosphere then undoubtedly the first stage of the reaction would be the establishment of a chemisorbed layer of gas on the metal surface. This phase of the reaction would take place with extreme rapidity and it is unlikely that it would be observed except at low temperatures. Following the establishment of the chemisorbed film it would then be possible for an oxide film to form by one of the thin film mechanisms discussed previously in section 2.3. Such films are extremely thin and it is unlikely that they have a structure characteristic of the bulk oxide. For example, magnesium oxide normally has a cubic structure, but oxide films on magnesium have been found[94] to be hexagonal like the metal. Similarly crystalline alumina grown on aluminium prefers a face-centred cubic lattice[95,96] following that of the aluminium substrate.

Although the solubility of oxygen in iron is

generally considered to be very low some sub-surface penetration of oxygen must accompany the early stages of the reaction. In support of this view Rees[34] has calculated the mean diffusion paths for a number of gas/metal systems and has shown that at 500°K some gas atoms will certainly be found below the surface after one second's exposure. Thus it is possible to visualize two processes competing for the available oxygen at the gas/metal interface. Under certain conditions such as high rates of solution of oxygen in the metal and only weakly oxidizing conditions at the gas/metal interface it is probable that the oxide film would not start to form until an appreciable quantity of oxygen had dissolved in the metal.

According to the views of Rees[34], and to those of Benard and his colleagues[97], the oxide nuclei form as a result of the metal becoming superficially saturated with oxygen. The oxide nuclei thus form in the layers of metal adjacent to the surface and not in the initial thin film. Recent work on copper[30] and cadmium[98] has allowed the incubation time (the time observed to elapse before the nuclei make their first appearance) to be identified as the time necessary to accomplish the superficial saturation of the metal with oxygen. These studies have also shown that varying the oxygen content of the metal can have some effect on the number of nuclei produced, and

in some cases even alter their mode of formation.

In most cases it was not possible to obtain a gravimetric record which corresponded to the formation of the nuclei as this phase of the reaction was either over too quickly to be observed or it had already taken place during the vacuum anneal. However, at 396°C - the lowest temperature studied - it was possible to obtain this information and the data is shown in Fig. 25. It can be seen that the rate of oxygen uptake decreased until a total weight-gain of approximately 0.7 $\mu g/cm^2$ had been achieved. This would correspond to the formation of a magnetite film 50 Å thick or alternatively, if the oxygen was uniformly distributed throughout the metal, would correspond to a solid solution having an overall oxygen content of 0.206×10^{-6} weight percent. If this stage of the reaction involves the solution of oxygen in the metal then according to Crank[99] the relationship between the oxygen uptake ΔM, and time t, should be of the form

$$\Delta M = 2C_1 (Dt/\pi)^{1/2}.$$

Where D is the diffusion coefficient of oxygen in the metal, and

C_1 the concentration of oxygen at the metal/gas interface which is assumed to remain constant.

Consequently a plot of ΔM against $t^{1/2}$ should yield a

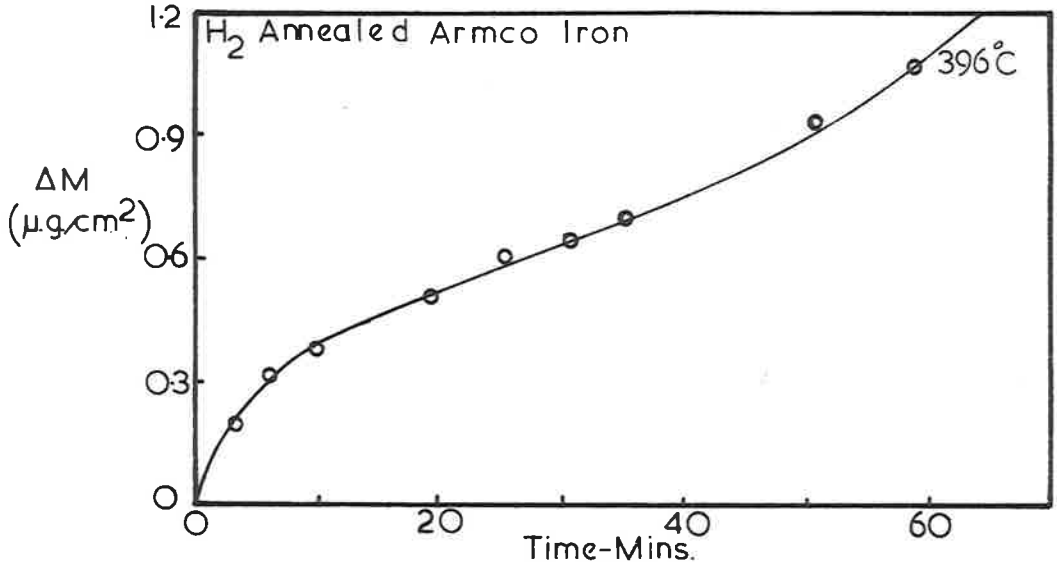

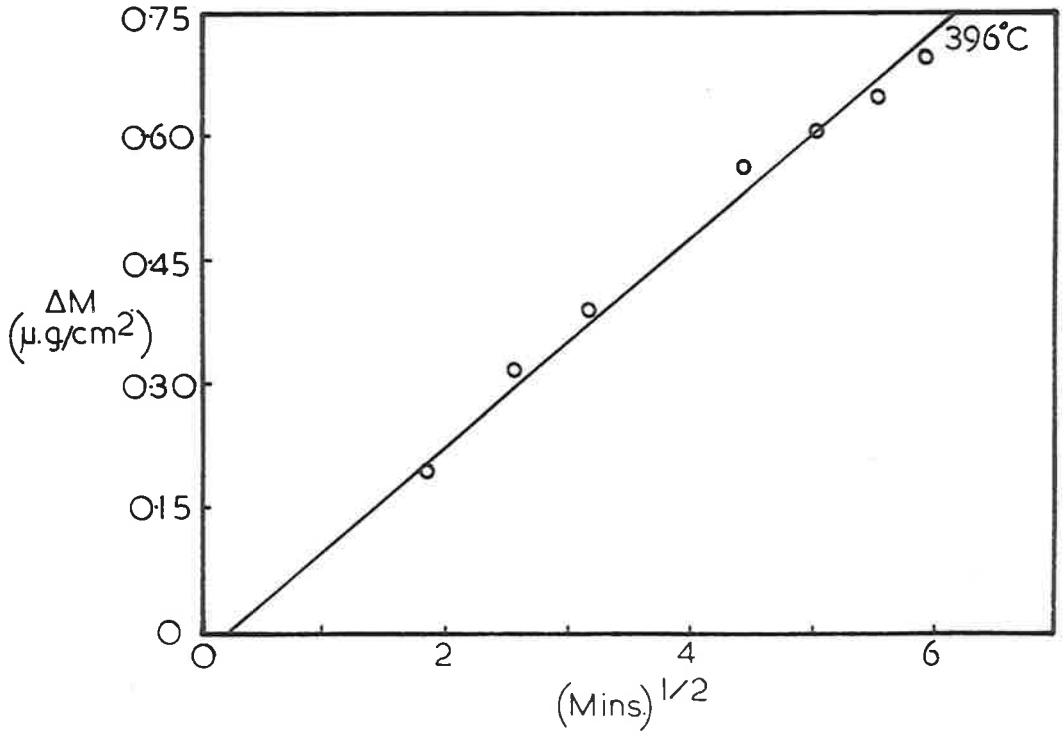

Fig.25 Gravimetric record for the formation of oxide nuclei.

straight line. The results have been plotted in this fashion in Fig.25 from which it can be seen that a reasonable fit of the data has been obtained. Thus this stage of the gravimetric record could correspond to the solution of oxygen in the metal and would be evidence to support the view that the nuclei form as a result of the metal becoming superficially saturated with oxygen.

5.3.2 The Growth of Oxide Nuclei.

At most of the temperatures studied the nuclei had either formed during the vacuum anneal or they formed very soon after the admission of carbon dioxide to the system. Hence the majority of the gravimetric results for the early stages of the reaction deal with the growth rather than the formation of oxide nuclei. As discussed previously in section 4.3 microscopic examination of the specimens revealed that some time after the nuclei had formed they were surrounded by a thin oxide film, the thickness of which varied from grain to grain of the underlying metal. The gravimetric results were thus a measure of the amount of oxygen consumed by the growth of this oxide film as well as that consumed by the growth of the nuclei. However, the film was extremely thin and the amount of oxygen composing the film would be small in comparison with that composing the nuclei, and it would

therefore be a valid approximation to take the measured weight-gains as being due to the oxygen consumed by the nuclei alone.

Rees[34] has stated that only those pre-nuclei with built-in conditions for growth (e.g. screw dislocations) can become nuclei and under these conditions it would be expected that the rate of growth would be limited by the supply of oxygen. According to Benard[27] the rate of growth is limited by the rate of surface diffusion of material over the surface of the basal film, but another possibility is that the nuclei are being supplied from the adjacent areas of oxygen rich metal by the lateral diffusion of oxygen through the sub-surface layers of metal. As a nett result of either mechanism the nuclei would receive oxygen by supply to their outer peripheries and the rate of growth would depend upon the area of this interface. For oxide nuclei based either on or in the surface layers of the metal, the area of this interface would be proportional to the perimeter of the base of the nuclei.

5.3.3 The Rate of Growth of Oxide Nuclei.

Recently published photomicrographs[99,100,101] of oxidized and sputtered metal surfaces show that in a large number of cases the nuclei grow in the form of

tetrahedra. It has been assumed that the nuclei formed in this study also have this shape and for the sake of simplicity they have been treated as being regular in shape. Then for a single nucleus

$$\frac{dw}{dt} = kp.$$

Where :- w is the weight of oxygen in an individual nucleus at time t.

p is the length of the perimeter of the base of the nucleus.

k is a constant at any temperature, the magnitude of which depends upon whether the trasport to or the incorporation of oxygen into the nucleus is the rate determining factor. Quantitatively k is a measure of the amount of oxygen crossing unit length of the perimeter in unit time.

By introducing ρ the density of oxygen in the oxide it is possible to relate p to w. Thus for the simple model outlined above

$$p = \frac{sw^{1/3}}{\rho^{1/3}}.$$

Where :- s is a geometrical factor having the value

$$3(6\sqrt{2})^{1/3}.$$

Substitution of this value of p in the original expression yields

$$\frac{dw}{dt} = \frac{ksw^{1/3}}{\rho^{1/3}}.$$

If the number of nuclei per unit area remains constant at a value n then M, the weight-gain per unit area of surface can be expressed as follows:-

$$\Delta M = nw$$

and

$$\frac{d(\Delta M)}{dt} = \frac{n^{2/3}ks(\Delta M)^{1/3}}{\rho^{1/3}}.$$

Integration of this expression yields

$$\Delta M^{2/3} = \frac{n^{2/3}kst}{\rho^{1/3}} + C,$$

or

$$\Delta M^{2/3} = Kt + C.$$

Where C is a constant of integration.

K is a bulk constant. At a given temperature K is a function of the number of nuclei per unit area, the shape and density of the nuclei, and the rate at which they grow.

It should be noted that the above derivation requires that:-

1) Once having formed, the number of nuclei remains constant.

2) There is no impingement of the nuclei.

With regard to the first restriction numerous workers [21,22,36] have shown that the number of nuclei is independent of time, while with regard to the second restriction

Benard and his colleagues[97] have shown that each nuclei is a discrete entity which is surrounded by a 'zone of influence' from which it collects material for its growth. Impingement would only occur when the nuclei had reached a sufficient size to actually touch one another.

Although this expression has been derived on the basis that the nuclei exist as regular tetrahedra, similar expressions, differing only in the value of s, could have been derived for other regular and irregular solid shapes.

The gravimetric results, up until the point of inflection in the weight-gain versus time curves, have been expressed in the form of $\Delta M^{2/3}$ against time in Appendix B.2.1 and the results obtained above 570°C are shown plotted in this form in Fig. 26. It can be seen that the results are consistent with the proposed model and that good straight line fits of the data have been obtained. The results below 570°C could not be plotted in this manner due to the large numbers of nuclei which were present. Interaction and impingement of the nuclei occurred very early in the reaction and it was not possible to observe the growth of individual nuclei at these temperatures.

The straight line data presented in Fig. 26 has been analysed by the method of least squares and the slopes of the lines, or values of K, are contained in table 8.

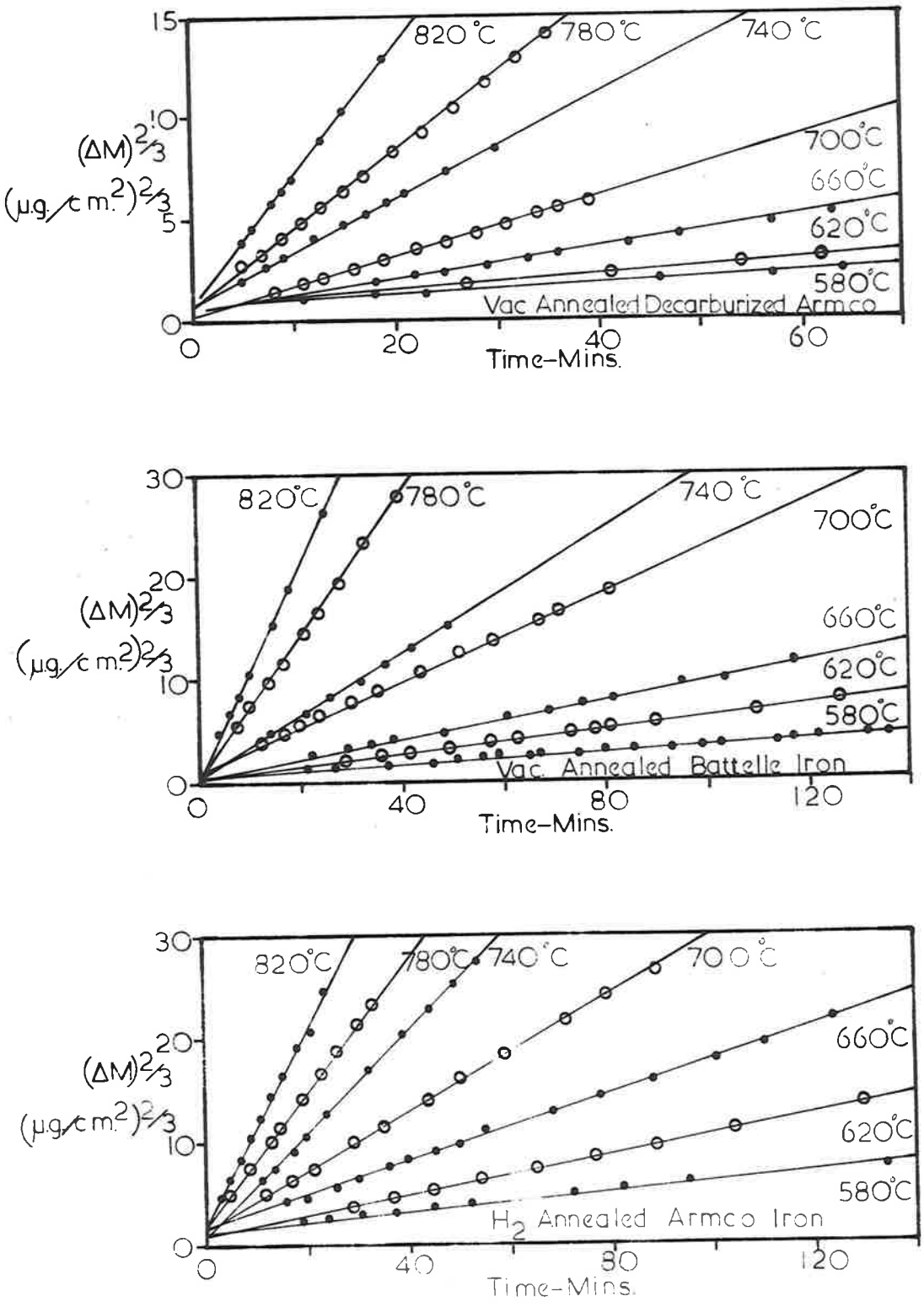

Fig.26 Gravimetric records for the growth of oxide nuclei.

Table 8.

Constants for the growth of oxide nuclei.

T °C	K values $(\mu g/cm^2)^{2/3}/min.$ Vac. annealed Armco iron.	Vac. annealed Battelle iron.	H_2 annealed Armco iron.
580	0.0234	0.0291	0.0457
580		0.0327	
620	0.0423	0.0608	0.0978
660	0.0777	0.0944	0.1537
660		0.1039	
700	0.1464	0.2152	0.2847
700		0.1875	
740	0.2511	0.3002	0.4904
780	0.3770	0.7158	0.6516
780		0.6267	
820	0.6322	1.0018	0.9520

Since K is a bulk constant, composed of a number of temperature dependent factors, there is little point in making an Arrhenius plot of the K values. For the sake of convenience these values have been plotted in the form of log K against $T^{o}C$, and the resulting graphs are shown in Fig.27. Up until $740^{o}C$ the graphs corresponding to the different forms of iron are parallel to one another and lie in the following order of increasing magnitude of K:-

vacuum-annealed (decarburized) Armco iron,

vacuum-annealed Battelle iron, and

hydrogen-annealed Armco iron.

This is also the order of decreasing initial oxygen content of the iron used in these experiments. It would appear that these results show the effect of the initial oxygen content on the number of nuclei which form under a given set of oxidizing conditions. Similar behaviour has been observed in the past for cadmium[98] and germanium[101]. Above $740^{o}C$ the graph for the Battelle iron specimens increases at a greater rate than that observed for either of the forms of Armco iron. It is thought that the difference in behaviour is due to the effect of impurities in the Armco iron hindering recrystallization during the vacuum-annealing stage which preceded the oxidation experiments. Different surface orientations would be produced which would affect the number of nuclei and hence the value of K.

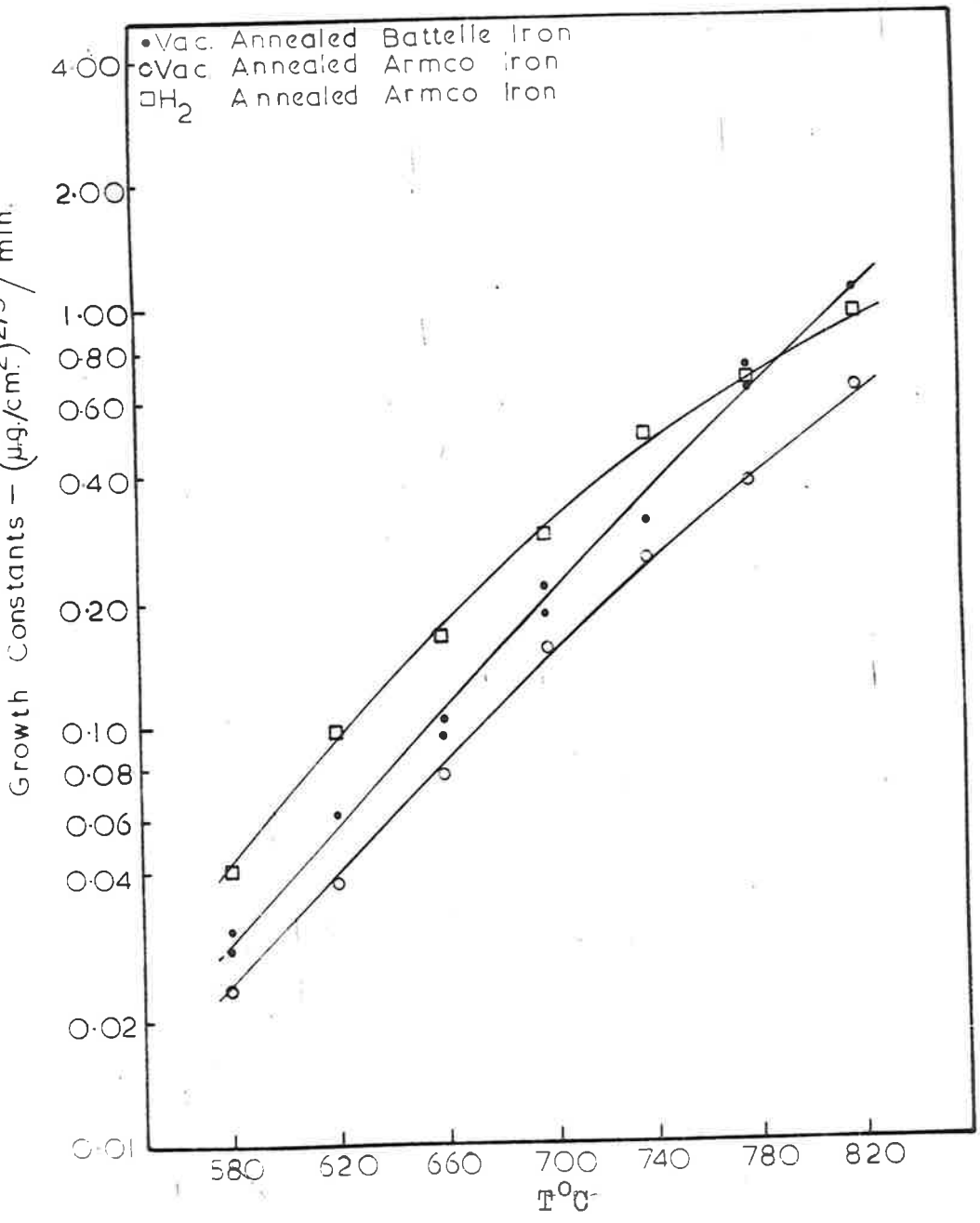

Fig.27 Constants for the growth of oxide nuclei vs temperature of formation.

5.4 The Mechanism of Magnetite Scale Formation.

Electrometric analysis of the oxide formed at temperatures below 570°C showed that, for the times of oxidation studied in this project, the oxide consisted wholly of magnetite. This finding was confirmed by x-ray diffraction analysis of the oxide. Microscopic examination of metallographic sections through the oxidized specimens also revealed the presence of only one oxide phase and showed that, except for the early stages of the reaction, the oxide formed a compact adherent layer which was free from cracks and voids.

The kinetics of the reaction, as represented by the weight-gain versus time curves of Fig. 19, showed that the rate decreased with increasing thickness of the oxide layer. This suggested that the rate of oxidation was controlled by the diffusion of material through the oxide layer. If this were the case then the gravimetric data should obey the parabolic law :-

$$\Delta M^2 = k_p t + C$$

Where ΔM is the weight-gain per unit area at time t.

k_p is the parabolic rate constant.

C is a constant.

According to this expression a plot of ΔM^2 versus time, t, should yield a straight line, the slope of which would be k_p.

Fig. 28 shows the data plotted in this fashion and it can be seen that, apart from the early stages of the reaction, the above expression provides a good fit of the experimental data. The corresponding values of the parabolic rate constants are presented in table 9.

Since the rate of magnetite formation is diffusion controlled the rate of growth would be a function of the diffusion coefficient and the concentration gradient across the oxide layer. Reference to the binary iron-oxygen phase diagram[2] shows that below 600°C the range of existence of the magnetite phase field is confined to very narrow composition limits. Consequently it would not be expected that the driving force for diffusion across the scale layer would vary much with temperature. Under these circumstances an Arrhenius plot of log k_p against the reciprocal of the absolute temperature should yield a straight line. This results from the fact that the growth rate would be a simple function of the average diffusion coefficient for the components of the scale.

An Arrhenius plot of the parabolic rate constants has been made in Fig. 29. It was found that the slope of the best fit straight line drawn through the experimental points corresponded to an activation energy of 38 kcals/mole. Paidassi[102] and Davies et al[6] have oxidized hydrogen reduced iron in air and oxygen respectively. At

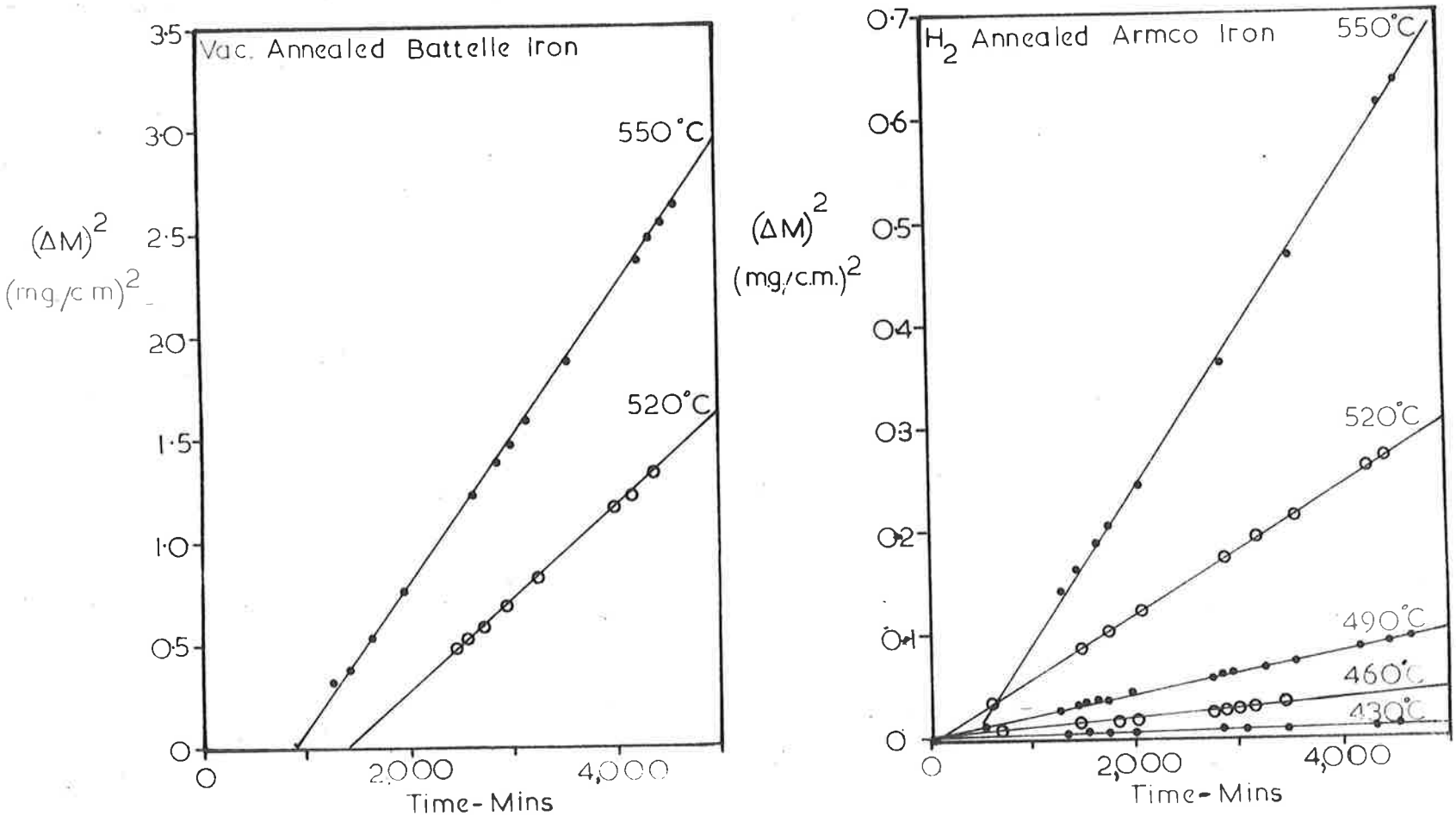

Fig.28 (Weight-gain)^2 vs time curves for magnetite scale formation.

Table 9.

Parabolic rate constants for magnetite scale formation.

T°C	k_p (mg/cm^2)^2/min.	
	H_2 annealed	Vac. annealed
	Armco iron	Battelle iron
395	0.763	
430	3.03	
460	9.84	
490	19.7	
520	73.6	433.0
550	158.0	719.0

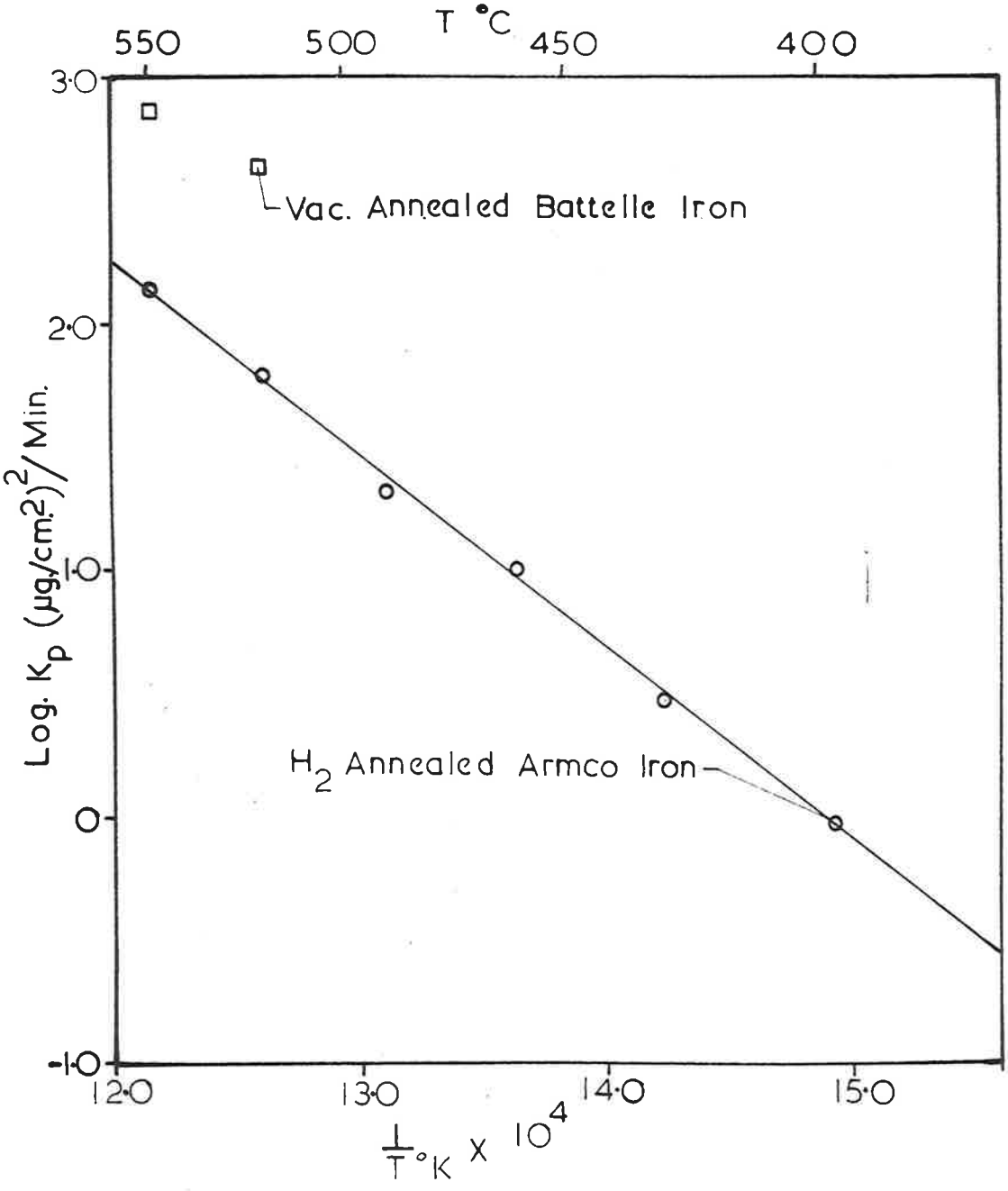

Fig.29 Arrhenius plot of the parabolic rate constants.

temperatures below 600°C they have both shown that the activation energy for the diffusion controlled process was approximately 39 kcals/mole. Davies and his associates conducted marker measurements concurrently with their gravimetric studies and from the position of the markers they concluded that the magnetite grew largely by oxygen ion diffusion, although there was an appreciable contribution of about 20% from iron ion diffusion.

So far no mention has been made of the fact that magnetite formed at a greater rate on specimens of vacuum-annealed Battelle iron than it did on specimens of hydrogen annealed Armco iron. The difference in oxidation rates is attributed to the effect of impurities present in the Armco iron. The oxygen ion diffusion occurs by way of oxygen ion vacancies in the magnetite lattice and since monovalent and divalent cations increase these vacancies oxidation of iron containing them will be greater than on iron itself. Such cations are

Cu^{+}, Cu^{++}, Ni^{++}, and Co^{++}.

On the other hand cations with valencies greater than two decrease the oxidation rate of iron. Any of the following cations would have this effect

Cr^{+++}, Al^{+++}, V^{+++}, Mn^{+++}, V^{+++++}.

As mentioned in section 3.3.1 the impurity level of the Armco iron is fairly high, the major impurities being

Mn 0.07%, and Cu 0.04%. From the preceding discussion it can be seen that the effect of the copper would be to increase the rate of oxidation, whereas the effect of the manganese would be to decrease the rate. Evidently the large manganese concentration counteracts the effect of the copper, and the nett effect is a reduction in the rate of oxidation of the Armco iron compared to that observed on the Battelle iron.

5.5 The Mechanism of the Linear Rates of Wustite Scale Formation.

X-ray diffraction analysis of the oxide formed above 570°C has shown that under the experimental conditions, and for the times of oxidation studied in this project the scale was composed of only one component, namely wustite. The oxidation kinetics (as represented by the gravimetric results) which correspond to this stage of the reaction can be represented by a linear relationship between weight-gain and time. Since the oxidation kinetics are independent of the instantaneous thickness of the oxide layer it was concluded that the oxide was either non-protective or that the rate of reaction was controlled by a phase boundary reaction.

Microscopic examination of metallographic sections through the scale layer has confirmed the presence of

only one component and has established that the oxide formed as a compact adherent layer which was free from cracks and voids, that is the oxide formed as a protective barrier between the metal and the gas phase and the oxidation kinetics cannot be explained on the basis of the cracking or blistering of this layer. Under these circumstances the linear oxidation kinetics indicate that the rate was controlled by a reaction at either the metal/oxide or the oxide/gas interface. Since the results of this and other studies[45,51] have shown that wustite was the only phase present during this stage of the reaction it has been concluded that the reaction was not limited by the supply of Fe^{++} ions at the metal/oxide interface.

Linear scaling kinetics would be observed if the reaction at the oxide/gas interface was limited by the gas phase transport of either carbon dioxide to, or carbon monoxide from the interface. The reaction at the interface would proceed to equilibrium and the driving force for diffusion would be $(p_b - p_i^*)$, where p_b is the partial pressure of the component in the gas phase, and p_i^* the partial pressure of the component in equilibrium with the oxide. This latter quantity may be evaluated from the work of Darken and Gurry[2]. By estimating the diffusion coefficient of carbon dioxide, and by assuming a value of the gas 'film thickness' over which it is assumed that the bulk

of the resistance to gaseous diffusion lies, it can be shown that the reaction would not be limited by the rates of gaseous diffusion until temperatures of the order of 1300 - 1400°C had been attained. Also the activation energy for gaseous diffusion is very small; reference to Fig. 30 an Arrhenius plot of the linear rate constants for the wustite scaling reaction shows that the activation energy for this process is quite considerable, consequently it was concluded that the reaction was not limited by the rates of gaseous diffusion.

The reaction at the oxide/gas interface involves the production of electron holes - $\oplus$ - and cation vacancies - $Fe_{\square}^{++}$ - and can be represented by the following equation :-

$$CO_2(g) = CO(g) + Fe_{\square}^{++} + 2\oplus.$$

By applying the principles of the law of mass action to the above equation an expression can be derived for r, the rate of reaction. Thus

$$r = k' p_{CO_2} - k'' p_{CO} [Fe_{\square}^{++}][\oplus]^2,$$

where k' and k'' are the velocity constants for the forward and reverse reactions respectively. At equilibrium the nett rate is zero, and

$$K = \frac{p^*_{CO_2}}{p^*_{CO}}$$

$$= \frac{k''}{k'}[Fe_{\square}^{++*}][\Theta^*]^2,$$

where the equilibrium values of the terms are denoted by an asterisk. Use of this expression to eliminate k'' from the rate equation yields,

$$r = k'(p_{CO_2} - \frac{K[Fe_{\square}^{++}][\Theta]^2 p_{CO}}{[Fe_{\square}^{++*}][\Theta^*]^2}) \qquad - (A).$$

The reaction at the oxide/gas interface may be sub-divided into a number of elementary reaction steps. Smeltzer[45] assumed that the carbon dioxide dissociated at the oxide surface to yield chemisorbed oxygen ions, carbon monoxide gas and electron holes in the oxide. The dissociation was followed by the incorporation of the chemisorbed oxygen ions into the wustite lattice which resulted in the formation of cation vacancies. The elementary reactions are represented by the following equations :-

$$CO_2(g) = O^{=}(ads.) + 2\Theta + CO(g) \qquad - (B).$$

$$O^{=}(ads.) = FeO + Fe_{\square}^{++} \qquad - (C).$$

According to Smeltzer the rate of linear scaling was determined by the rate of incorporation of chemisorbed oxygen into wustite at temperatures lower than 910°C, and by the dissociation of carbon dioxide and the incorporation of oxygen at higher temperatures.

5.5.1 Dissociation of Carbon Dioxide as the Rate-Determining Reaction.

If the dissociation of carbon dioxide, as represented by equation (B), is the rate-determining step in the reaction then the values of the concentrations of adsorbed oxygen ions, electron holes, and cation vacancies at the oxide surface would approach equilibrium values. Under these circumstances

$$\frac{[Fe_{\square}^{++}][\theta]^2}{[Fe_{\square}^{++*}][\theta^*]^2} \text{ approaches 1,}$$

and the expression for the rate simplifies to

$$r = k'(p_{CO_2} - Kp_{CO}).$$

By introducing the total pressure P, and the mole fraction of carbon dioxide N_{CO_2} and by rearranging,

$$r = k'P(K + 1)(N_{CO_2} - N^*_{CO_2}). \qquad - (D).$$

It should be noted that this expression is the same as that derived by Petit et al[50] for the dissociation of carbon dioxide.

By applying equation (D) to the linear rates of the wustite scaling reaction that have been measured by Smeltzer[45], Hauffe and Pfeiffer[48], Petit et al[50], and to the results of this study (contained in table 4), it is possible to evaluate k' over a wide range of temperature, pressure, and composition of the gas phase. The results

obtained by Fischbeck et al[43] have not been included in the analysis since their results above 900°C show considerable scatter. Their work can be criticized on the grounds of the heating procedure that they adopted; namely heating the specimens from room temperature to the reaction temperature in a very short time. Such a procedure would be conducive to cracking and spalling of the oxide which could explain the large amount of scatter in their results. To calculate k' it is necessary to know K and $N^*_{CO_2}$. These values have been obtained by interpolation between the data of Darken and Gurry[2], and are shown, together with the corresponding values of k', in table 10.

An Arrhenius plot of the velocity constant k' against the reciprocal of the absolute temperature is shown in Fig. 30. It can be seen that the plot is curved over its whole extent and that there is no justification for breaking the plot at the $\alpha-\gamma$ change point in iron (i.e. at 910°C). This treatment differs from that given by Smeltzer who broke the plot at 910°C and divided it into two straight line regions.

As discussed in section 2.5 modern kinetic theory indicates that the 'A' term in the Arrhenius equation is no longer constant but is directly dependent on the temperature. Since Fig. 30 covers a temperature range of 500°C it would be expected that over such a wide range of temperat-

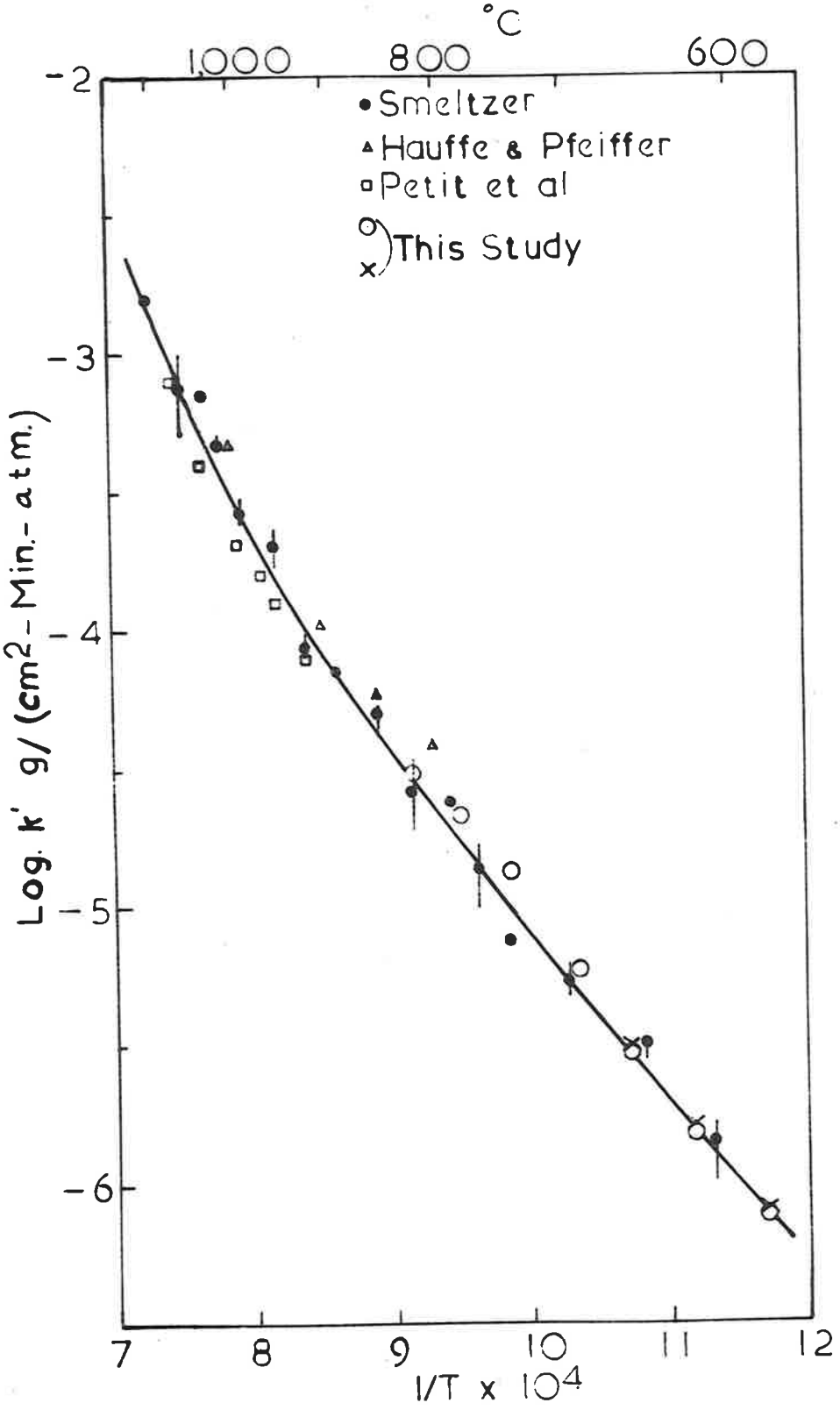

Fig.30 Arrhenius plot of the linear rate constants.

Table 10.

The evaluation of k' the velocity constant for the linear rates of the wustite scaling reaction.

Smeltzer's[45] results.

-obtained in pure CO_2 at 1 atma.-

T^oC	$1/T^oK$ x10^4	Log K_L g/(cm^2-min.)	K	$N^*_{CO_2}$	Log k' g/(cm^2-min.-atma.)
1100	7.28	-2.80	0.352	0.260	-2.80
1060	7.50	-3.00,-3.12,-3.30	0.368	0.269	-3.00,-3.12,-3.30
1030	7.67	-3.15	0.381	0.276	-3.15
1010	7.79	-3.29,-3.33,-3.40	0.391	0.280	-3.29,-3.33,-3.40
990	7.92	-3.54,-3.58,-3.61	0.401	0.285	-3.54,-3.58,-3.61
950	8.18	-3.63,-3.70,-3.77	0.422	0.297	-3.63,-3.70,-3.77
920	8.38	-4.02,-4.06,-4.11	0.440	0.305	-4.02,-4.06,-4.11
890	8.60	-4.15	0.460	0.314	-4.15

Table 10 (cont'd.)

Wheltzer's[45] results cont'd.

$T^{o}C$	$1/T^{o}K$ $\times 10^{4}$	$\log K_1$ $g/(cm^2\text{-min.})$	X	$N^{*}_{CO_2}$	$\log k'$ $g/(cm^2\text{-min.-atm.})$
850	8.90	-4.05,-4.30,-4.38	0.487	0.388	-4.23,-4.30,-4.38
820	4.46	-4.46,-4.58,-4.73	0.511	0.340	-4.46,-4.55,-4.73
790	9.41	-4.61	0.546	0.353	-4.61
765	9.63	-4.77,-4.87,-5.01	0.571	0.364	-4.77,-4.87,-5.01
740	9.87	-5.12	0.604	0.376	-5.12
700	10.28	-5.21,-5.27,-5.32	0.666	0.389	-5.21,-5.27,-5.32
650	10.83	-5.47,-5.50,-5.56	0.755	0.428	-5.47,-5.50,-5.56
610	11.33	-5.77,-5.80,-6.01	0.846	0.456	-5.77,-5.82,-6.01

Table 10 (cont'd.)

Haufe & Pfeiffer's[48] results.

-obtained in a 70:30;CO_2:CO mixture at 1 atm.-

T^oC	$1/T^oK$ x10^4	Log K_I $g_{CO_2}/(cm^2\text{-min.})$	K	$P^*_{CO_2}$	Log K' $g/(cm^2\text{-min.-atm.})$
1000	7.85	-0.56	0.395	0.283	-3.38
900	8.50	-1.22	0.452	0.311	-3.97
850	8.90	-1.56	0.487	0.336	-4.24
800	9.30	-1.68	0.532	0.348	-4.41

Table 10 (cont'd.)

Petit et al's[30] results.

-obtained in CO_2:CO mixtures.-

(results already corrected.)

t^oC	$1/T^oK$ $x10^4$	Log k' g/(cm^2-sec.-atms.)	Log k' g/(cm^2-min.-atms.)
1075	7.42	-6.5	-3.1
1038	7.65	-6.8	-3.4
993	7.90	-7.1	-3.7
967	8.07	-7.2	-3.8
950	8.18	-7.3	-3.9
925	8.35	-7.5	-4.1

Table 10 (cont'd.)

The results of this study.

-obtained in pure CO_2 at 100 mm Hg.

T^oC	$1/T^oK$ x10^4	K_b g/(cm^2-min.)	K	$P^*_{CO_2}$	log k' g/(cm^2-min.-atm.)
		(vac. annealed Battelle iron.)			
580	11.72	0.202	0.926	0.480	-7.29
620	11.20	0.429	0.820	0.449	-6.91
660	10.72	0.777	0.734	0.422	-6.47
700	10.28	1.51	0.655	0.398	-6.05
740	9.87	3.11	0.604	0.376	-5.82
780	9.50	5.46	0.546	0.357	-5.52
820	9.15	7.54	0.511	0.340	-5.48
		(O_2 annealed Armco iron.)			
580	11.72	0.207	0.926	0.480	-7.90
620	11.20	0.403	0.820	0.449	-7.89
660	10.72	0.803	0.734	0.422	-6.18

ure some curvature resulting from this source would become apparent and show up over the experimental scatter of the results. However, the magnitude of the curvature exhibited by Fig. 30 is more than can be accounted for by this explanation and part of the curvature must be attributed to a characteristic of the reaction.

A curved Arrhenius plot would also result if the reaction was exothermic and the liberation of a fair amount of heat accompanied the reaction. The temperature of the specimen would rise above the temperature of its surroundings (and hence the usual measured temperature) by an amount depending upon the rate of the reaction and the rate of heat transfer to its surroundings. However, since the reaction between iron and carbon dioxide is slightly endothermic, the curvature of the Arrhenius plot cannot be explained on the basis of 'over-temperatures'.

Since the rate-determining reaction occurs at the oxide/gas interface the composition of wustite throughout the oxide layer would approach that in equilibrium with the iron interface. Engell[4] has studied the range of existence of the wustite phase field and has shown that the number of positive holes in equilibrium with iron decreases from a value of 7.5% of the total iron sites, at 600°C, to a value of approximately 5% at 1100°C. Examination of Fig. 30

shows that the slope of the Arrhenius plot, which is directly related to the activation energy, increases with decreasing defect concentration of the wustite. The activation energy varies between the approximate limits of 30 and 60 kcals/mole. It thus appears that the wustite is acting as a catalyst for the dissociation of carbon dioxide and the variable activation energy reflects the changing defect composition of wustite with temperature. The activation energy for the dissociation of carbon dioxide (i.e. dissociation in the gas phase, unassisted by a catalyst) is 67.6 kcals/mole[45,50]. From Fig. 30 it can be seen that as the number of positive holes in the wustite decreases so the value of the activation energy approaches closer to that for the uncatalysed reaction.

To support the above view that, over the temperature range 600 - 1100°C the linear rates of the wustite scaling reaction are controlled by the dissociation of carbon dioxide at the wustite surface; and that the curvature of the Arrhenius plot is due to the effect of the variation of activation energy with wustite composition, it is appropriate to make reference to the work of Schwab and Block. These workers investigated the relation between the semi-conducting nature of a number of materials and their catalytic properties, and the results of their work have been reported by Garner[103]. For the oxidation of carbon

monoxide it was demonstrated that nickel oxide (a p-type semiconductor like wustite) with minor additions of lithium oxide to enhance the number of positive holes gave a significantly lower activation energy than in the case of the same oxide in which the number of current carriers had been reduced by the addition of chromic oxide. Similarly the addition of lithium oxide to zinc oxide (an n-type semiconductor) decreased the number of current carriers and increased the activation energy over that observed when the number of current carriers was increased by the addition of chromic oxide. This work demonstrated the dependence of the activation energy for the oxidation of carbon monoxide on the semi-conducting nature of the oxide. It would be expected that similar effects would apply to the reverse reaction and that a varying activation energy would be obtained for the dissociation of carbon dioxide on wustite surfaces of different composition.

5.5.2 Incorporation of Oxygen into the Wustite Lattice as the Rate-Determining Reaction.

If the rate of incorporation of chemisorbed oxygen into the wustite lattice, rather than the rate of dissociation of carbon dioxide, was the rate-determining step in the reaction then the concentration of adsorbed oxygen on the surface would change from a value in equil-

ibrium with wustite to a value in equilibrium with the gas phase. The increased negative charge on the surface would be balanced by changes in the surface concentrations of electron holes and positive vacancies, both of which are involved in equation (A), the general expression for the rate of reaction. Although it is not known how these quantities alter with respect to different surface coverages of adsorbed oxygen ions, it is considered highly unlikely that they would vary in a manner which would enable equation (A) to predict the observed experimental results - namely a linear dependence of the rate of reaction on the total pressure and the composition of the gas phase.

The main point in Smeltzer's argument in favour of the incorporation mechanism is the fact that below 910°C the activation energy for the reaction is approximately 30 kcals/mole which is in good agreement with the value of the activation energy for vacancy diffusion in wustite. (As discussed in section 2.6.1 Smeltzer has drawn an analogy between the activation energies for the diffusion and incorporation processes and claims that they should have the same value of the activation energy.) However, as one process operates in the bulk phase while the other operates at an interface, (where the conditions are different to those in the bulk phase) it is considered that the analogy is of little value and that the agreement

between the values of the activation energy is fortuitous.

Thus it is not considered that the incorporation mechanism is responsible for the linear rates of the wustite scaling reaction but rather that the dissociation of carbon dioxide is determining the rate of reaction over the whole of the temperature range from 600 to 1100°C.

5.6 Recommendations for Further Work.

1. The significance of the electrical capacity and resistance measurements requires further investigation and it is suggested that a more fruitful approach than the one adopted in the present project would have been to investigate the electrochemical behaviour of oxides formed by thermal oxidation. Such a method of producing the oxide films would have the following advantages :-

a) By choosing the appropriate conditions of temperature and partial pressure of the oxidizing environment (see for example the work of Davies, Evans and Agar[56]) it would be possible to produce oxide films consisting wholly of Fe_3O_4 or γFe_2O_3, the compositions of which could be checked by x-ray diffraction analysis.

b) By carrying out the oxidation on the microbalance it would be possible to produce oxide films containing accurately known amounts of oxide.

Iron specimens carrying oxide films produced by such means could then be transferred to the electrochemical apparatus where their behaviour to oxidation or reduction could be tested under any desired conditions of pH and potential.

2. The nucleation and growth stage of the reaction between iron and carbon dioxide warrants further intensive study. Since the number of nuclei that form on a given surface is strongly influenced by the crystallographic orientation of that surface it is recommended that any future fundamental studies be conducted on single crystal surfaces.

As hot-stage microscopes are now readily available it would be interesting to examine the metal surfaces while they were actually oxidizing, and to make use of these observations to provide quantitative information regarding the way in which the number of nuclei are affected by :-

A) The partial pressure of the oxidizing enviroment.

B) The temperature of oxidation.

C) The nature and crystallographic orientation of the metal surface.

Such information could then be used, in conjunction with microbalance measurements, to determine the rate of growth of the individual nuclei and thus allow some definite

conclusions to be drawn as to the mechanism of their growth.

3. During the closing stages of the project , when some of the results for the early stages of oxidation were being checked, one set of windings on the non-inductively wound furnace was inadvertently open-circuited, and as can be seen from Fig. 31 the effect on the gravimetric record was quite marked. This result was reproducible and when the winding was reconnected the usual type of gravimetric record was obtained. With the inductive winding the weight gain was initially greater than that obtained with the non-inductive winding but after a short period of time the overall oxygen uptake was much less.

It is thought that the difference in the results can be explained on the basis of the magnetostrictive effect. When a crystal is placed in a magnetic field it tends to expand along some directions and contract along others so that the total volume of the crystal tends to remain the same. Whether a crystal expands or contracts along a given direction depends upon the orientation of the crystal relative to the direction of the applied magnetic field. Thus polycrystalline specimens (such as those used in this project) would be subjected to internal stress, when they were placed in a magnetic field, due to the interaction of differently orientated grains. The nett

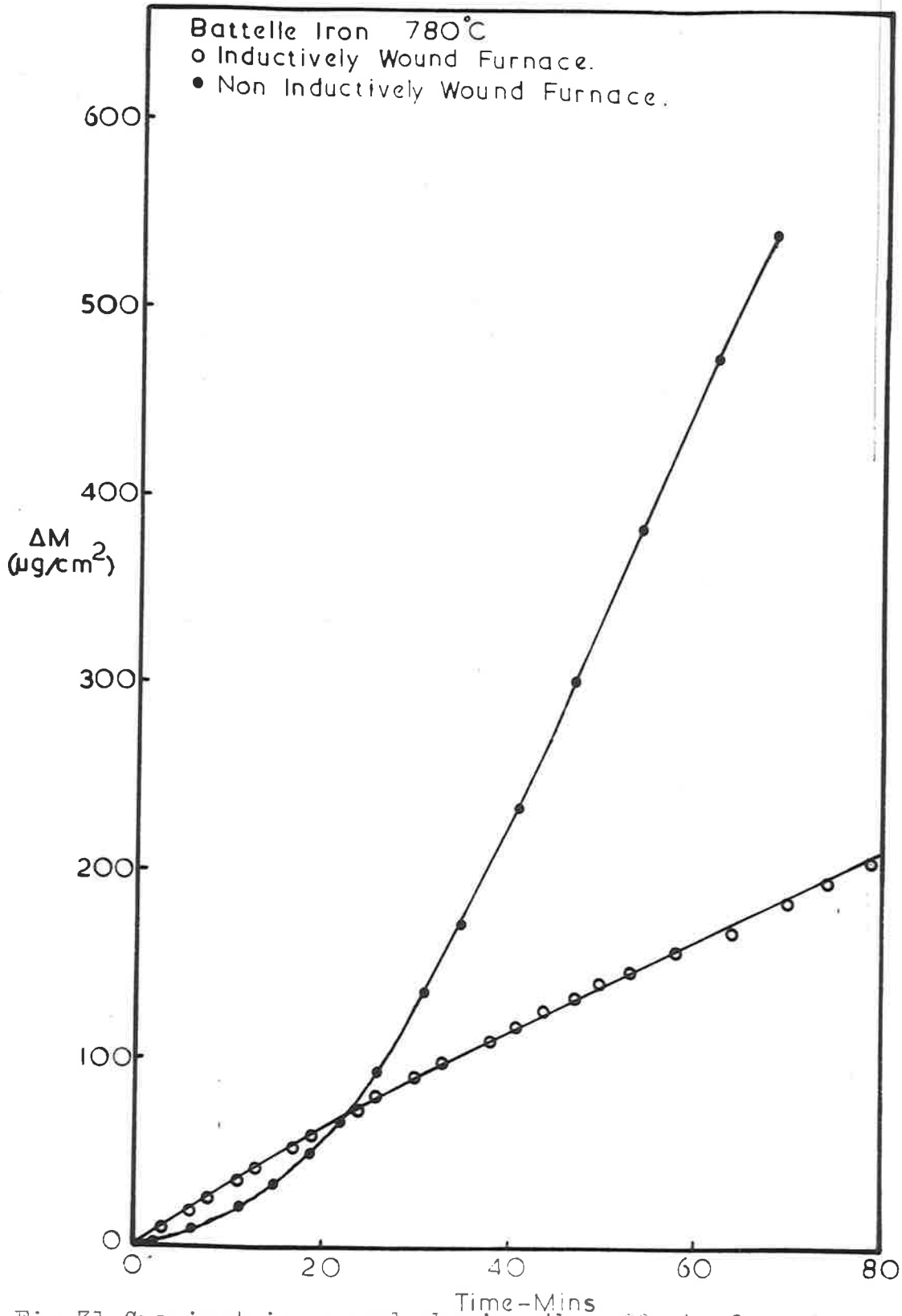

Fig.31 Gravimetric record showing the effect of an inductive furnace winding.

effect of the inductive winding would then be to subject the specimen to a periodic reversal of stress at the rate of 50 cycles per second. Evidently the effect of such stress reversals is to give a large increase in the number of nuclei, this would account for the weight-gain record obtained with the inductive furnace being initially greater than that obtained with the non-inductive furnace. Clearly such effects require further investigation and merit extension to other metals.

6. CONCLUSIONS.

The following progress has been made towards the attainment of objectives 1 and 2 as set out on page 3 of section 1 - the introduction.

1. The oxidation of iron in carbon dioxide at 200 mm Hg total pressure has been studied over the range of temperature from 400 - 800°C. It was found that the mechanism of oxidation varied for short and long periods of exposure and also depended upon whether the temperature of oxidation was above or below the wustite eutectoid temperature (i.e. 570°C). Above this temperature, and for the times of oxidation studied in this project, the oxide layer consisted wholly of wustite, while below this temperature it consisted wholly of magnetite.

It has been established that :

a) The early stages of the reaction proceed by a mechanism involving the nucleation and growth of an oxide phase on the metal surface. It appears that the nuclei form as a result of the surface layers of the metal becoming saturated with oxygen, and a model has been developed to account for their subsequent growth. The model is based upon the growth of individual nuclei as discrete entities, and it has been assumed that their growth is limited by the rate of supply of oxygen to their outer peripheries. The

growth equation derived from this model has the following form.

$$\Delta M^{2/3} = Kt + C.$$

Where ΔM is the weight-gain per unit area at time t.

K is a bulk constant which is a function of the number of nuclei per unit area, their shape, and the rate at which they grow.

C is a constant of integration.

This equation has been applied to the gravimetric results for the initial stages of the reaction. Above 570°C good fits of the experimental data were obtained but below this temperature the results were not amenable to this treatment, due to the large numbers of nuclei which were present. Impingement and ingestment of the nuclei took place very early in the reaction and thus it was not possible to treat this data in a quantitative manner.

In the range of temperature where the gravimetric results are amenable to analysis the growth of the nuclei has been studied on three different forms of iron. It was found that the values of K were dependent upon the type of iron used in the experiments, and the results appear to show the effect of the initial oxygen content of the iron on the number of nuclei which form on a given surface.

b) When the surface roughening produced during the nucleation and growth stage of the reaction had subsided, and a uniform oxide layer of magnetite had been interposed between the metal and the gas phase, the oxidation kinetics obeyed the parabolic law.

$$(\Delta M)^2 = k_p t + C.$$

Where ΔM is the weight-gain per unit area at time t.

k_p is the parabolic rate constant.

C is a constant.

An Arrhenius plot of the parabolic rate constants yielded an activation energy of 38 kcals/mole and by analogy to similar values of the activation energy it has been concluded that the rate of reaction was largely limited by the diffusion of oxygen ions via vacancies in the magnetite lattice.

In support of this mechanism it was found that specimens of high purity iron oxidized at a much greater rate than specimens of Armco iron. The difference in rates was probably due to the presence of manganese as an impurity in the Armco iron. The manganese entered the magnetite lattice and decreased the number of oxygen ion vacancies which in turn resulted in a decreased rate of reaction.

c) At temperatures above 570°C, and for the times of

oxidation studied in this project, the kinetics of the latter stages of the reaction were represented by a linear relationship between weight-gain and time. Since the oxide layer that formed was protective, and since wustite (and not one of the higher oxides) constituted the scale, it was concluded that the rate of reaction was limited by the reaction at the oxide/gas interface. In this case the impurities present in the Armco iron were not observed to affect the rates of reaction due to the very large defect composition of wustite.

Use was made of published data, obtained at higher temperatures than those studied in this project, to extend the experimental data to cover the temperature range 580 - 1100°C. The reaction has been critically examined and a general expression formulated for the rate of reaction. When the reaction is controlled by the dissociation of carbon dioxide this expression simplifies to

$$r = k'P(K + 1)(N_{CO_2} - N^*_{CO_2}).$$

Where r is the rate of reaction.

k' the velocity constant for the reaction.

P the total pressure.

K the value of p_{CO_2}/p_{CO} that is in equilibrium

with iron and wustite.

N_{CO_2} is the mole fraction of carbon dioxide in the gas phase. The asterisk denotes an equilibrium value.

It was subsequently shown that, over the whole of the above temperature range, the linear rates of the wustite scaling reaction were controlled by the dissociation of carbon dioxide at the wustite surface. In support of this view it was found that an Arrhenius plot of the linear velocity constants was curved, and it was concluded that the curvature was due to the effect of the changing composition of wustite with temperature on the activation energy for the dissociation process. These conclusions are different from those of previous workers in the field who claim that different mechanisms operate above and below the $\alpha - \gamma$ change point in iron at 910°C.

d) When iron containing carbon is oxidized the carbon tends to diffuse to the surface and react to form gaseous oxidation products. In some circumstances the iron may preferentially decarburize, in which case the iron will not oxidize until the carbon content of the surface has been reduced to such an extent that oxide formation becomes possible. The thermodynamics of the Fe-C-O system have been examined

and an equilibrium diagram constructed. It was concluded that iron will preferentially decarburize until the carbon content of the surface has been reduced to a level corresponding to the Fe/FeO limit, at which point oxide formation becomes thermodynamically possible. This conclusion was checked against the small amount of experimental data available.

The present study has elucidated the mechanism of the reaction between iron and carbon dioxide and provided basic data on the rates of reaction; thus the main objective of this project has been fulfilled. Although certain aspects of the nucleation and growth stage of the reaction require further investigation it is felt that a solid foundation has been laid on which the further study of the oxidation behaviour of iron alloys in carbon dioxide could well be based.

2. Oxide films were formed by the anodic oxidation of iron electrodes in borate buffer solutions covering the range of pH from 8 to 10. During the course of the anodic oxidation measurements of the electrical capacity and resistance of the electrode were made with an A.C. bridge. In the range of potential where it is thermodynamically possible for the electrode to be covered by an oxide film the capacity measurements exhibited the following behaviour.

Peak values of the capacity, of the order of thous-

ands of $\mu F/cm^2$, were observed to occur at potentials near the Fe_3O_4/Fe_2O_3 equilibrium potential. The peak values appear to correspond to a rapid reversible equilibrium between Fe^{++} and Fe^{+++} sites in the film. At more noble values of the potential the capacity rapidly fell to values which were equal to or less than double layer capacity. In this range of potential the oxide film appears to behave as an inert dielectric film which has been placed between the electrode and the solution.

It was not possible to estimate the magnitude of the oxide films formed by the anodic oxidation method and thus it was not possible to treat the results in a quantitative manner. It has been recommended that further work be done in this field and that future studies be conducted on oxide films formed by thermal oxidation.

The pursuit of objectives 1 and 2 necessitated the construction of a considerable amount of equipment. In particular the gravimetric work, which was directed towards the attainment of objective 1, required the construction of a vacuum microbalance. The balance operates as a null point instrument and relies on electromagnetic compensation to counteract the effect of weight changes in the specimen. Departures of the beam from the null position are detected with a very sensitive optical lever. The detector system

is capable of great sensitivity and it is felt that, if effect were given to the recommendations for improving the performance of the balance (made in section 3.1.9), an instrument could be built which would make a major contribution to the field of vacuum microbalance techniques.

APPENDIX A - THERMODYNAMIC CALCULATIONS.

A.1 Basic Data.

1. Wustite $FeO^{(104)}$ ± 3 kcals.

$Fe + 1/2O_2 = FeO$, $\Delta G^\circ = -62{,}050 + 14.95T$ 298-1642°K

For the sake of simplicity wustite has been written as being of stoichiometric composition.

2. Magnetite $Fe_3O_4^{(104)}$ ± 3 kcals.

$3FeO + 1/2O_2 = Fe_3O_4$, $\Delta G^\circ = -74{,}620 + 29.90T$ 298-1642°K

3. Ferric Oxide $Fe_2O_3^{(104)}$ ± 3 kcals.

$2Fe_3O_4 + 1/2O_2 = 3Fe_2O_3$, $\Delta G^\circ = -59{,}620 + 33.62T$ 298-1460°K

4. Cementite $Fe_3C^{(104)}$ ± 1 kcal.

$3Fe + C = Fe_3C$, $\Delta G^\circ = 6{,}380 - 5.92T$ 463-1115°K

5. 'Iron percarbide' $Fe_2C^{(105)}$ ± 1 kcal.

$2Fe + C = Fe_2C$ $\Delta G^\circ = 4{,}930 - 2.60T$ 298-800°K

6. Carbon in ferrite$^{(105)}$ ± 1 kcal.

$C = C(0.01\%\text{ in Fe})$, $\Delta G = 20{,}000 - 21.40T$ 273-1071°K

The free energy change accompanying the solution of carbon in ferrite may be represented thus -

$$\Delta G = \mu_C - \mu_C^*.$$

Where μ_C^* = the chemical potential of solid carbon, and

μ_C = the chemical potential of carbon in solution in ferrite.

The chemical potential of carbon in solution is related to the activity and the chemical potential at some arbitrary standard state by the following expression :-

$$\mu_C = \mu_C^\circ + RT \ln a.$$

Thus $(\Delta G)_1 = \mu_C^\circ + RT \ln (a)_1 - \mu_C^*,$

and

$$(\Delta G)_2 = \mu_C^\circ + RT \ln (a)_2 - \mu_C^*.$$

Therefore

$$(\Delta G)_2 = (\Delta G)_1 + RT \ln \frac{(a)_2}{(a)_1}.$$

It has been assumed that dilute solutions of carbon in ferrite obey Henry's Law and that the solutions are sufficiently dilute for the mole fraction to be proportional to the wt.% of carbon in solution.

Under these circumstances

$$(\Delta G)_2 = (\Delta G)_1 + RT \ln \frac{(wt.\%)_2}{(wt.\%)_1}.$$

This equation together with the above data for the 0.01 wt.% solution has been used to estimate the following :-

C = C (0.020% in Fe), $\Delta G = 20,000 - 20.02T$

C = C (0.015% in Fe), $\Delta G = 20,000 - 20.60T$

C = C (0.010% in Fe), $\Delta G = 20,000 - 21.40T$

C = C (0.007% in Fe), $\Delta G = 20,000 - 22.13T$

C = C (0.005% in Fe), $\Delta G = 20,000 - 22.78T$

C = C (0.004% in Fe), $\Delta G = 20,000 - 23.22T$

C = C (0.003% in Fe), $\Delta G = 20,000 - 23.79T$

C = C (0.002% in Fe), $\Delta G = 20,000 - 24.60T$

C = C (0.001% in Fe), $\Delta G = 20,000 - 25.97T$

7. Ferrite to Austenite transformation.

Temperatures at which various carbon contents in ferrite are in equilibrium with austenite have been read from Smith's[106] diagram.

8. Carbon Monoxide CO,[104] ± 1 Kcal.

$C + 1/2O_2 = CO$, $\Delta G^\circ = -26,700 - 20.95T$

298-2500°K

9. Carbon Dioxide CO_2[104] ± 1 Kcal.

$C + O_2 = CO_2$, $\Delta G^\circ = -94,200 - 0.20T$

298-1642°K

10. Methane CH_4[104] ± 1 kcal.

$C + 2H_2 = CH_4$, $\Delta G^\circ = -16,520 + 12.25 \log T - 15.62T$

298-1200°K

A.2 Equations derived from the basic data.

In the following equations p_{CO} and p_{CO_2} are denoted by CO and CO_2 respectively.

11. Fe_2O_3/Fe_3O_4.

$2\ Fe_3O_4 + CO_2 = 3\ Fe_2O_3 + CO$, $\quad \Delta G^\circ = +7{,}880 + 12.8T$

$\text{Log } CO/CO_2 = \frac{-1{,}720}{T} - 2.180.$

12. Fe_3O_4/FeO.

$3\ FeO + CO_2 = Fe_3O_4 + CO$, $\quad \Delta G^\circ = -7{,}120 + 9.15T$

$\text{Log } CO/CO_2 = \frac{+1{,}556}{T} - 2.000.$

13. FeO/Fe.

$Fe + CO_2 = FeO + CO$, $\quad \Delta G^\circ = +5{,}450 - 580T$

$\text{Log } CO/CO_2 = \frac{-1{,}192}{T} + 1.269.$

14. Fe_3O_4/Fe.

$3\ Fe + 4\ CO_2 = Fe_3O_4 + 4\ CO$, $\quad \Delta G^\circ = +9{,}230 - 8.25T$

$\text{Log } (CO/CO_2)^4 = \frac{-2{,}018}{T} + 1.269.$

15. FeO/Fe_3C.

$Fe_3C + 4\ CO_2 = 3\ FeO + 5\ CO$, $\quad \Delta G^\circ = +50{,}770 - 53.8T$

$\text{Log } CO^5/CO_2{}^4 = \frac{-11{,}090}{T} + 11.62.$

16. Fe_3O_4/Fe_3C.

$Fe_3C + 5\ CO_2 = Fe_3O_4 + 6\ CO$, $\quad \Delta G^\circ = +43{,}650 - 44.0T$

$\text{Log } CO^6/CO_2{}^5 = \frac{-9{,}560}{T} + 9.64.$

17. $'Fe_2C/Fe_3O_4$.

$3Fe_2C + 11CO_2 = 2Fe_3O_4 + 14CO$, $\Delta G^\circ = 126,070 - 133.76T$

$\text{Log } CO^{14}/CO_2^{11} = \frac{-27,610}{T} + 29.2$

18. Fe_3C/Fe.

$3Fe + 2CO = Fe_3C + CO_2$, $\Delta G^\circ = -34,420 + 35.78T$

$\text{Log } CO^2/CO_2 = \frac{-7,530}{T} + 7.81$

19. $Fe_3C/'Fe_2C'$

$2Fe_3C + 2CO = 3Fe_2C + CO_2$, $\Delta G^\circ = -38,770 + 45.70T$

$\text{Log } CO^2/CO_2 = \frac{-8,460}{T} + 9.49$

20. C in ferrite.

$C + CO_2 = 2CO$, $\Delta G^\circ = 40,800 - 41.70T$

$C = C(0.01\% \text{ in Fe})$, $\Delta G = 20,000 - 21.40T$

$C(0.01\% \text{ in Fe}) + CO_2 = 2CO$, $\Delta G^\circ = 20,800 - 20.30T$

The values obtained at other carbon levels are shown below.

0.020%	$\Delta G^\circ = 20,800 - 21.68T$
0.015%	" = " $-21.10T$
0.010%	" = " $-20.30T$
0.007%	" = " $-19.57T$
0.005%	" = " $-18.92T$
0.004%	" = " $-18.48T$
0.003%	" = " $-17.91T$
0.002%	" = " $-17.10T$
0.001%	" = " $-15.73T$

21. C in Austenite.

Equilibrium carbon levels have not been calculated, as austenite is only stable at temperatures above those studied in this investigation.

A.3 Method of Calculation.

The equilibria denoted by equations 11-14 (inc.) are pressure independent and the equilibrium gas compositions can be calculated directly from these equations. However, the reactions represented by equations 15-20 (inc.) are accompanied by a change in the number of gas molecules so that the equilibria are pressure dependent. Under these circumstances calculation of the equilibrium gas composition involves the simultaneous solution of the two equations obtained by considering the thermodynamic and pressure restrictions imposed upon the system. As the present work was conducted at a total pressure of 200 mm Hg the equation representing the pressure restriction is as follows :-

22. $CO_2 + CO = 0.2632.$

It was found that the equilibria represented by equations 14,15 and 17 did not appear on the final form of the equilibrium diagram (which is shown in Fig. 1), and no further mention will be made to these equations.

Equilibrium gas compositions for equations 18, 19 and 20 have been determined in the following manner.

As an example consider the equilibrium of carbon in ferrite; for any given carbon level and for any given temperature it is always possible to evaluate Log CO^2/CO_2 and hence CO^2/CO_2. Let this quantity equal M. Then

$$CO^2/CO_2 = M,$$

and from equation 22,

$$CO + CO_2 = 0.2632.$$

Eliminating one of the unknowns yields

$$CO^2 = M (0.2632 - CO).$$

This is a standard quadratic equation the positive solution of which is

$$CO = \frac{- M + (M^2 - 1.053M)^{1/2}}{2}.$$

Equation 16 involves the term CO^6/CO_2^5; graphical solution has been used to solve this equation and equation 22 to yield the equilibrium composition of the gas phase.

Equilibrium gas compositions determined in the above manner are presented in the following section and this data has been used to construct Fig. 1.

A.4. Calculated equilibrium values.

Over the temperature range 500 - 900°C the equilibrium gas compositions for the Fe_2O_3/Fe_3O_4 equilibrium are very nearly 100% CO_2, thus these values have not been presented, and this equilibrium has been represented on the equilibrium diagram by a mere thickening of the 100% CO_2 line.

Table 11.

Gas compositions for the Fe_3O_4/FeO equilibrium.

T°C	Log CO/CO_2	CO/CO_2	%CO
500	0.015	1.0351	50.2
550	- 0.110	0.7763	43.8
600	- 0.217	0.6067	37.7
650	- 0.312	0.4875	32.8
700	- 0.401	0.3972	28.4
750	- 0.480	0.3311	25.1
800	- 0.551	0.2812	21.9
850	- 0.614	0.2432	19.6
900	- 0.672	0.2128	17.6

Table 12.

Gas compositions for the FeO/Fe equilibrium.

T°C	Log CO/CO_2	CO/CO_2	%CO
500	- 0.275	0.5308	34.7
550	- 0.180	0.6607	39.8
600	- 0.099	0.7962	44.3
650	- 0.024	0.9462	48.6
700	0.042	1.1015	52.6
750	0.104	1.2706	56.0
800	0.158	1.4388	58.8
850	0.207	1.6106	61.8
900	0.251	1.7824	64.1

Table 13.

Gas compositions for the Fe_3O_4/Fe_3C equilibrium.

(graphical solution).

T^oC	CO/CO_2	%CO
500	0.0825	31.4
550	0.1020	38.8
600	0.1195	45.5

Table 14.

Gas compositions for the Fe_3C/Fe equilibrium.

T^oC	Log CO^2/CO_2	M	CO	%CO
500	- 1.93	0.01175	0.0505	19.2
550	- 1.34	0.04575	0.892	33.9
600	- 0.82	0.1529	0.138	52.6
650	- 0.35	0.4486	0.186	70.8
700	0.07	1.178	0.221	84.1
750	0.45	2.816	0.243	92.4
800	0.79	6.197	0.253	96.1
850	1.11	12.74	0.259	98.5
900	1.39	24.58	0.260	98.9

Table 15.

Gas compositions for the Fe_3C/'Fe_2C' equilibrium.

T°C	Log CO^2/CO_2	M	CO	%CO
500	- 0.98	0.1047	0.120	45.5
550	- 0.29	0.5129	0.192	72.9
600	0.30	1.992	0.235	89.4
650	0.82	6.662	0.253	95.3
700	1.30	19.73	0.260	98.9

Table 15.

Equilibrium gas compositions for the 0.020% carbon level.

T°C	Log CO^2/CO_2	M	CO	%CO
650	- 0.187	0.6503	0.201	76.3
700	0.066	1.165	0.216	82.1
750	0.295	1.971	0.235	89.3
800	0.502	3.176	0.245	93.0
850	0.691	4.904	0.251	95.2
900	0.863	7.296	0.254	96.7

Table 17.

Equilibrium gas compositions for the 0.015% carbon level.

T°C	Log CO^2/CO_2	M	CO	%CO
700	- 0.314	0.4856	0.189	71.9
750	- 0.065	0.8616	0.211	80.3
800	0.168	1.472	0.228	86.6
850	0.564	3.661	0.247	93.8
900	0.736	5.448	0.252	95.6

Table 18.

Equilibrium gas compositions for the 0.010% carbon level.

T°C	Log CO^2/CO_2	M	CO	%CO
600	- 0.771	0.1695	0.143	54.3
650	- 0.489	0.3246	0.172	65.4
700	- 0.235	0.5814	0.197	74.7
750	- 0.007	0.9840	0.216	82.0
800	0.200	1.580	0.230	87.3
850	0.389	2.451	0.240	91.3

Table 19.

Equilibrium gas compositions for the 0.007% carbon level.

T°C	Log CO^2/CO_2	M	CO	%CO
500	- 1.246	0.1174	0.097	36.9
600	- 0.930	0.1174	0.127	48.1
650	- 0.648	0.2248	0.156	59.1
700	- 0.395	0.4027	0.181	69.0
750	- 0.167	0.6812	0.203	77.1
800	0.040	1.098	0.219	83.3
850	0.229	1.695	0.232	88.0
900	0.402	2.522	0.240	91.3

Table 20

Equilibrium gas compositions for the 0.005% carbon level.

T°C	Log CO^2/CO_2	M	CO	%CO
550	- 1.389	0.04082	0.080	30.5
600	- 1.073	0.08461	0.113	42.9
650	- 0.798	0.1592	0.140	53.2
700	- 0.537	0.2902	0.161	63.5
750	- 0.309	0.4911	0.190	72.1
800	- 0.102	0.7912	0.208	79.2
850	0.087	1.222	0.225	88.5
900	0.260	1.818	0.233	88.7

Table 21.

Equilibrium gas compositions for the 0.004% carbon level

T°C	Log CO^2/CO_2	M	CO	%CO
650	- 0.887	0.1298	0.131	49.8
700	- 0.633	0.2326	0.157	59.7
750	- 0.405	0.3936	0.180	68.6
800	- 0.198	0.6342	0.200	76.0
850	- 0.009	0.9793	0.216	82.0
900	0.163	1.457	0.228	86.5

Table 22.

Equilibrium gas compositions for the 0.003% carbon level

T°C	Log CO^2/CO_2	M	CO	%CO
700	- 0.758	0.1746	0.144	54.8
750	- 0.530	0.2954	0.168	63.8
800	- 0.323	0.4756	0.188	71.6
850	- 0.133	0.7354	0.206	78.2
900	0.039	1.093	0.219	83.4

Table 23.

Equilibrium gas compositions for the 0.002% carbon level.

T^oC	Log CO^2/CO_2	M	CO	%CO
700	- 0.935	0.1161	0.126	47.9
750	- 0.707	0.1965	0.147	56.0
800	- 0.500	0.3162	0.171	64.9
850	- 0.311	0.4888	0.190	72.1
900	- 0.138	0.7273	0.205	78.0

Table 24.

Equilibrium gas compositions for the 0.001% carbon level.

T^oC	Log CO^2/CO_2	M	CO	%CO
800	- 0.780	0.1585	0.140	53.1
850	- 0.610	0.2453	0.160	60.6
900	- 0.438	0.3649	0.177	67.4

The data contained in the preceding tables have been used to construct Fig. 1. It should be noted that this figure shows that the solid phases Fe_3O_4, FeO, Fe and Fe_3C can all coexist at 570°C. This state of affairs is purely coincidental and has arisen from the total pressure of the system being 200 mm Hg. At other values of the total pressure the equilibria represented

by equations 14, 15 and 17 would appear on the diagram.

A.5 Decarburizing by dry hydrogen at 800°C.

The Armco iron used in this project contained 0.02% carbon. Calculation of the maximum amount of decarburizing involves the graphical solution of two simultaneous equations, one of which is derived from the overall mass balance on the system, while the other is derived from thermodynamic considerations.

Equilibrium Line

Calculation of the equilibrium gas ratios involves the following equations:-

$$C + 2H_2 = CH_4 \qquad (X)$$

$$C = C\ (\text{in Fe}) \qquad (Y)$$

$$C\ (\text{in Fe}) + 2H_2 = CH_4 \qquad (Z)$$

The standard free energy change for reaction (X) can be calculated from equation (10). At 800°C.

$$\Delta G^{\circ}_{X} = +6,534 \text{ cals.}$$

The free energy change for reaction (Y) depends upon the carbon content, these values have been calculated from equation (6) and are shown in Table 25. ΔG°_{Z} has been determined from ΔG°_{Y}, and these values, along with the corresponding values of the equilibrium gas ratios, are also shown in Table 25.

Table25.

Equilibrium gas compositions for the hydrogen decarburizing reaction.

wt.%C	ΔG	ΔG_{800}	ΔG^{o}_{z}	log p	p
	C = C(in Fe)	C= C(in Fe)			
0.00005	20,000 - 31.92T	-14,250 cals	20,784 cals	-4.2348	5.8×10^{-5}
0.00010	" - 30.55T	-12,780 "	19,314 "	-3.9352	11.6 "
0.00015	" - 29.74T	-11,911 "	18,445 "	-3.7582	17.5 "
0.00020	" - 29.17T	-11,299 "	17,833 "	-3.6330	23.3 "
0.00025	" - 28.73T	-10,827 "	17,361 "	-3.5373	29.0 "

Operating Line.

To calculate the equation of the operating line, it is necessary to know the total amounts of hydrogen and carbon in the system. As the specimens weighed in the vicinity of 0.55g it has been calculated that they contained 9.17×10^{-6}g moles of carbon. The amount of hydrogen was calculated as follows:-

$$n = \frac{PV}{RT}$$

where $P = 1$ atma.

$V = 5$L.

$R = 0.80205$ liter - atma - deg.$^{-1}$ mole^{-1}.

$T = 25^{\circ}$C (except for the small amount of gas at 800°C in the furnace tube.)

Therefore $n = 0.204$g moles of hydrogen.

Two points on the operating line can be found for the limiting conditions of complete and zero reaction. Carbon is the limiting reactant so for complete reaction 9.17×10^{-6}g moles of methane would be formed. The production of this amount of methane would have a negligible effect on the total amount of hydrogen in the system. Thus

$$\frac{P_{CH_4}}{P_{H_2}^2} = \frac{9.17 \times 10^{-6}}{(0.204)^2} = 22.1 \times 10^{-5}.$$

P_{CH_4} is linearly related to the amount of carbon in the

specimen. Since p_{H_2} has been assumed constant then the value of the pressure ratio term is also linearly related to the carbon content of the specimen. Hence the operating line has been drawn on Fig. 32 as a straight line passing through the following pair of points :-

$$0\%C \; ; \quad \frac{p_{CH_4}}{p^2_{H_2}} = 22.1 \times 10^{-5}$$

$$0.02\% \; C \; ; \quad " \quad = \quad 0$$

From Fig. 32 it can be seen that it is thermodynamically possible for the hydrogen to reduce the carbon content of the specimens from 0.02% to 0.00018%.

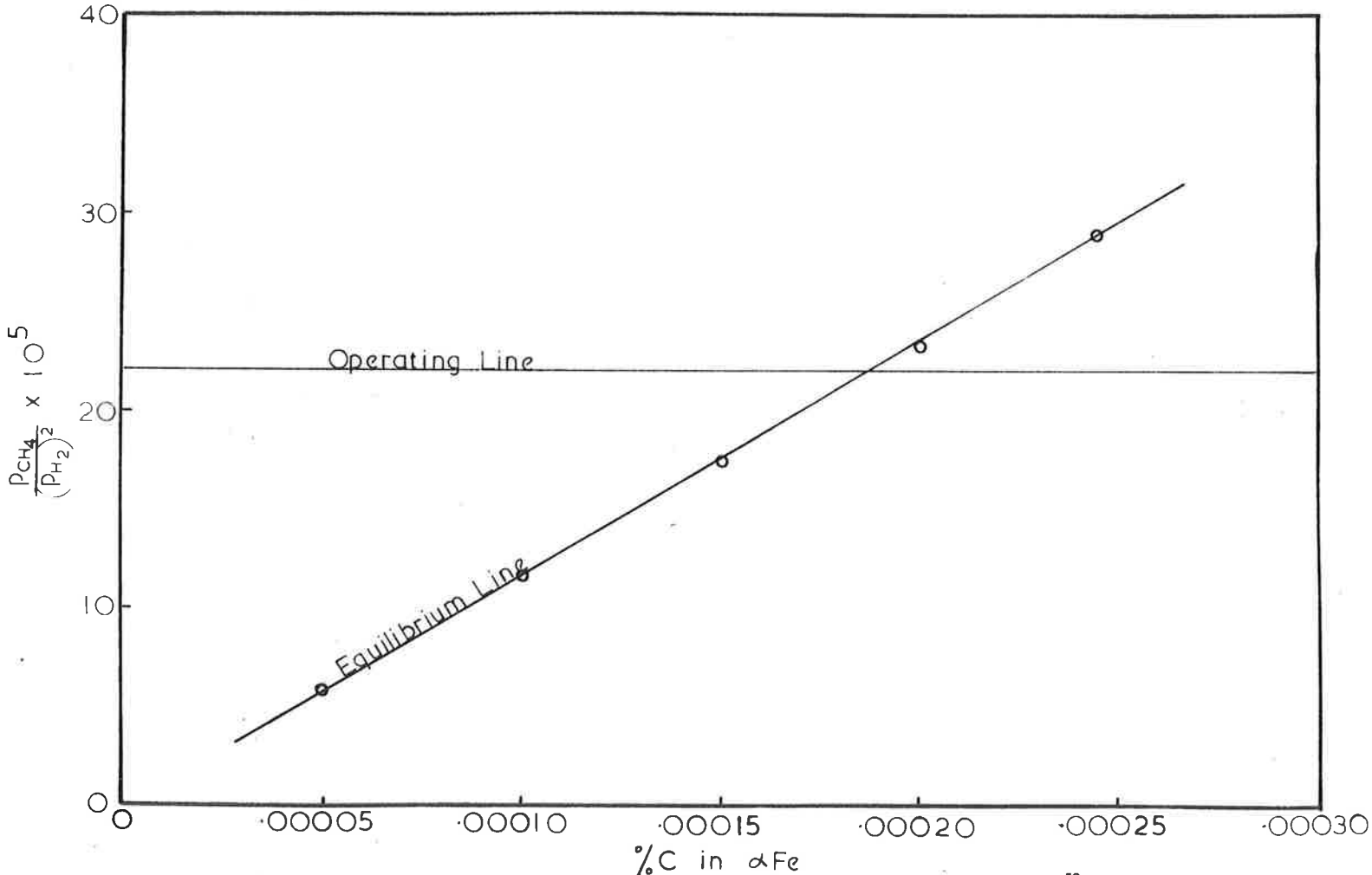

Fig.32 Decarburizing by hydrogen (graphical sol^{n}.)

APPENDIX B - GRAVIMETRIC DATA.

The following gravimetric results have been used to calculate reaction rate constants. All the data was obtained for the oxidation of iron in carbon dioxide at 200 mm Hg total pressure. The letters listed below have been used to designate the various forms of iron used in the particular experiments.

(X) : Vacuum-Annealed Battelle Iron.

(Y) : Hydrogen-Annealed Armco Iron.

(Z) : Vacuum Annealed decarburized Armco Iron.

B.1 Results for the later stages of oxidation.

B.1.1 Results obtained above 570°C.

mins.	$\mu g/cm^2$	mins.	$\mu g/cm^2$
580°C(X)		620°C(X)	
773	103	1316	459
884	127	1399	493
901	139	1484	529
1004	154	1649	595
1103	178	1715	620
1332	203	2687	1038
2212	396	2782	1078
2375	430	2890	1128
2537	464	3066	1208
2675	493	3178	1259

mins.	$\mu g/cm^2$
660°C(X)	
678	404
1177	753
1267	816
1368	890
1480	967
1544	1013
1619	1067
1677	1110
2004	1363
700°C(X)	
681	1675
1381	2430
1711	3480
2141	3460
2796	4840
3036	5310
3246	5370
740°C(X)	
1170	3032
1410	4243
1680	5702
2090	6195
2735	8941
3005	10275

mins.	$\mu g/cm^2$
740°C(X) cont'd.	
3127	9519
780°C(X)	
1030	3760
1330	6490
2150	12020
2290	13080
2450	13090
2655	12400
820°C(X)	
601	4126
1220	9310
1486	12306
1715	13659
2520	13973
580°C(Y)	
535	102
1300	256
1817	369
1949	398
2847	611
2988	643
3174	686
3179	686

min.	$\mu g/cm^2$
620°C(Y)	
602	220
1254	450
1324	484
1442	529
1552	574
1635	605
1746	650
2058	772
2749	1092
2824	1133
2950	1208
3093	1289
3193	1343
660°C(Y)	
585	474
1278	1038
1320	1060
1380	1091
1430	1142
1493	1188
1561	1245
1622	1299
1715	1377
1757	1408

T.1.2 Results obtained below 570°C.

520°C(X)			550°C(X) cont'd.		
mins.	$\mu g/cm^2$	$(mg/cm^2)^2$	mins.	$\mu g/cm^2$	$(mg/cm^2)^2$
2464	702	0.493	3000	1215	1.477
2513	715	0.511	3155	1260	1.588
2570	732	0.536	3564	1371	1.880
2639	749	0.561	4213	1534	2.353
2706	769	0.591	4381	1572	2.471
2870	814	0.663	4476	1597	2.550
2945	834	0.696	4608	1623	2.634
3221	900	0.810	396°C(Y)		
3904	1056	1.115	1291	22.5	5.06×10^{-1}
4005	1077	1.160	1320	23.1	5.33
4161	1111	1.234	1601	27.9	7.78
4346	1152	1.327	1672	28.3	8.00
550°C(X)			1909	31.6	9.99
1289	566	0.320	2673	39.2	15.37
1342	588	0.346	2778	40.2	16.16
1419	625	0.391	2849	41.1	16.89
1495	666	0.444	3089	43.0	18.49
1567	696	0.484	3138	43.9	19.27
1664	740	0.548	3335	45.8	20.97
1714	762	0.581	4154	55.6	30.91
1989	873	0.762	4255	56.4	31.81
2643	1108	1.228	4420	57.6	33.18
2882	1180	1.392	4508	52.8	34.57

mins.	$\mu g/cm^2$	$(mg/cm^2)^2$	mins.	$\mu g/cm^2$	$(mg/cm^2)^2$
	430°C(Y)			460°C(Y) cont'd.	
1333	43.4	24.40×10^{-4}	1584	117	136.8×10^{-4}
1400	51.4	26.42	1635	119	142.2
1450	52.8	27.88	1701	121	147.6
1515	54.2	29.38	1375	111	123.2
1573	55.8	31.14	1463	115	132.3
1636	57.5	33.06	1535	118	139.2
1698	58.7	43.46	1632	122	148.8
1777	60.6	36.72	1698	126	157.5
1986	65.2	42.51	1834	131	170.4
2798	79.3	62.89	1955	135	182.3
2857	81.1	65.77	2024	138	190.4
2981	83.6	69.89	2785	163	264.1
3081	85.0	72.25	2862	164	269.0
3204	87.0	75.69	3062	168	282.2
3480	92.3	85.19	3125	172	294.2
4312	105	110.25	3247	175	304.5
4549	110	121.00	3434	182	329.5
	460°C(Y)			430°C(Y)	
1275	102	104.0×10^{-4}	1283	165	272.3×10^{-4}
1328	105	110.3	1345	169	285.6
1371	107	114.5	1447	176	309.8
1411	109	119.9	1510	180	324.0
1468	112	125.4	1570	185	432.2
1516	114	131.1	1632	188	353.4

mins.	$\mu g/cm^2$	$(mg/cm^2)^2$
	490°C(Y) cont'd.	
1696	191	304.8×10^{-4}
1747	194	376.4
1978	207	428.5
2755	242	585.6
2837	246	605.2
2943	250	625.0
3054	255	650.0
3268	261	681.2
3528	272	739.8
4170	293	858.5
4298	297	882.1
4426	302	912.0
4590	307	942.5
4654	303	954.8
	520°C(Y)	
1471	296	87.6×10^{-3}
1500	298	88.8
1762	323	104.3
2077	354	125.0
2894	421	177.2
3186	442	195.4
3515	465	216.2
4234	512	262.1
4413	521	271.4

mins.	$\mu g/cm^2$	$(mg/cm^2)^2$
	550°C(Y)	
1304	373	143.6×10^{-3}
1366	390	152.1
1457	406	164.4
1560	421	177.2
1645	436	190.1
1757	455	207.0
2041	494	244.0
2869	603	366.0
3513	685	469.2
4407	783	613.1
4548	796	633.6

3.2 Results for the early stages of oxidation.

3.2.1 Results obtained above 570°C.

mins.	$\mu g/cm^2$	$(\mu g/cm^2)^{2/3}$	mins.	$\mu g/cm^2$	$(\mu g/cm^2)^{2/3}$
	580°C(x)			580°C(x) cont'd.	
13	0.759	0.83	122	8.28	4.09
16	0.937	0.96	132	9.24	4.40
23	1.465	1.29	136	9.73	4.56
27	1.658	1.40	139	9.90	4.61
32	1.897	1.53	142	10.3	4.73
37	2.15	1.67	151	11.2	5.00
42	2.46	1.82	155	11.4	5.09
46	2.63	1.91		580°C(x)	
51	2.88	2.02	20	0.148	0.28
56	3.31	2.22	28	0.297	0.44
59	3.51	2.31	35	0.396	0.54
65	3.89	2.51	41	0.573	0.77
67	4.04	2.54	45	0.890	0.93
73	4.39	2.68	50	1.19	1.12
75	4.64	2.78	55	1.49	1.30
80	4.95	2.90	59	1.68	1.41
85	5.38	3.07	65	2.12	1.65
93	5.81	3.31	72	2.48	1.83
99	6.47	3.47	74	2.77	1.97
103	6.83	3.60	80	3.17	2.15
114	7.45	3.81	88	3.67	2.38
117	7.69	3.90			

mins.	$\mu g/cm^2$	$(\mu g/cm^2)^{2/3}$	mins.	$\mu g/cm^2$	$(\mu g/cm^2)^{2/3}$
	620°C(X)			660°C(X) cont'd.	
14	1.05	1.03	19	3.84	2.45
18	1.53	1.33	22	4.78	2.84
24	2.29	1.74	25	5.52	3.12
29	2.95	2.06	30	6.46	3.47
33	3.54	2.32	34	7.86	3.95
36	3.90	2.48	39	9.64	4.53
42	4.89	2.88	50	12.9	5.50
50	6.23	3.38	111	41.6	12.0
52	6.59	3.51		660°C(X)	
57	7.43	3.81	22	3.50	2.31
63	8.29	4.10	25	4.33	2.65
68	9.14	4.37	30	5.30	3.04
71	9.81	4.58	39	8.14	4.05
74	10.3	4.73	45	9.81	4.58
78	11.2	5.00	53	12.1	5.27
82	11.9	5.22	61	15.3	6.16
90	13.7	5.73	69	18.0	6.87
110	18.1	6.90	75	20.7	7.54
126	22.6	7.99	82	22.6	8.00
166	31.7	10.0	95	29.7	9.59
	660°C(X)		103	31.0	9.87
12	1.84	1.51	117	38.4	11.37
14	2.60	1.89	144	51.5	13.84
17	3.23	2.18			

mins.	$\mu g/cm^2$	$(\mu g/cm^2)^{2/3}$
	700°C(X)	
7.50	2.43	1.81
8.50	2.96	2.06
13.50	5.29	3.04
14.50	5.65	3.17
16.75	7.02	3.67
19.50	8.54	4.18
22.25	10.1	4.67
25.25	11.9	5.22
28.25	13.91	5.81
36.50	20.0	7.37
45.50	26.9	8.98
41.50	30.3	9.72
56.50	36.9	11.08
	700°C(X)	
8	4.55	2.75
12	7.44	3.81
17	11.0	4.95
20	13.3	5.61
24	17.1	6.63
30	22.2	7.90
35	26.9	8.98
42	33.9	10.48
48	40.1	11.72
51	43.9	12.45

mins.	$\mu g/cm^2$	$(\mu g/cm^2)^{2/3}$
	700°C(X) cont'd.	
58	51.4	13.82
67	62.4	15.73
71	67.1	16.51
81	79.9	18.55
	740°C(X)	
11	7.12	3.70
12	8.03	4.01
13	9.08	4.35
14	10.1	4.67
16	11.7	5.61
19	15.0	6.08
21	16.9	6.59
26	22.8	8.04
32	30.7	9.80
37	38.1	11.32
42	46.3	12.89
49	60.3	15.38
	780°C(X)	
5	6.34	3.43
6	7.75	3.92
7	9.48	4.48
8	11.4	5.07
9	13.6	5.70
10	15.6	6.24

mins.	$\mu g/cm^2$	$(\mu g/cm^2)^{2/3}$
	780°C(X) cont'd.	
11	17.6	6.77
12	19.9	7.34
13	22.5	7.97
15	27.8	9.17
18	36.8	11.05
21	48.3	13.26
24	60.8	15.47
	780°C(Y)	
7	12.9	5.50
10	20.6	7.51
14	30.3	9.72
17	40.0	11.70
21	54.6	14.40
24	67.6	16.60
28	86.5	19.56
33	113	23.39
39	147	27.85
44	178	31.65
48	203	34.54
57	259	40.64
	820°C(X)	
2	4.94	2.90
3	7.86	3.45
4	10.90	4.92

mins.	$\mu g/cm^2$	$(\mu g/cm^2)^{2/3}$
	820°C(X) cont'd.	
5	13.9	5.78
6	17.4	6.72
7	21.1	7.63
8	25.2	8.60
9	29.4	9.52
10	33.9	10.48
11	38.8	11.48
15	61.1	15.51
18	81.5	18.80
25	134	26.21
30	176	31.41
40	256	40.31
	580°C(Y)	
13	3.24	2.19
19	3.80	2.43
24	4.39	2.68
31	5.22	3.01
37	6.02	3.31
45	7.05	3.68
52	7.88	3.96
61	9.40	4.45
72	11.1	4.96
82	12.7	5.44
95	14.8	6.03

mins.	$\mu g/cm^2$	$(\mu g/cm^2)^{2/3}$
	580°C(Y) cont'd.	
134	21.0	7.61
	620°C(Y)	
11	2.40	1.79
13	2.96	2.06
17	4.14	2.58
24	5.93	3.28
29	7.41	3.80
37	9.94	4.62
45	12.6	5.42
54	15.9	6.32
65	20.4	7.47
77	25.3	8.62
89	30.1	9.68
104	37.0	11.11
130	49.0	13.39
	660°C(Y)	
4	2.44	1.81
5	2.79	1.98
7	3.75	2.42
9	4.51	2.73
11	5.02	2.93
13	6.60	3.52
16	8.37	4.12
20	10.5	4.79

mins.	$\mu g/cm^2$	$(\mu g/cm^2)^{2/3}$
	660°C(Y) cont'd.	
26	14.0	5.81
30	16.5	6.48
36	20.8	7.57
40	23.6	8.23
45	27.4	9.09
50	31.4	9.95
55	35.5	11.08
68	46.4	12.91
78	54.8	14.42
88	63.9	15.98
101	76.0	17.95
110	83.9	19.17
124	97.4	21.17
	700°C(Y)	
5	4.82	2.85
7	6.67	3.54
8	7.59	3.86
9	8.62	4.20
12	11.4	5.07
15	14.6	5.97
17	16.7	6.53
21	21.5	7.73
26	22.6	7.99
29	31.8	10.03

mins.	$\mu g/cm^2$	$(\mu g/cm^2)^{2/3}$
	700°C(Y) cont'd.	
35	48.2	11.74
44	53.4	14.18
47	59.0	15.15
50	64.2	16.03
54	70.9	17.13
59	80.0	18.57
63	87.2	19.66
71	103	21.90
79	118	24.04
89	137	26.50
	740°C(Y)	
2	3.10	2.13
3	4.44	2.70
5	7.43	3.81
6	8.66	4.22
9	13.2	5.58
11	16.5	6.48
13	20.1	7.39
17	28.4	9.31
20	35.3	10.77
24	45.9	12.83
32	70.1	17.00
39	92.9	20.50
44	110	22.96

mins.	$\mu g/cm^2$	$(\mu g/cm^2)^{2/3}$
	740°C(Y) cont'd.	
43	127	25.25
54	144	27.41
	780°C(Y)	
3	7.56	3.65
4	9.98	4.37
5	13.1	5.07
7	15.5	6.35
9	19.4	7.54
11	23.0	8.75
13	30.7	10.20
15	38.9	11.79
19	48.5	14.21
23	57.9	16.94
26	67.2	18.91
30	82.4	21.52
33	92.0	23.21
36	107	24.88
	820°C(Y)	
1	3.22	2.18
2	6.98	3.62
3	10.8	4.89
4	14.0	5.81
5	17.5	6.74
7	25.7	8.71

mins.	$\mu g/cm^2$	$(\mu g/cm^2)^{2/3}$
	820°C(Y) cont'd.	
8	30.4	9.74
9	34.8	10.66
11	44.8	12.62
13	56.2	14.67
15	67.4	16.56
18	85.7	19.43
21	94.4	20.73
24	124	24.88
	580°C(z)	
11	1.09	1.06
18	1.32	1.20
23	1.55	1.34
36	2.41	1.80
46	2.91	2.04
57	3.36	2.24
64	3.73	2.40
71	4.09	2.56
83	4.68	2.80
91	5.00	2.92
99	5.46	3.10
	620°C(z)	
14	0.69	0.78
17	1.04	1.03
22	1.47	1.29

mins.	$\mu g/cm^2$	$(\mu g/cm^2)^{2/3}$
	620°C(z) cont'd.	
27	1.99	1.58
41	3.55	2.33
54	4.66	2.79
62	5.22	3.01
70	6.00	3.30
78	6.87	3.61
86	7.73	3.91
	660°C(z)	
9	0.94	0.96
12	1.43	1.27
16	2.15	1.67
18	2.51	1.85
22	3.09	2.12
25	3.67	2.38
29	4.61	2.77
33	5.28	3.03
36	6.22	3.38
43	7.11	3.70
48	8.59	4.19
57	10.4	4.76
63	11.9	5.22
	700°C(z)	
6	1.04	1.03
8	1.75	1.45

mins.	$\mu g/cm^2$	$(\mu g/cm^2)^{2/3}$
	700°C(z) cont'd.	
11	2.57	1.88
13	3.24	2.19
16	4.41	2.69
19	5.45	3.08
22	6.58	3.51
25	7.54	3.85
28	9.04	4.34
31	10.4	4.76
34	11.9	5.22
36	13.1	5.56
39	14.6	5.97
	740°C(z)	
5	3.03	2.09
8	4.54	2.74
9	5.78	3.22
12	8.10	4.03
14	9.52	4.52
15	10.4	4.76
17	12.0	5.24
19	13.8	5.75
21	15.5	6.25
25	19.2	7.17
30	24.3	8.39

mins.	$\mu g/cm^2$	$(\mu g/cm^2)^{2/3}$
	780°C(z)	
5	4.50	2.73
6	5.26	3.03
7	6.22	3.38
9	8.42	4.14
11	10.6	4.82
13	13.2	5.58
15	15.8	6.30
17	18.7	7.05
20	23.4	8.18
23	28.2	9.26
26	33.9	10.48
29	39.7	11.65
32	45.9	12.83
35	52.7	14.06
	820°C(z)	
5	7.89	3.96
6	9.35	4.44
8	13.9	5.78
9	16.1	6.37
10	18.4	6.97
13	26.1	8.80
15	32.2	10.13
19	45.8	12.81

REFERENCES.

1. D.I.Cameron, J. Aust. Inst. Metals 7, 197 (1962).
2. L.S.Darken, and R.W.Gurry, J. Am. Chem. Soc. 68, 798 (1946).
3. E.R.Jette, and F.Foote, Trans. A.I.M.E. 105, 275 (1933).
4. H.J.Engell, Arch. Eisenhuttenw. 28, 109 (1957).
5. F.Marion, Docum. Metall. 24, 87 (1954).
6. M.H.Davies, M.T.Simnad, and C.E.Birchenall, J. Metals 3, 888 (1951).
7. R.F.Mehl, E.L.McCandless, and F.N.Rhines, Nature 134, 1009 (1934).
8. H.J.Goldschmidt, J. Iron and Steel Inst. 146, 157 (1942).
9. N.B.Pilling, and R.E.Bedworth, J. Inst. Metals, 29, 529 (1923).
10. C.Wagner, Z. Phys. Chem. 213, 25 (1933).
11. N.Cabrera, and N.F.Mott, Rep. Prog. Phys. 12, 163 (1948-49).
12. N.F.Mott, Trans. Faraday Soc. 35, 1175 (1939).
13. T.Mills, and U.R.Evans, J. Chem. Soc., 2182 (1956).
14. O.Kubaschewski, and B.E.Hopkins, Oxidation of Metals and Alloys, Butterworths, London (1960).
15. U.R.Evans, The Corrosion and Oxidation of Metals, Edward Arnold, London (1960).
16. J.Bardolle, and J.Benard, C. R. Acad. Sci. Paris 232, 231 (1951).

17. F.Gronlund, and J.Benard, C. R. Acad. Sci. Paris 240, 624 (1955); J. Chem. Phys. 53, 660 (1956).

18. E.Menzel, and W.Stossel, Naturwissen . Schaften. 41, 302 (1954).

19. E.Menzel, and C.Menzel-Topp, Z. Naturf. 13), 985 (1958).

20. U.Martius, Canadian J. Phys. 33, 466 (1955).

21. W.Harris, F.Hall, and A.Gwathmey, Acta Met. 5, 574 (1957).

22. J.Moreau, and J.Benard, J. Inst. Met. 83, 87 (1954).

23. J.Moreau, and J.Benard, J. Chim. Phys. 53, 787 (1956).

24. W. Hibbert, and C.Dunn, Acta Met. 4, 306 (1956).

25. J.Faidassi, M.L.Pointud, R.Caillat, and R.Darras, Acta Met. 9, 515 (1961).

26. P.Garcia, and D.Fuller, Acta Met. 9, 79 (1961).

27. J.Benard, Acta Met. 8, 272 (1960).

28. E.A.Gulbransen, and T.P.Copan, Faraday Soc. Disc. 28, 229 (1959); Nature 186, 961 (1960).

29. T.N.Rhodin, Z. Elektrochem. 62, 707 (1958).

30. F.Bouillon, G.Van Der Schrick, and C.Maeckenbeeck, Acta Met. 10, 647 (1962).

31. W.Hibbert, and C.Dunn, Acta Met. 4, 306 (1956).

32. J.Cabrera, J. Chem. Phys. 53, 675 (1956).

33. F.Young, Acta Met. 8, 117 (1960).

34. A.L.G.Rees, paper presented at the Solid State Chemistry Symposium, Australian and New Zealand Association for the Advancement of Science Conference, 1961; paper presented at the First Australian Conference on Electrochemistry, 1963.

35. E.R.Lawless, and A.Gwathmey, Acta Met. 4, 153 (1956).

36. J.Pardolle, Rev. Metall. 51, 833 (1954).

37. E.R.Lawless, F.W.Young, and A.Gwathmey, J. Chim. Phys. 53, 667 (1956).

38. R.E.Bloomer, Brit. J. Appl. Phys. 8, 321 (1957).

39. S.Wagener, Proc. Inst. Elec. Engrs., Part 3 99, 135 (1952).

40. U.R.Evans, Trans. Faraday Soc. 41, 365 (1945).

41. A.Ronnquist, J. Inst. Met. 91, 89 (1962-63).

42. S.Glasstone, K.J.Laidler, and H.Eyring, The Theory of Rate Processes p.13, Mc Graw-Hill, New York (1941).

43. K.Fischbeck, L.Neundeubel, and F.Salzer, Z. Electrochem. u angew Physik. Chem. 40, 517 (1934).

44. N.G.Schmall, H.Baumann, and H.Schenck, Arch. Eisenhuttenw. 29, 147 (1958).

45. W.W.Smeltzer, Acta Met. 8, 377 (1960).

46. U.R.Evans, Trans. Electrochem. Soc. 46, 247 (1924).

47. J.Benard, and J.Talbot, C. R. Acad. Sci. Paris 226, 912 (1948).

48. K.Hauffe, and H.Pfeiffer, Z. Electrochem. 56, 390 (1952); Z.Metallk 44, 27 (1953).

49. H.Pfeiffer, and C.Laubmeyer, Z. Electrochem. 59, 579 (1955).

50. F.Petit, R.Yinger, and J.F.Wagner, Acta Met. 8, 217 (1960).

51. V.I.Arkharov, V.P.Mar'evich, M.Reinkhol'd, and M.I.Simonova, Fiz. Metal. Metalloved 3, 251 (1957).

52. H.J.Engell, Acta Met. 6, 439 (1958).

53. W.W.Smeltzer, Trans. A.I.M.E. (Metall) 218, 674 (1960).

54. L.S.Darken, and R.W.Gurry, Physical Chemistry of Metals p.357, Mc Graw-Hill, New York (1953).

55. E.A.Gulbransen, Rev. Sci. Instruments 15, 201 (1944).

56. D.E.Davies, U.R.Evans, and J.N.Agar, Proc. Roy. Soc. A, 225, 443 (1954).

57. H.G.Oswin, and M.Cohen, J. Electrochem. Soc. 104, 9 (1957).

58. M.H.Huob, A.F.Beck, and M.Cohen, J. Electrochem. Soc. 105, 74 (1958).

59. P.Hancock, and J.E.O.Mayne, J. Chem. Soc., 4167 (1958).

60. U.R.Evans, and D.E.Davies, J. Chem. Soc., 4373 (1956).

61. W.H.J.Vernon, E.I.Akeroyd, and E.G.Stroud, J. Metals 65, 301 (1939).

62. D.Caplan, and M.Cohen, Corrosion 15, 141t (1959).

63. W.T.Denholm, J. Aust. Inst. Metals 7, 141 (1962).

64. W.T.Denholm, paper presented at the First Australian Conference on Electrochemistry, 1963.

65. P.L.Firk, and F.L.Schaffer, Rev. Sci. Instruments 19, 777 (1948).

66. P.L.Kirk, R.E.Craig, J.E.Gullberg, and R.Q.Boyer, Anal. Chem. 19, 427 (1947).

67. H.Barrett, A.Birnie, and M.Cohen, J. Am. Chem. Soc. 62, 2839 (1940).

68. A.W.Czanderna, and J.M.Honig, Anal. Chem. 29, 1206 (1957).

69. E.A.Gulbransen, Trans. Electrochem. Soc. 81, 327 (1942).

70. T.N.Rhodin, J. Am. Chem. Soc. 72, 4343 (1950).

71. T.N.Rhodin, Advances in Catalysis Vol. 5, p.51, Academic Press, New York (1953).

72. R.V.Jones, and J.C.S.Richards, J. Sci. Instruments. 15, 90 (1959).

73. R.V.Jones, J. Sci. Instruments 38, 37 (1961).

74. R.Bowers, and E.A.Long, Rev. Sci. Instruments 26, 337 (1955).

75. E.A.Gulbransen, Vacuum Microbalance Techniques p.11, (Edited by M.J.Katz), Plenum Press, New York (1961).

76. T.Mills, and G.M.Willis, Trans. Electrochem.Soc.

100, 452 (1953).

77. W.T.Denholm, Thesis, The University of Adelaide (1959).

78. R.E.Heffelfinger, D.L.Chase, G.W.P.Rengstorff, and W.M.Henry, Anal. Chem. 30, 112 (1958).

79. A.Draycott, and R.Smith, AAEC/E52, 1 (1960).

80. A.Draycott, and P.J.Fox, AAEC/E97, 4 (1962).

81. A.Draycott, and A.C.Kerr, AAEC/E58, 8 (1960).

82. N.V.Sidgwick, The Chemical Elements and Their Compounds, Vol. 2, p283, Clarendon Press, Oxford (1952).

83. M.Pourbaix, Thermodynamics of Dilute Aqueous Solutions, (English translation by J.N.Agar) p.89, Edward Arnold, London (1949).

84. C.D.Stockbridge, P.E.Sewell and M.Cohen, J. Electrochem. Soc. 108, 922 (1961).

85. J.V.Hardy, and A.D.Hopkins, Metallurgia 306, 209 (1955).

86. D.C.Grahame, J. Electrochem. Soc. 99, 370 (1952).

87. D.C.Grahame, J. Electrochem. Soc. 76, 4819 (1954).

88. E.Deltombe, and M.Pourbaix, Proc. C. I. T. C. E. (6th meeting) p.124, Butterworths, London (1955).

89. C.Upthegrove, and D.W.Murphy, Trans. Am. Soc. Steel Treatment 21, 73 (1933).

90. H.J.Engell, Z. Electrochem. 637, 835 (1959).

91. N.A.Warner, Kinetics of the gaseous reduction of hematite, a paper presented at the A.I.M.M. annual conference (1963).

92. C.Wagner, and K.Grunewald, Z. Phys. Chem. 40, 435 (1939).

93. R.F.Tylecote, J. Inst. Metals 81, 681 (1952-53).

94. G.I.Finch, and A.G.Quarrell, Nature 131, 877 (1933); Proc. Roy. Soc. 141, 398 (1933).

95. K.Thomas, and M.W.Roberts, J. App. Phys. 32, 70 (1961).

96. A.Steinheil, Ann. Phys. 19, 465 (1934).

97. J.Benard, F.Gronlund, J.Oudar, and M.Duret, Z. Electrochem. 63, 799 (1959).

98. F.Bouillon, and M.Jardinier Offergeld, Acta Met. 11, 287 (1963).

99. J.Crank, Mathematics of Diffusion, p.30, Oxford Univ. Press, Oxford (1957).

100. C.A.Neugebauer, J.B.Newkirk, and D.A.Vermilyea, Structure and Properties of Thin Films p.37, John Wiley, New York (1959).

101. J.W.Faust, Acta Met. 11,1077 (1963).

102. J.Paidassi, J. Metals 4, 536 (1952).

103. W.E.Garner, Chemistry of the Solid State p.142, Butterworths, London (1955).

104. O.Kubaschewski, and E.L.Evans, Metallurgical Thermochemistry, Pergamon Press, London (1958).

105. F.D.Richardson, J. Iron and Steel Inst. 173, 46 (1953).

106. R.P.Smith, J. Am. Chem. Soc. 68, 1163 (1946).